UNIVERSITÀ DEGLI STUDI DI PAVIA

DOTTORATO IN SCIENZE CHIMICHE E FARMACEUTICHE E INNOVAZIONE INDUSTRIALE
(XXXVII Ciclo)
Coordinatore: Chiar.mo Prof. Giorgio Colombo

R&D for gas recovery systems and study of eco-friendly gas mixtures for new gas detectors for the Experiments at the CERN Large Hadron Collider

Tesi di Dottorato di
Maria Cristina Arena

AA 2023/2024

Tutor
Chiar.ma Prof.ssa Antonella Profumo

Dott. Roberto Guida

Co-tutor
Chiar.mo Prof. Daniele Dondi

Summary

This PhD was conducted at the Chemistry Department of the University of Pavia in collaboration with the EP-DT-FS group at CERN, which manages the gas systems of the gaseous detectors used in LHC experiments. The LHC gas systems share a common structure, consisting of several main modules: primary gas supply, mixer, gas distribution, pump, exhaust, purifier, and gas analysis module. At the CMS and LHCb experiments, the analysis module is equipped with integrated systems for gas chromatography, to perform analyses on selected sample lines. These analyses provide a more comprehensive measurement of all the components in the gas mixture and are conducted every two weeks. The results are published on the CERN network, allowing everyone to check the status of the gas mixtures for each detector.

LHC gaseous detectors are filled with expensive greenhouse gases, such as hydrofluorocarbons (HFCs), sulphur hexafluoride (SF_6), and CF_4, all of which have a high Global Warming Potential (GWP). This PhD project specifically focused on the recovery systems for CF_4 (CMS CSC and LHCb RICH2), $C_2H_2F_4$ (CMS RPC), and C_4F_{10} (LHCb RICH1). The GWPs of these gases are 7390, 1430, and 9200, respectively. Recovering these freon gases is crucial for reducing emissions, especially since the existing gas recirculation systems still require some gas to be sent to the exhaust. These recovery efforts also necessitate dedicated research and development studies to separate specific gas mixture components.

The CMS CSC gas recuperation system was designed to separate CF_4 from other mixture components, namely argon (Ar) and carbon dioxide (CO_2). The purification plant comprises four main parts:

1. A membrane module for bulk separation of CO_2,

2. A molecular sieve (4Å) for residual CO_2 removal,

3. A molecular sieve (13X) for CF_4 adsorption and recovery,

4. CF_4 compression and storage.

Since the system became operational in 2012, the recovery efficiency has significantly improved due to extensive testing and upgrades, reaching an average efficiency of over 65% in the past year. Further advancements in separation efficiency and nitrogen (N_2) removal (which is present at 1%

as a non-separable impurity) are still achievable. This is particularly relevant given the variable concentration of CF_4 in the CSC mixture and the purity standards for the recuperated gas, which may necessitate the development of new materials for improved separation devices.

Recently, a prototype for the CMS RPC recovery system was developed to separate $C_2H_2F_4$ from other gaseous mixture components (iC_4H_{10}/SF_6 in a ratio of 4.5/0.3). The $C_2H_2F_4$ recovery process consists of three main steps:

1. Removal of SF_6 and N2 through the condensation of iC_4H_{10} and $C_2H_2F_4$ (cooling the gas mixture from 20°C to -35°C),

2. Separation of $C_2H_2F_4$ from the azeotropic mixture of iC_4H_{10}/ $C_2H_2F_4$ via sequential distillation processes,

3. Compression, storage, and purity analysis of $C_2H_2F_4$.

The recovery plant for CF_4 at LHCb RICH2 employs a membrane separation process, which can be adjusted according to the fraction of CF_4 in the gas mixture from the detector. In contrast, the LHCb RICH1 separation process uses a single-step distillation method to separate C_4F_{10} from other components for storage.

Throughout the development of these plants, gas composition measurements using gas chromatography (GC) and gas chromatography-mass spectrometry (GC/MS) have proven to be essential tools for optimizing various parameters.

In addition to developing recovery systems, research was conducted on long-term alternatives to the freon gases currently used in gaseous detectors. Most alternative hydrofluoroolefins (HFOs) have a lower GWP and behave similarly to traditional freon-based gases for refrigeration purposes, but they do not perform as effectively in detector ionization processes. Moreover, these gases can undergo breakdown processes when exposed to high radiation rates, especially in the presence of a strong electric field. This breakdown can release highly reactive products, which may adversely affect detector operation by causing polymerized deposits, etching materials, or reacting with water (present at 40% relative humidity in RPC detectors) to form hydrofluoric acid. Such reactions could undermine detector performance and accelerate aging.

One goal of this PhD project was to characterize these processes through various chemical analyses, including UV-Visible spectroscopy, ion-selective electrodes (ISE), and GC/MS. After establishing a suitable setup for laboratory measurements, F^- measurements were performed at

the LHC ALICE experiment for MID detectors, aiming to better understand F^- production under real conditions across different radiation levels.

A critical parameter for assessing the performance of a gas in LHC operations is its absorbance spectrum, which ranges from vacuum ultraviolet (UV) to visible light. R&D activities focused on both traditional and newer, more environmentally friendly gases for RPC detectors, specifically examining their performance across the energy range between 9 eV and 1 eV.

Contents

Chapter 1
“Muon Systems and Gaseous detectors at the LHC”

1.1 CERN at LHC

The European Organization for Nuclear Research (CERN) primarily focuses on particle physics, particularly through studies of the Standard Model and the search for New Physics. To support this mission, the Large Hadron Collider (LHC) has been constructed. Additionally, CERN conducts various other research activities, including "fixed-target" experiments, antimatter experiments, and non-accelerator experiments, along with other experimental facilities.

The LHC is the world’s largest and most powerful particle accelerator, and it consists of a 27-kilometre ring of superconducting magnets, lying 100m underground, with several accelerating structures to boost the energy of the particles along the way.

The functioning of the accelerator is based on two high-energy particle beams travelling at close to the speed of light before they are made to collide. The beams travel in opposite directions in separate beam pipes kept under ultra-high vacuum. They are guided around the accelerator ring by a strong magnetic field ensured by superconducting electromagnets.

The working temperature of this magnets is -271.3°C (1.8 K) a temperature colder than outer space.

Primary protons are obtained from Helium, and they are accelerated in a first linear accelerator (LINAC4), to be then injected in the chain of circular accelerators that allows the achievement of their maximum energy (6.5TeV). Protons pass through the Proton Synchrotron (PS, 25GeV), the Super Proton Synchrotron (SPS, 450GeV) and finally are injected in the LHC (Figure 1).

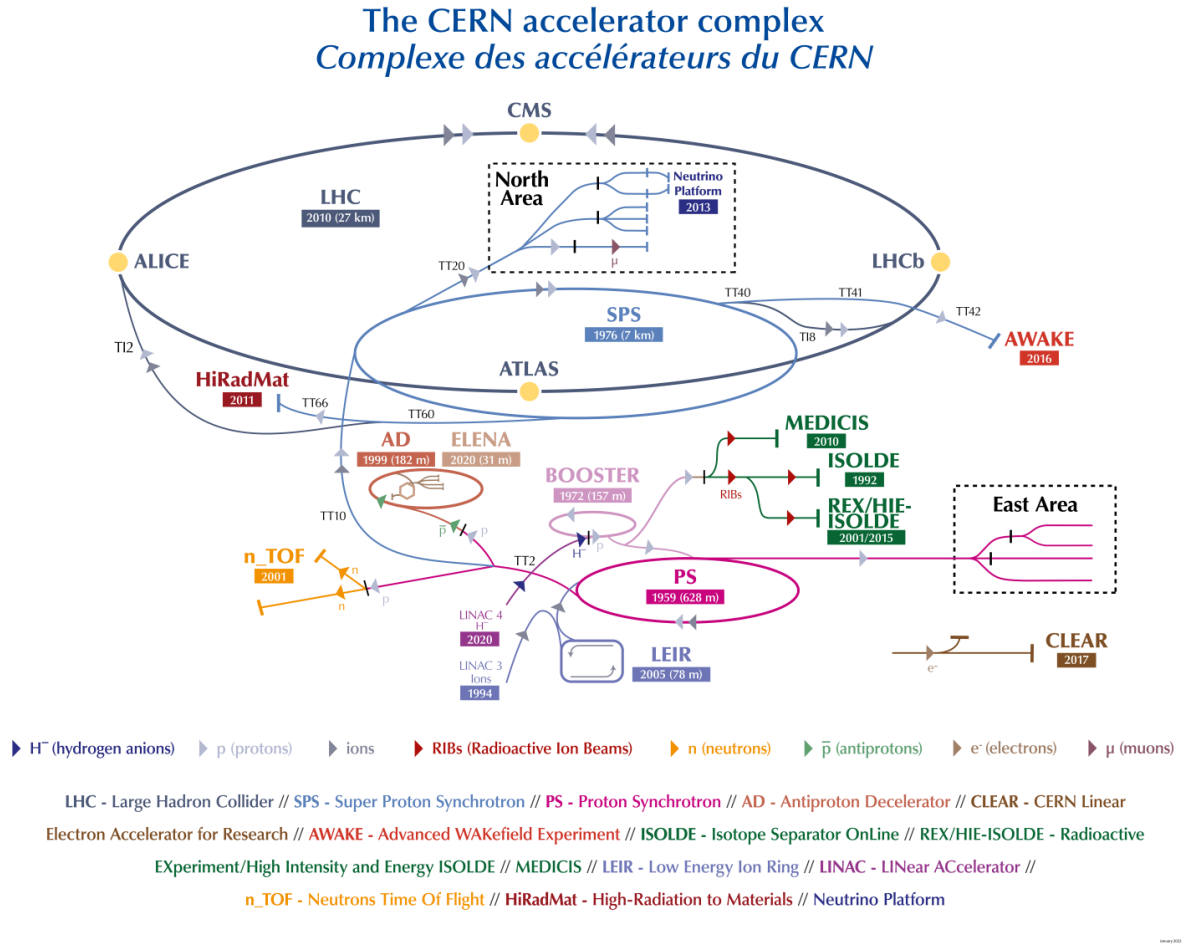

Figure 1 Schematic drawing of the LHC complex layout, with accelerators and experiments.

The CERN accelerator complex accelerates protons, but also nuclei of ionized atoms of lead (Pb), argon (Ar) or xenon (Xe). Some LHC runs are thus dedicated to lead-ion collisions. The beams inside the LHC are made to collide at four locations around the accelerator that correspond to the four Experiments: ATLAS, ALICE, CMS and LHCb.

ATLAS (A Toroidal LHC apparatus) and CMS (Compact Muon Solenoid) are the two general purpose Experiments that were developed for exploring all the possible aspects of the LHC physics (from the search for the Higgs boson to extra dimensions and particles that could make up dark matter) and for searching new particles. ALICE (A Large Ion Collider) Experiment is designed to study the physics of strongly interacting matter at extreme energy densities, while LHCb (Large Hadron Collider beauty) Experiment specializes in investigating the differences between matter and antimatter by studying a type of particle called the "beauty quark", or "b quark".

Although each experiment has a specific purpose, the requirements for the detectors they utilize are largely similar:

- *Inner Detectors*:

  Located close to the collision points, they track and measure the momentum of charged particles, as well as Interaction Point and vertices reconstruction.

- *Hadronic and Electromagnetic Calorimeters*:

  They measure the energy of hadrons, photons and electrons crossing their volume, based on the energy loss of emerging particles.

- *Muon systems*:

  Due to their ability to penetrate the calorimeter, muons necessitate a specialized Muon system, typically positioned in the outermost layers of experiments. This arrangement ensures the unambiguous identification of signatures pertinent to numerous significant events. Discussion of these systems will be deferred, as the current focus of this thesis is on the gas analysis pertinent to gaseous detectors.

1.2 LHC gaseous particles detectors

In the past nearly all High Energy Physics experiments successfully used gaseous detectors, exploring their features, like good spatial resolution, big and fast signals, good energy deposition per unit length (d*E*/d*x*), low radiation length, etc. Their performance and adaptability to the needs of the experiments make them still indispensable today. Good examples are the numerous and diverse gaseous detectors employed in the Large Hardron Collider (LHC) experiments, such as the proportional counter and later the Multi-Wire Proportional Chamber (MWPC), microstructure devices, now known as Micro-Pattern Gaseous Detectors (MPGD), the Gas Electron Multiplier (GEM) and the MICRO MEsh GAseous Structure (MICROMEGAS). Finally, Resistive Plate Chamber (RPC) combines fast signal response with good rate capability.

ALICE [1]

The ALICE high-energy heavy-ion experiment is strongly based on gaseous detectors (Figure 2). Technologies include: the high momentum particle identification system (HMPID, 100% of CH_4), the transition radiation detector (TRD, 100% of Xe), a large time projection chamber (TPC, $Ne/CO_2/N_2$ in a ratio 89/8/3), the muon identifier detectors (MID R134a/iC_4H_{10}/SF_6 in a ratio 89.7/10/0.3) in the muon arm trigger, the time of flight system (TOF, R134a/SF_6 in a ratio 93/7), and the muon tracking chambers (MCH, Ar/CO_2 in a ratio 80/20) [2].

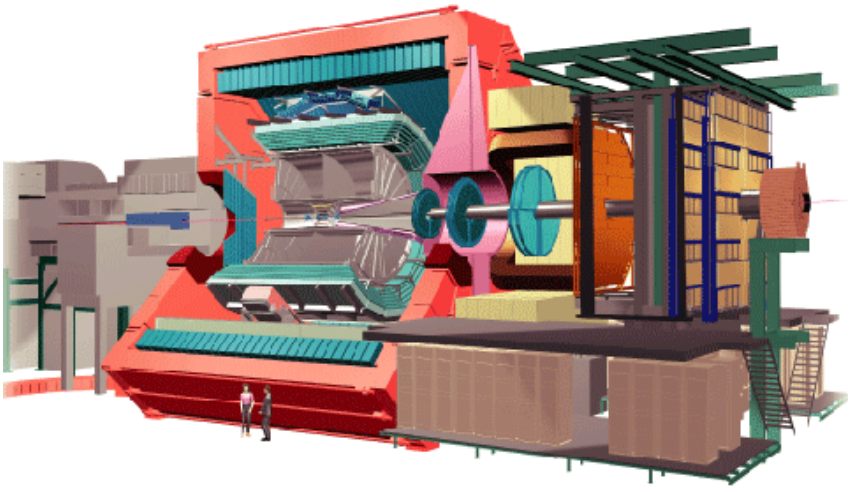

Figure 2 ALICE experiment layout.

ATLAS [3]

The outer layer of the ATLAS experiment (Figure 3) is made of gaseous detectors for muon detection. They identify and measure the momenta of muons – particles similar to electrons but 200 times heavier, which allows them to cross the thick layers of the ATLAS Calorimeters.

Five different detector technologies are used: Thin Gap Chambers (TGC, CO_2/n-C_5H_{12} in a ratio 45/55), Resistive Plate Chambers (RPC, R134a/CO_2/iC_4H_{10}/SF_6 in a ratio 64.7/30/5/0.3), Monitored Drift Tubes (MDT, Ar/CO_2 in a ratio 93/7), Transition Radiator Tracker (TRT, Xe/Ar/O_2 in a ratio 65/34/1), and Micromegas (MMG, Ar/CO_2/iC_4H_{10} in a ratio 93/5/2) [4].

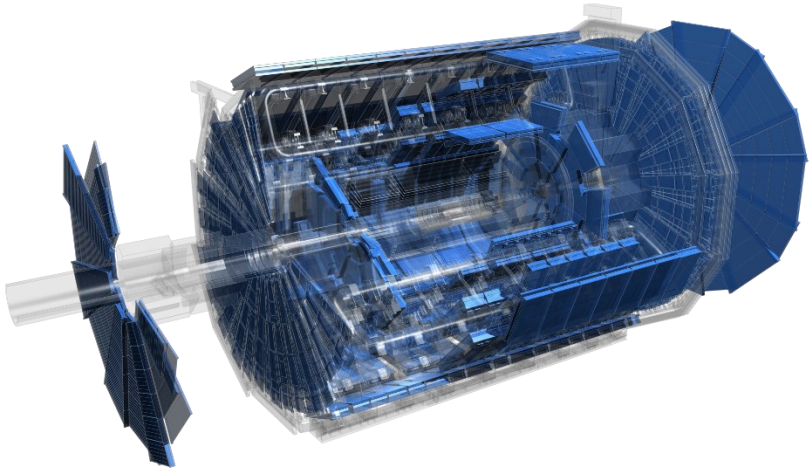

Figure 3 ATLAS muon system layout.

CMS [5]

The experiment is equipped with four types of gaseous detectors, shown in Figure 4. They use different technologies: Drift Tubes (DT, Ar/CO_2 in a ratio 85/15) measure muon positions in the barrel part of the detector, Resistive Plate Chambers (RPC, R134a/iC_4H_{10}/SF_6 in a ratio 95.2/4.5/0.3) give a quick measure of the muon momentum, which is then used by the trigger to make immediate decisions about whether the data are worth keeping. Cathode strip Chambers (CSC, CO_2/Ar/CF_4 in a ratio 50/40/10) are used in the endcap disks where the magnetic field is uneven and particle rates are high. Finally, Gas Electron Multiplier (GEM, Ar/CO_2 in a ratio 70/30) complement and extend the existing muon system coverage detectors in the forward regions close to the beampipe.

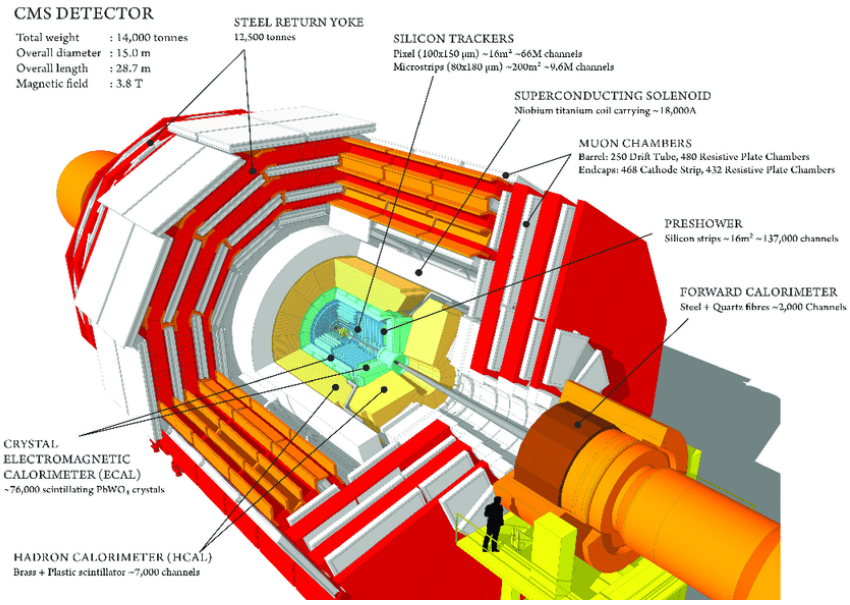

Figure 4 CMS experiment layout.

LHCb [6]

Gaseous detectors at the LHCb experiment (Figure 5) are used for muon detection and particle identification.

The Muon system is composed of five stations (M1-M4) and each station is equipped with 276 Multi Wire Proportional Chambers (MWPCs, $Ar/CO_2/CF_4$ in a ratio 38/57/5). The stations consist of two mechanically independent parts, side A and C, that can be horizontally moved to access the beam pipe and the chambers for maintenance, and each of them is divided into four regions (R1-R4) with increasing distance from the beam axis.

The particle identification system consists of two RICH detectors. The upstream detector, RICH1 (100% C_4F_{10}), covers the low momentum charged particle range ~1-60 GeV/c using aerogel and C_4F_{10} radiators, while the downstream detector, RICH 2 (CF_4/CO_2 in a ratio 92/8), covers the high momentum range from ~15 GeV/c up to and beyond 100 GeV/c using a CF_4 radiator [7].

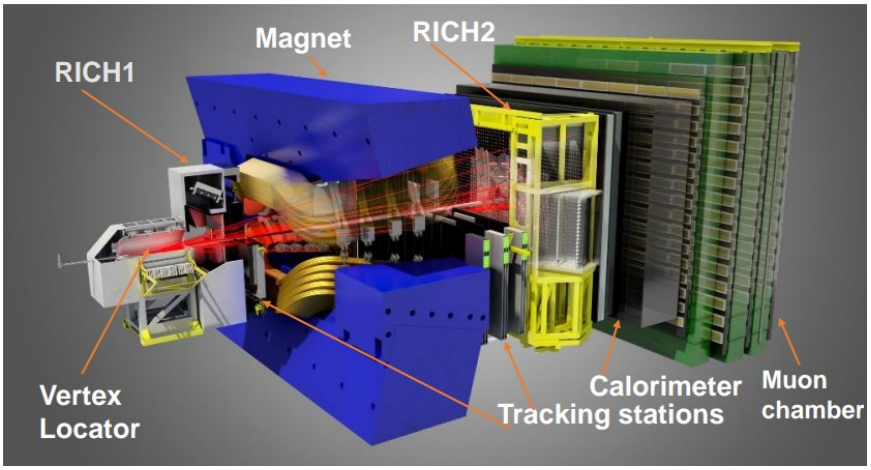

Figure 5 LHCb experiment layout.

1.3 Gaseous ionization detector

Gaseous detectors used in muon systems exploit the gaseous ionization capability for detecting the presence of particle. These detectors typically consist of a gas-filled chamber, an electrode configuration, and a voltage applied across the electrodes to create an electric field.

When the electric field is applied, the positive and negative specimens are attracted to cathode and anode, respectively, while, if the electric field is absent, ions and electrons move away from the point of creation by diffusion. Based on the geometry of the gaseous detector, the electric filed can be:

- Radial → it is typical of wire chambers (e.g. DT) and it is generated in cylindrical geometries, where the electrodes are concentric, such as proportional counters and Geiger-Müller tubes. It is characterized by high gain and good timing resolution but the disadvantages are related to the non-uniform field.
- Planar → it is generated by two parallel plate electrodes and is used in ionization chamber (RPC) and TPCs. The advantages lie in the uniform field and the possibility to have larger volume; on the other hand it is characterized by lower gain and slower signal.

If the electric field has properly strength, the applied voltage prevents the ions-electrons recombination and these specimens reach the electrodes and collected.

The signal is produced by the drift of electrons and ions (not by the collection of charge at the electrodes) [8], the gas parameters influencing the ionization detectors performance are:

- Ionisation potential (eV)
- Energy loss required to produce an electron ion pair (eV). Part of the energy is lost to excite the medium. Noble gases are preferred due to the absence of vibration and rotation states, so ionisation dominates.
- Number of primary electrons reduced by:
    - Recombination: $X^+ + e^- \rightarrow X + \gamma$
    - e^- attachment: $X + e^- \rightarrow X^- + \gamma$

Gaseous detectors may be operated in different operation modes depending on the applied high voltage, as shown in Figure 6:

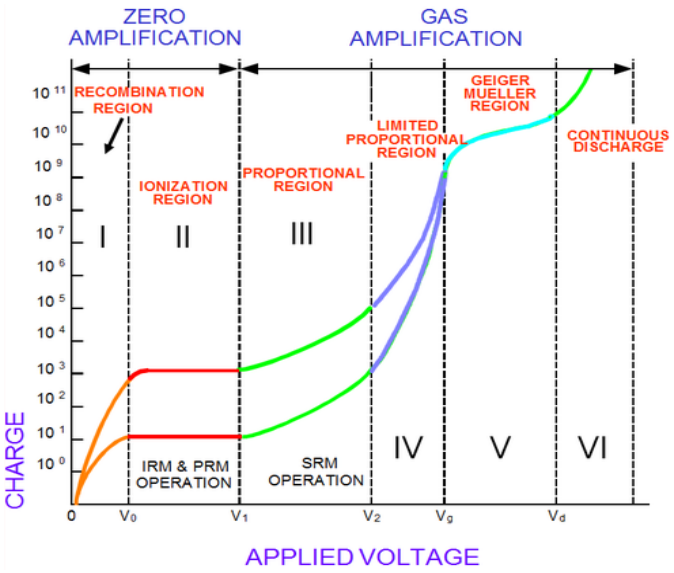

Figure 6 Relationship between the pulse size produced and the potential applied across the electrodes.

- The *Ionization Region* operates at a voltage which allows full collection of charges, but it is not high enough for the amplification of signal. This means that electric field has not the strength to accelerate the electrons and no secondary ions are created. All created pairs are collected and a further increase in the applied voltage shows no effect.

- In the *Proportional region* the voltage applied produces an electric field strong enough to accelerate free electrons. At this point free primary electrons have enough energy to ionise again gas molecules inducing secondary electrons. The electrons released in these secondary ionizations are accelerated to produce still more ionization giving rise to a cascade of electrons known as “avalanche”. The result is a proportional amplification of the current. The number of electron-ion pairs in the avalanche is directly proportional to the number of primary electrons.
- In the *Limited proportional Region and Geiger Muller region* the voltage is increased, ionization becomes sufficiently large that the charge created warps the electric field about the anode. As a result, proportionality is lost. Continuing to increase voltage, the energy becomes so large that a discharge occurs in the gas and chain reaction of many avalanches takes place all along the anode. These secondary avalanches are caused by photons emitted by de-energised molecules. The output current becomes saturated and gives the same amplitude regardless of the energy of the initial event. To stop the discharge a quenching gas must be present to absorb the photons.

1.3.1 Fill Gases

Each detector utilizes a specific gaseous mixture tailored to its purpose. This paragraph describes the main gases and their characteristics.

Noble gases are employed mainly in wire chambers and multipattern detectors for his very low *electron attachment coefficient*, allowing for most of the free electrons to reach the multiplication region without significant interference. However, it should be considered that, besides to a simple ionization, the collision between electrons and neutral gas molecules may give rise to excitation, without the creation of a secondary electron. The excited molecules decay to their ground state, through the emission of a visible or ultraviolet photon, that may create additional ionization elsewhere in the gas. These events are normally undesirable since they may reduce the proportionality. Furthermore, they cause the avalanche to spread. The addition of a certain quantity of polyatomic gas, such as Carbon Dioxide (CO_2) or the iC_4H_{10}, can suppress the photon-induced effects by absorbing the photons in a way that does not lead to further ionization. Traces of oxygen or other impurities must be removed since they can cause a significant loss of free electrons [9].

CF_4 contains fluorine atoms, which are highly reactive. Under the high-energy conditions inside a wire chamber (such as during ionization or electrical discharges), CF_4 can break down and release free fluorine radicals, causing etching of surface. Thanks to its etching property, CF_4 is sometime added to the gaseous mixture in small concentration to clean the wires by removing contaminants or deposits that form due to prolonged operation. Moreover, CF_4 is a key component in RICH detectors because of its unique optical and physical properties, such as high transparency to UV light and low refractive index, which optimize the detection and imaging of Cherenkov radiation.

R134a is used as main component of resistive plate detectors' gas mixtures for its excellent timing properties due to the higher electron drift velocity compared to that of other gases, and its quenching capability. SF_6, thanks to its electron affinity, is added to the gas mixture in small quantities in order to reduce the streamer probability [10].

Finally, C_4F_{10} is used in RICH detectors due to its higher refractive index, which makes C_4F_{10} particularly suitable for identifying particles within a lower momentum range, and it works well alongside other radiators in RICH systems.

1.4 The LHC gas systems for gaseous detectors

The main component of gaseous detectors is the gas mixture that must be correct and stable for the properly functioning of systems. Each type of detector system has its own specific gas system, tailored to its particular utilisation.

The role of the gas systems is to mix the different component of the gas mixture in the right proportion and to distribute the resulting mixture to the corresponding detectors. High reliability is necessary to guarantee the stability and quality of gas mixture, since it is the primary element influencing the detector performance. The LHC gas systems are characterized by a common structure that, if needed, can be adapted to each gas detector requirements; it is made of many modules, each of which has its own function and their pipes extension can reach several hundreds of meters.

The modules are associated with a Programmable Logic Controller (PLC) unit, that manages and controls the units. The software used for controlling the system is based on the WinCC-OA

(SIMATIC WinCC Open Architecture) SCADA tool, where is possible to find information about the status of the system, to control the device, and have information about the interactions between two modules. The collected data are stored in a database and is possible to consult them through a custom graphical user interface [11].

The gas system modules of LHC Experiments are located in three different places: in the Surface room (SG), in the Underground service room (US) and in the Experimental cavern (UX). From the SG, the gas mixture is sent to the US where there is the pre-distribution system as well as part of the gas system parameters regulation. The latter part of gas distribution takes place in the UX, from the service gas balcony racks. The figure below reports a schematic layout of an LHC gas system. The schematic layout of the gas system structure is shown in Figure 7.

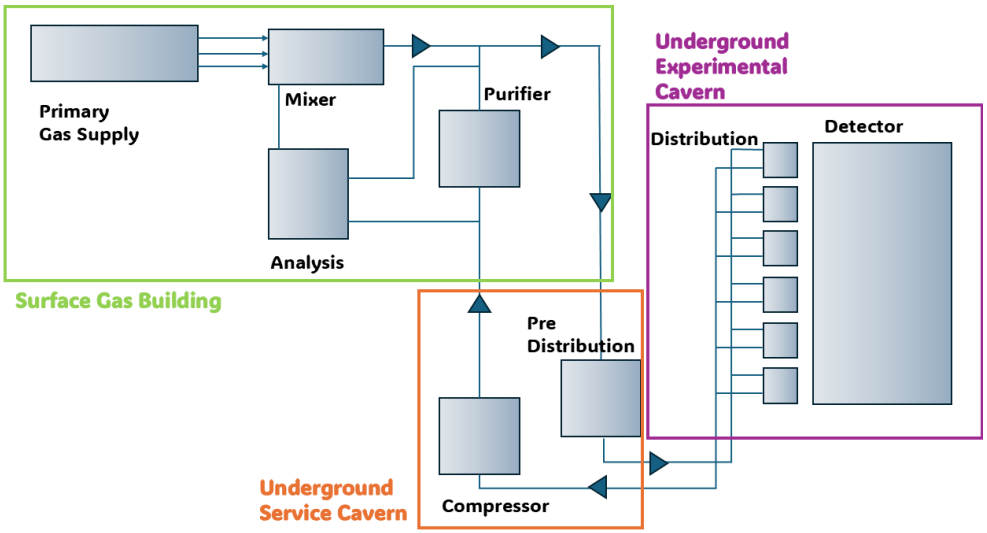

Figure 7 Layout of basic modules of an LHC gas system.

The single modules are briefly described in the followings.

- **Primary Gas Supply**:

  For each gas there are two independent supply sources, one in use and one in stand-by, that can compensate when there is a failure in the main one and during replacement of the storage tanks.

- **Mixer Module**:

  Primary gases are used to prepare the gas mixture for each detector. Mixer modules have up to four input lines, equipped with Mass Flow Controllers (MFCs), controlled via the software control system to set the correct concentration of each component of the gas mixture. In particular, for each fresh gas, two MFCs are installed with different volume flow ranges, since the gas systems needs different flows according to the operation status (run, fill, purge). The gas mixture is prepared with a precision given by the MFCs which is: $0.5\%\ Rd\ (reading) \pm 0.1\%\ FS(Full\ Scale)$.

- **Gas Distribution:**

  Several steps are needed to distribute the gas mixture to each detector, with precise gas volume flow and pressure. Pre-distribution modules are located in the US, and they are related to different detector sectors of the Detector System. The gas is sent from the US to the UX, where the final distribution modules are located, and each gas line is split into several smaller lines, to distribute the gas with the required granularity. The UG and US distribution levels can be accessed and controlled during LHC runs if necessary. The gas mixture coming from the exhaust of the chambers is re-grouped into return modules.

- **Pump Module:**

  Once the gas has flown from the UX into the return modules, the pump module compresses the gas to a higher pressure in way to send it back to the surface.

- **Exhaust Module**:

  In the basic gas systems, the gas passes through the exhaust module, where volume flow and pressure regulations allow to manage the gas emission in relation to the gas system parameters which are subject to specific requirements, for example the chamber pressure stability.

- **Purifier Module:**

  In the recirculation gas systems, the return gas is re-injected in the system and a purifier module allows to remove or reduce the impurities typically accumulated along the gas path, in the gas system elements or directly in the detectors volume. Impurities can be

originated in various ways leaks or chemical reaction occurring when the gas is subject to irradiation and electric field (creation of avalanche, which creates further e- that can easily break the molecules). The most common impurities are N_2, O_2 and H_2O: the last two can be easily removed by adsorption filters.

They consist of two 24-liters cartridges, filled with suitable material that interacts with the specific impurity. Molecular sieves used for H_2O removals, whilst metallic catalysts are employed for O_2 absorption.

- **Gas Analysis Module**:

  The gas analysis module allows a continuous monitoring of the gas mixture quality in the critical gas system points (after mixer, in the exhaust, after purifier). Normally, O_2, H_2O and InfraRed (iC_4H_{10}, CO_2) analysers are present, to measure the concentration of impurities and relevant mixture components. In some cases, the analysis module has an integrated system to perform Gas Chromatograph analysis on selected sample lines, in a way to obtain a more complete measurement of all the gas mixture components.

1.5 Gas Analysis at the LHC

To ensure the proper functioning of the LHC experiments' gas systems, the monitoring of the gas mixture is fundamental. This allows for constant information about the status of the system. For this purpose, different analytical instruments were employed during this PhD project, such as micro gas chromatograph (μGC), gas chromatograph coupled with mass spectrometer (GC/MS), Infrared (IR) devices, UV-Visible and Vacuum-UV (VUV) spectrophotometers. A brief overview of these techniques is given following.

1.5.1 Gas Chromatograph

The instrument of choice for the LHC gas systems is generally a micro-GC, a compact Gas Chromatograph created by the integration of micro-fabricated components. The advantage of this type of device is to have analytical columns that are much shorter than the ones of a standard Chromatograph, allowing to perform analysis in the time span of some minutes.

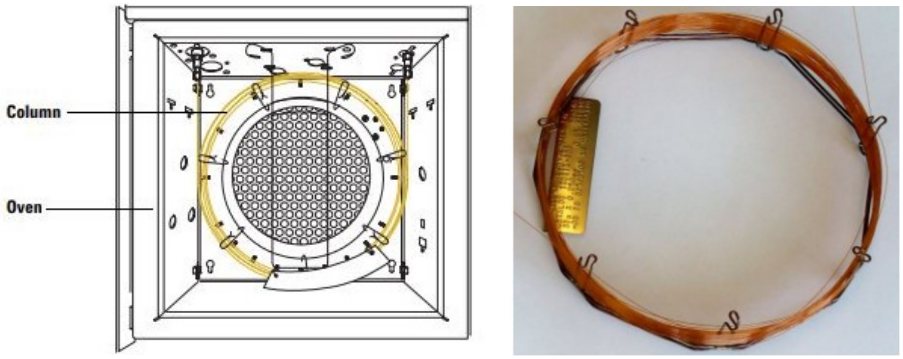

Figure 8 Drawing of a capillary column in an oven: a typical uGC column.

The gas mixture under analysis is injected into the micro-GC through a micro injector, along with a carrier gas which can be Ar, He, H_2 or N_2, depending on the specific properties of the column type of choice and the analysed mixture. The column temperature is controlled by an oven and separates the mixture into its component gases in typically less than 180 seconds (Figure 8). The separation occurs thanks to the specific chemical species that coats the inside surface of column which has different interaction strength with the mixture components, as represented in Figure 9. Basically, achieving quality separations involves understanding and optimizing the effect of many variables including column type and length, choice of the carrier gas and temperature of the column.

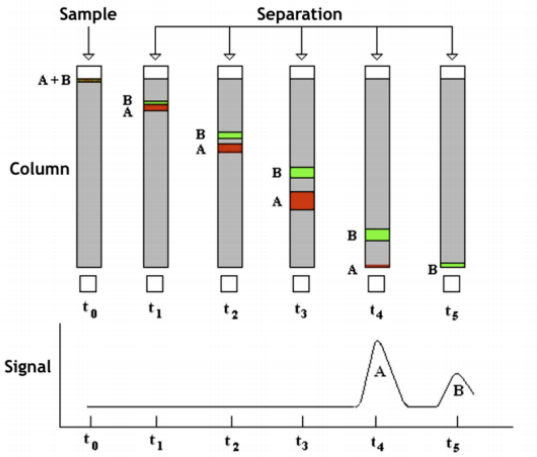

Figure 9 Schematic representation of the separation process inside a µGc column.

The different components are detected by a Thermal Conductivity Detector (TCD, shown in Figure 10), which output signal is proportional to the amount of gas exiting from the column. The plot over time of the electrical signal is a chromatogram, where each peak represents a different component. The peak retention time is used to identify each component while the peak size (height or area) is a measurement of the concentration.

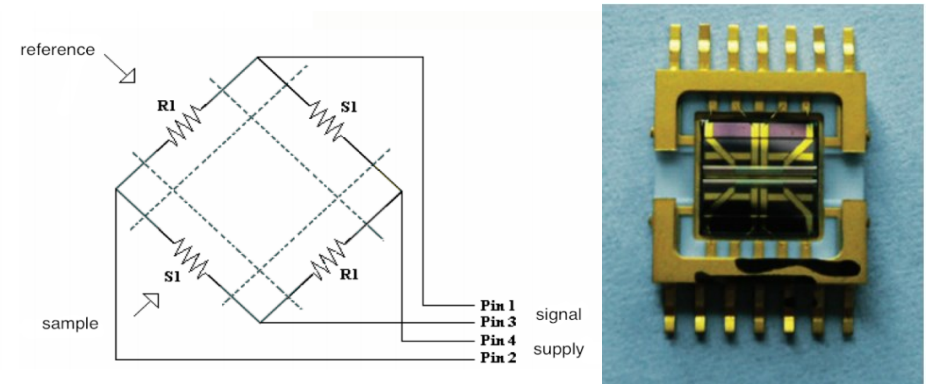

Figure 10 Wheatstone bridge scheme (left); universal detector based on Micro Electro-Mechanical System (MEMS) 10 times more sensitive than conventional Thermal Conductivity Detectors (right).

Once the chromatogram is obtained, it is processed offline. The voltage signal produced by the TCD is then proportional to the concentration of the analyte: the dynamic response starts from few ppm to 100%, with a linear proportionality area-concentration in the range 0-20%, which flattens above the 20-30%. A proper calibration is needed to be able to compute the concentration value from the raw signal (measured in μV).

As concern μGCs installed at the LHC experiments, they are usually equipped with the following columns:

- **PPlotU**: Porous Layer Open Tubular column. Stationary phase is Divinylbenzene/Ethylen glycoldimethacrylate. It separates C_1 to C_4 hydrocarbons, CO_2, CH_4, H_2O, H_2S, SO_2, and N_2O.
- **MolSieve**: 5Å zeolite molecular sieve. It separates permanent and noble gases: Ne, H_2, O_2, Ar, N_2, CH_4, CO.

- **OV1:** made of 100% Polydimethylsiloxane, designed to separate hydrocarbons from C_4 to C_{12}, BTEX, and VOC.

An example of the chromatograms obtained for the LHC gaseous detectors is shown in Figure 11. Here the CMS CSC gas mixture chromatogram is reported: it was obtained with the PPU column, where the three gas mixture components, Ar/CO_2/CF_4, are well separated.

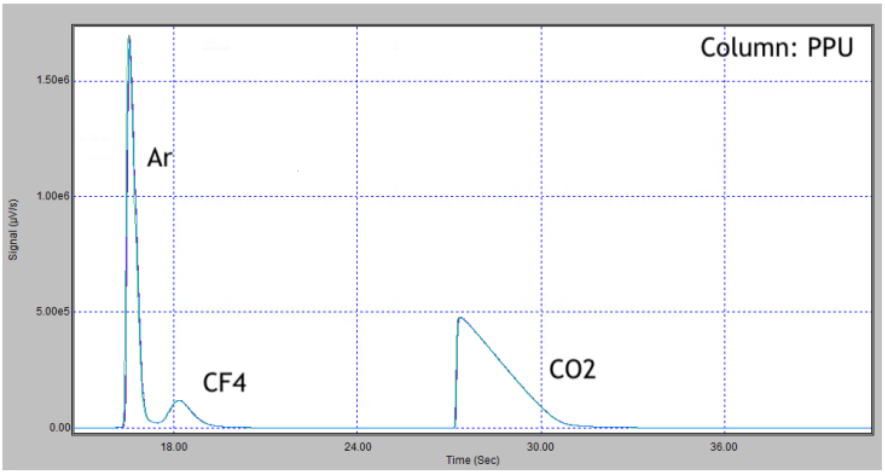

Figure 11 PPU chromatogram of the CMS CSC gas mixture.

Figure 12 presents the chromatograms obtained from the same gas mixture, analysed using the MolSieve 5A column. This column is typically employed to quantify oxygen and nitrogen, which are well separated into two distinct peaks. A noticeable difference can be observed between the chromatograms: the mixer line (purple) shows very low concentrations of O_2 and N_2 in parts per million (ppm), while the levels are higher in the Before Purifier line (green). After the purification process, the O_2 concentration decreases further in the After Purifier line (blue), attributed to the absorption capacity of the material within the module that targets oxygen.

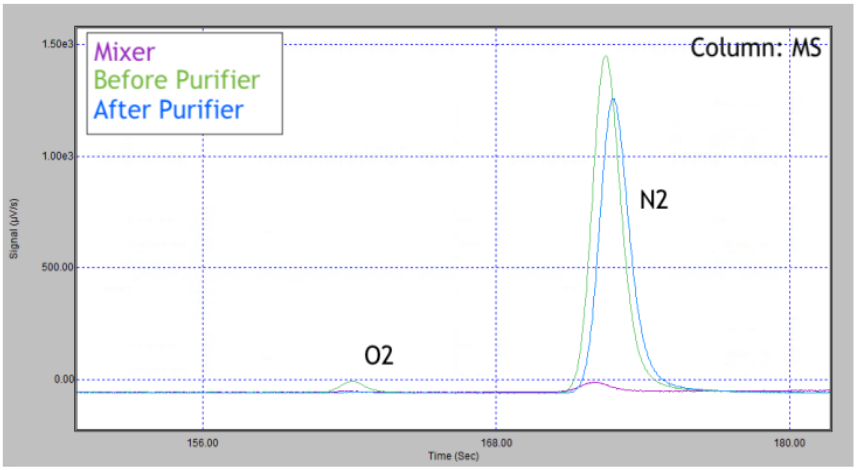

Figure 12 Comparison of three MolSieve 5A chromatograms of the CMS CSC gas mixture: Mixer, Before and After Purifier.

Finally, the Figure 13 reports the CF_4 calibration measurements realized for the CMS CSC gas mixture. The plot shows the trend of the conversion factor with respect to the nominal CF_4 concentration (5% - 100%). The trend is approximately linear up to 10% of CF_4, but then the curve slope progressively decreases. It is therefore fundamental to have a calibration with a reference mixture in which the concentration of the relevant component is as close as possible to the one of the sample mixtures, to avoid inaccuracies in the concentration calculation.

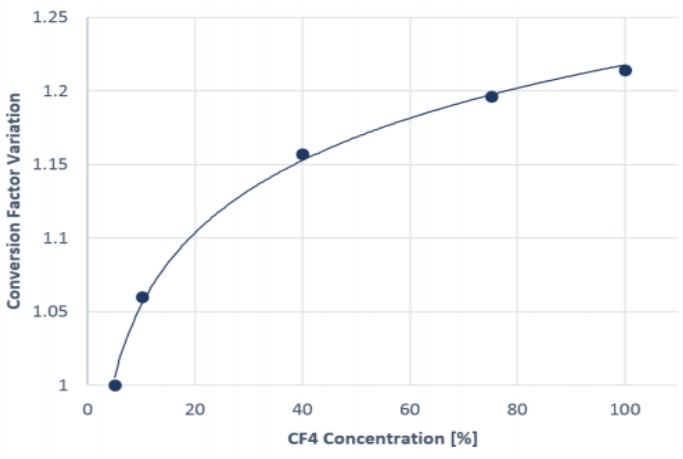

Figure 13 Example of CF_4 calibration curve, obtained analysing mixture with known concentration of CF_4 [12].

1.5.1.1 Biweekly µGC analysis of CMS and LHCb detectors' gas mixtures

The LHC gaseous detectors work with different gas mixtures depending on the purpose and on the geometry of the detector. Some of them use a single pure gas while others need mixtures with up to four components.

Due to the complexity of the gas systems and the sensitivity of the detectors to impurities accumulated in the gas mixtures, the monitoring of their quality and the stability is fundamental for the detector's operation. Even though all the four main LHC experiments use gaseous detectors, only CMS and LHCb decided to install a µGC to carefully monitor the status of the gas mixtures. The schema of the setups is shown in Figure 14.

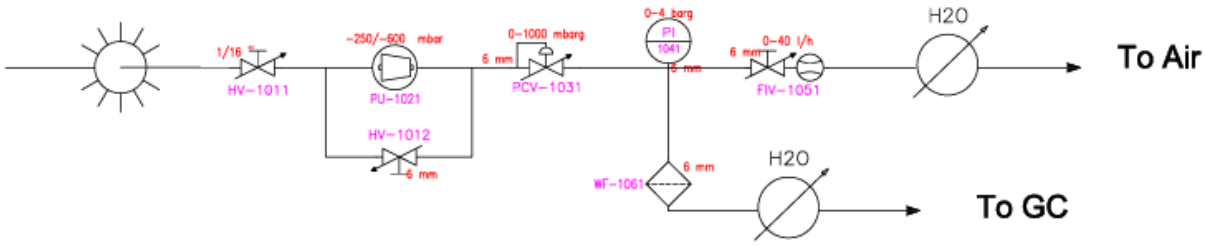

Figure 14 General P&ID of the µGC setups installed at the CMS and LHCb Experiments.

The gas mixtures used in these experiments are summarized in Table 1.

Detector	Gas
LHCb RI1	C4F10
LHCb RI2	CO2/CF4
LHCb MWPC	CO2/CF4/Ar
CMS CSC	CO2/CF4/Ar
CMS GEM	CO2/Ar
CMS DT	CO2/Ar
CMS RPC	C2H2F4/iC4H10/SF6

Table 1 Gas mixtures used in gaseous detectors at the CMS and LHCb Experiments.

Analyses are usually performed at different sampling points of the gas systems, such as:

- Mixer Module
- Exhaust module
- Before and After Purifier
- Exhaust to Distribution module

Moreover, μGC plays a key role to monitor the status of the detectors in presence of recovery systems. All the gas systems are designed to have an analysis module for monitoring the content of water and oxygen in the gas mixtures. For the detectors working with flammable gas mixtures also a dedicated IR analyser is installed in the analysis rack. Each module is equipped with pneumatic valves fully controlled by software which open daily or weekly, based on the expected contamination level of the gas.

μGC analyses are performed every two weeks in CMS and LHCb for all the gaseous detectors. The list of the lines usually analysed are summarized in the Table 2.

Detector	Mixer	Exhaust To Distribution	After Purifier
CMS CSC	X	X	
CMS GEM	X		
CMS DT	X	X	
CMS RPC	X	X	X
LHCb RI1			X
LHCb RI2			X
LHCb MWPC	X	X	X

Table 2 Summary of the modules analysed for each gaseous detector at the CMS and LHCb Experiments.

For the LHCb RICH detectors, the mixer lines are not analysed because the module does not inject continuously, but only to compensate the oscillations of atmospheric pressure. The gas from the purifiers is analysed either when monitoring the performance of the module is necessary or when a drastic reduction in oxygen or water in the gas mixture is required.

Each gas mixture is analysed using different μGC methods that differ on temperature and pressure values, especially for the PPU column used to quantify Ar, CO_2, CF_4, SF_6, $C_2H_2F_4$, iC_4H_{10} and C_4F_{10}. Each molecule has a different retention time due to different affinity with the column's coating material. For this purpose, tuning the temperature and the pressure of the run, allows to

well separate all the compounds of the gas mixture. Some examples of the analysis methods are reported in Figure 15 and Figure 16.

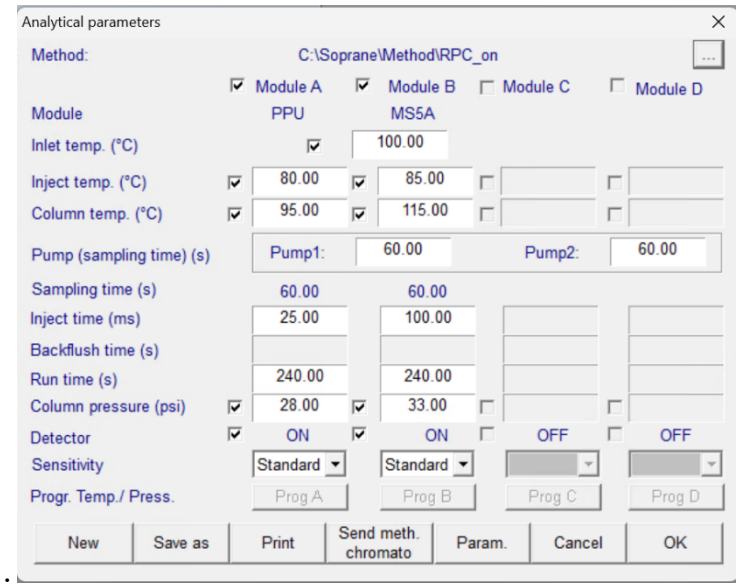

Figure 15 µGC method used for the analysis of the RPC gas mixture in CMS.

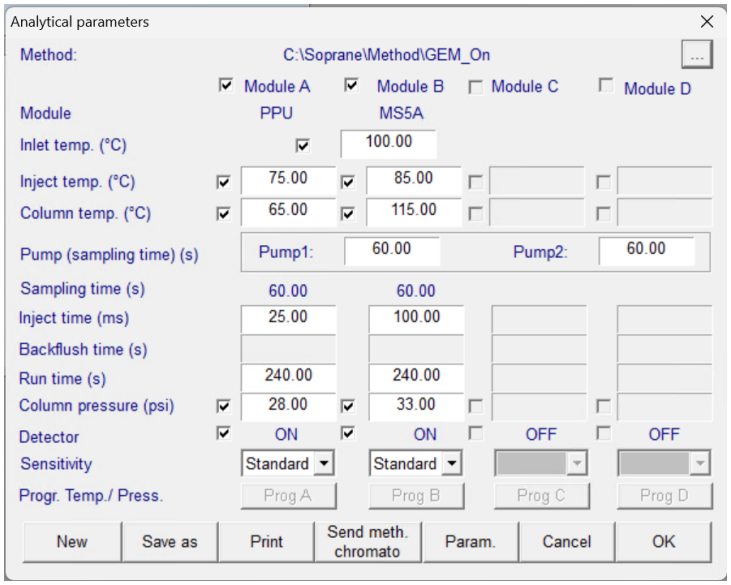

Figure 16 µGC method used for the analysis of the GEM gas mixture in CMS.

Even though the software is able to perform automatic integration, it is necessary to verify the results because even a small shift in the retention time may alter the integration outcomes. Then, the analyses are published in the CERN network to allow everyone to check the status of the gas mixtures for each detector. Thanks to the regular monitoring it is possible to follow the trend of contaminants and to spot possible problems in the gas system or in the detectors.

1.5.2 GC/MS

Gas chromatography-mass spectrometry (GC-MS) is a coupled method used to identify and quantify various substances within a test sample. In this process, molecules in the sample are retained by a column and then eluted at different retention times. This allows the mass spectrometer to separately capture, ionize, accelerate, deflect, and detect the ionized molecules. The mass spectrometer achieves this by breaking each molecule into ionized fragments and detecting these fragments based on their mass-to-charge ratio. A schematic view of this instrument is shown in Figure 17.

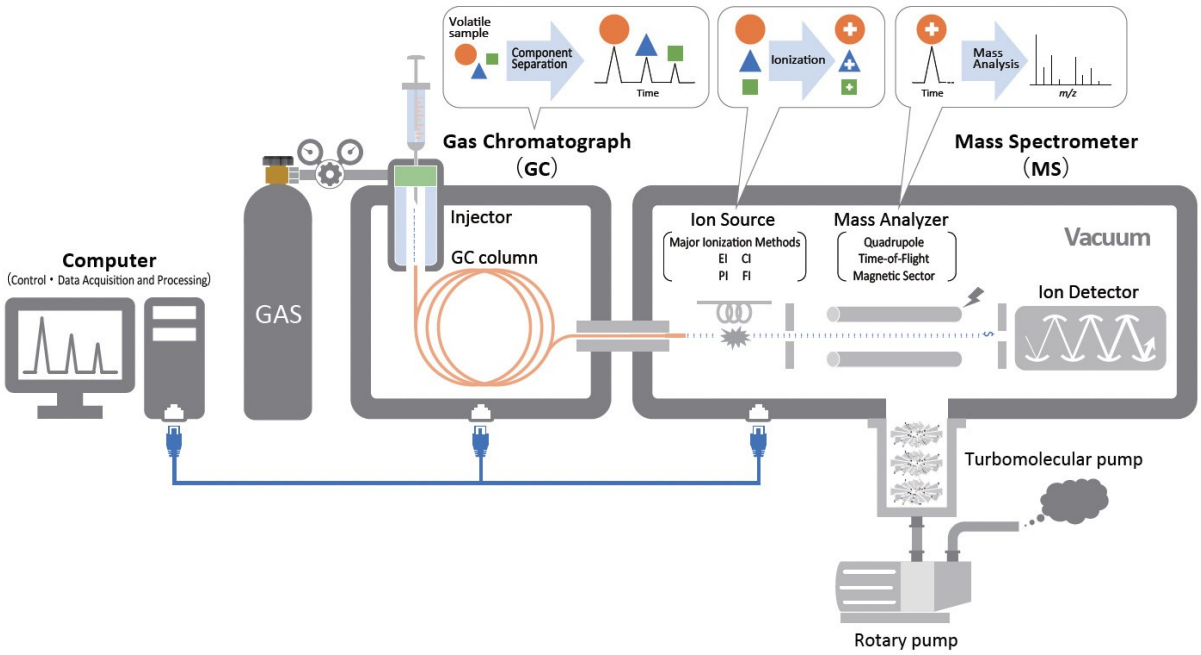

Figure 17 Scheme of a GC/MS instrument [13].

The combined use of these two components enables a significantly finer level of substance identification compared to using each unit separately. Neither gas chromatography nor mass spectrometry alone can provide an identification of a specific molecule. The mass spectrometry process generally necessitates a highly pure sample, while gas chromatography using a conventional detector such as a Flame Ionization Detector is unable to distinguish between multiple molecules that share the same retention time, resulting in their co-elution. Additionally, two different molecules may exhibit a similar mass spectrum. By integrating both processes, the likelihood of error is reduced, as it is highly improbable for two different molecules to behave identically in both a gas chromatograph and a mass spectrometer. Consequently, when a characteristic identifying mass spectrum is observed at a specific retention time in a GC-MS analysis, it significantly enhances the confidence that the analyte of interest is present in the sample.

In the MS, the fragments are detected using an electron multiplier, which produces an electrical signal. The mass spectrometer uses electron ionization, bombarding the molecules with free electrons, resulting in characteristic fragmentation. This technique creates fragments with low mass-to-charge ratio and is typically done using 70 eV electron energy.

The mass spectrometer used by our group at CERN, shown in Figure 18, employs a quadrupole as an analyser. The quadrupole consists of four parallel metal rods, with each opposing rod pair being electrically connected. A radio frequency (RF) voltage with a DC offset voltage is applied between one pair of rods and the other. Ions travel down the quadrupole between the rods. Only ions of a specific mass-to-charge ratio will reach the detector for a given voltage ratio; other ions will have unstable trajectories and will collide with the rods. This enables the selection of an ion with a particular m/z or allows the operator to scan for a range of m/z values by continuously varying the applied voltage.

Figure 18 Agilent MSD 5975 coupled with a µGC R3000 used to perform analyses during this PhD project.

1.5.3 Fluoride ISE

Ion Selective Electrode is a sensor for the potentiometric determination of ionic species and one of the most frequently used devices. In general, ISEs are electrochemical semi-cells consisting of an ion-selective membrane (i.e. a selective interphase for the ion in question), one internal solution of constant concentration of the analyte and an internal reference electrode. These electrodes allow selective and specific determination of the free ion activity. The ion activity can be expressed by:

$$\alpha_i = \gamma_i \times C_i$$

where γ_i is the activity coefficient of the specific ion and C_i its concentration in the solution. The whole electrochemical cell is obtained by coupling the ISE to an external reference electrode maintaining contact between the two half-cells by a salt bridge. The membrane potential results from the composition of two potential differences originating at each interface ‘’membrane/internal solution’’ and ‘’membrane/external solution’’. So the potential measured by the ISE electrode is that developed through the membrane (E_m):

$$E_m = E_e - E_i = \frac{RT}{nF} \times ln\frac{\alpha_{Ie}}{\alpha_{Ii}} = \frac{0.059}{n} \times ln\frac{\alpha_{Ie}}{\alpha_{Ii}}$$

Where:

- R: universal gas constant, R = 8.314482 $JK^{-1}mol^{-1}$

- T: temperature in Kelvin
- a: the activity of species involved
- F: faraday constant, the number of coulombs per mole of electrons, $F=9.648\times10^{4}Cmol^{-1}$
- N: ion charge

Since the concentration of the generic ion ''I'' of the internal filling solution is constant, the potential of the cell is given by:

$$E_{cell} = L' + \frac{0.059}{n} \times \log[I]_e$$

where L' is a constant that includes the logarithmic term of activity of the filling solution, the activity coefficients, the potentials of the reference electrodes, the potential of liquid junction and membrane asymmetry potential.

When compared to other analytical techniques, ion-selective electrodes show many advantages, such as cheapness, ease-of-use, durability, accuracy (± 2 - 3%), versatility in terms of use.

A Fluoride Ion Selective Electrode is a common device used to detect fluoride in aqueous solutions. Two different types of electrodes are presented in Figure 19. The first type, known as separated electrodes, consists of a reference electrode and an indicator electrode housed in separate cases. In contrast, the second type, called combined electrodes, has both the reference and indicator electrodes integrated into a single case.

Silver/silver chloride electrode is the most used and common reference electrode: it consists of a cylindrical glass containing 4 M solution of KCl saturated with AgCl. Half-cell can be written as follow:

$$Ag \mid AgCl\ (s), KCl\ (s) \mid\mid$$

Electrode's redox is:

$$AgCl_s + e^- \leftrightarrow\ Ag_s + Cl^-$$

Electrode potential E^0 for this half-cell is +0.2046 V with respect Standard Hydrogen Electrode at 25°C.

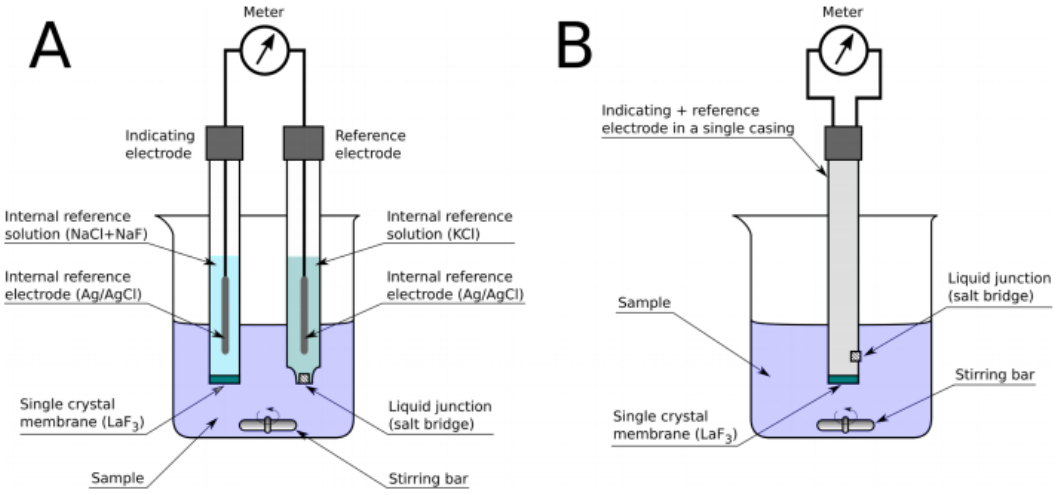

Figure 19 Scheme of a setup for ISE analysis using A) separated electrodes and B) combined electrode.

The indicator electrode consists of a solid state inorganic membrane of LaF_3 crystal placed into an epoxy body. Fluoride ions inside crystal lattice are mobile while lanthanum is in fixed positions, and the only one acceptable ion for these vacancies is fluoride because its compatibility in term of shape, size and charge. That's the reason why LaF_3 membrane is highly selective for fluoride ions. The internal part of the electrode is filled with a reference solution containing a note concentration of fluoride ions. At the two interfaces (membrane/ internal solution and membrane/ external solution) ionization creates a charge on the membrane according to the dissociation:

$$LaF_3 \leftrightarrow LaF_2^+ + F^-$$

The amount of charge depends on the concentration of F^- ions in ''test solution'' (the side of the membrane in contact with the solution at a lower concentration is positively charged compared to the other side).

This creates a potential across the membrane E_m:

$$E_{cell} = E_m - E_{rif} = L' - 0.059 \times \log[F]^-$$

Fluoride Ion Selective Electrode are influenced by the presence of other ions in the solution. TISAB (Total Ionic Strength Adjustment Buffer) is added to samples and standards in order to solve these problems. Hydroxide ion (OH-) is the only interfering anion. In fact, the following reaction can be carried out at pH values > 8 at the membrane surface:

$$LaF_3 + 3OH^- \leftrightarrow La(OH)_3 + 3F^-$$

Then a layer of $La(OH)_3$ is formed at the surface (as it has a solubility similar to LaF_3) compromising the measure. Even H^+ ions can create problems, in fact at acidic pH HF is formed and, by lowering the pH, the concentration of F decreases and this will lead to an increase in potential. Another interference is determined by the presence of polyvalent cations such as Fe^{3+}, Al^{3+}, that can complex F^- reducing the concentration of the free ion in solution thus altering the electrochemical response. Among the most used buffers TISAB is a solution containing both pH buffer and ionic strength that a complexing agent for cations (generally CDTA = 1.2-cyclohexylene-dinitrilo-tetraacetic acid).

1.5.4 Vacuum-UV and UV-Vis

1.5.4.1 VUV

The wavelengths below the Ultraviolet is called Vacuum Ultraviolet (VUV).

The VUV regions are surrounded by "above" the ultraviolet (UV) spectral region (from 200 nm) and the long wavelength side of the Hard X-Ray region below (around 1 nm) (Figure 20).

Three main regions make up the Vacuum Ultraviolet domain:

- The Far Ultraviolet (FUV): 200-120 nm
- The Extreme Ultraviolet (EUV): 120-10 nm
- The Soft X-Rays (Soft X): 15-0.2 nm

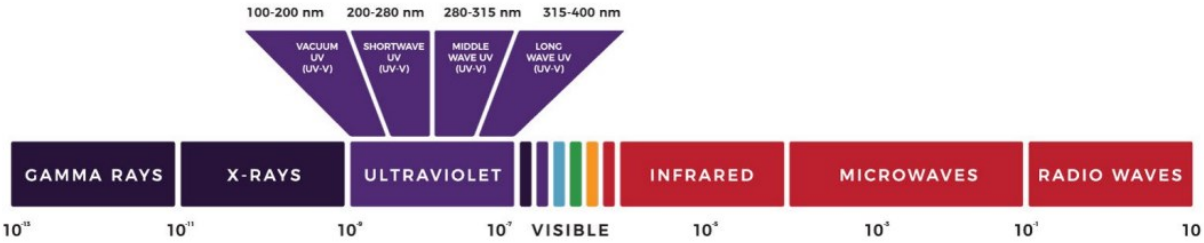

Figure 20 Electromagnetic spectrum.

In the last decades VUV has been widely used for the identification of chemical compounds in the field of analytical chemistry, often coupled with a gas chromatograph. High energy and short wavelength VUV induce electronic transitions in most chemical bonds including σ →σ* and π→π*, which provide for unique spectral fingerprints, as shown in Figure 21. Thanks to these transitions it is possible to unambiguously identify compounds, even positional isomers.

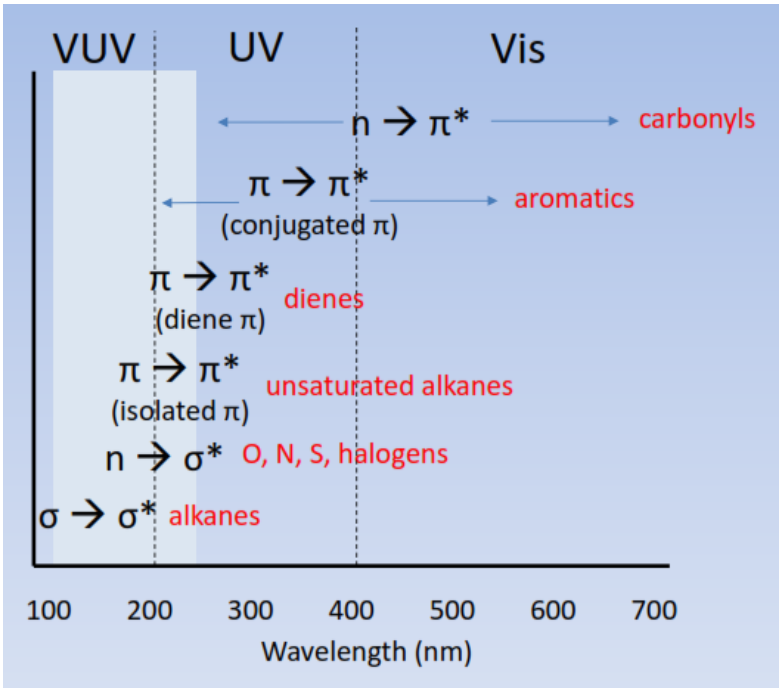

Figure 21 Typical electron transitions in the wavelength range between 100 and 700 nm.

VUV photon detection increasingly displays also a prospect in the field of space science, basic science (high-energy physics, physical chemistry, spectral physics, etc.), electronic industry, biomedicine, environmental protection, etc.

Light sources in VUV

- Synchrotron: The synchrotron radiation facilities provide intense continuum radiation from the microwave (harmonics of the driving RF field) to X-Ray spectral regions, emitted by high-energy electrons that are centripetally accelerated in the magnetic fields of a storage ring. Their beams are polarized and quasi-collimated.
- Free Electron Laser (FEL); A FEL is the fourth generation of synchrotron. It is a kind of laser using electrons accelerated up to the speed of light and then crossing a very long undulator (linear array made with magnets). Due to the alternation of polarities of the magnets, the electron path becomes sinusoidal. This effect produces an emission of radiation.
- Laser Produced Plasmas (LPP): When the output of a high-power pulsed laser is focused onto target materials, particularly the rare earths and neighbouring metals on the periodic table, a short-lived (nanosecond), high-temperature (50~100 eV), high-density (~1021 cm^{-3}) plasma is created. It generates a strong VUV quasi-continuum that is most intense in the 4 to 30 nm region, but often extend to about 180 nm.
- Others: Several VUV light sources emit VUV lines and/or continuum radiations. They are based on gas discharges, high-pressure arcs, low-pressure and vacuum sparks:
    - H_2 and D_2 Discharges: 115~350 nm, bulb material dependent.
    - Ar mini-Arc: from near UV to approximately 115 nm.
    - Inert Gas Discharges: Plasma discharges generated through He, Ar, Kr, and Xe cover mainly the 20 to 700 nm region. Some available designs are Penning, pumped hollow cathode, Capillary Plasma or Damany source.

Detector

The principles of the VUV detectors are those used for the visible and infrared detections – surface photoemission and electron-hole pair creation in semiconducting materials. But most of the time, VUV detectors should operate in an evacuated environment, especially when EUV or

Hard X-Ray radiations have to be detected. For this purpose, photodiodes or photomultipliers are usually used.

1.5.4.2 UV-Vis

Ultraviolet-visible (UV-Vis) spectrophotometry is used to quantify and qualify samples by the means of UV and visible light (mainly 200 to 900 nm). A single xenon lamp is commonly used as a high intensity light source for both UV and visible ranges. For instruments employing two lamps, a tungsten or halogen lamp is commonly used for visible light, whilst a deuterium lamp is the common source of UV light. As two different light sources are needed to scan both the UV and visible wavelengths, the light source in the instrument must switch during measurement, usually between 300 and 350 nm where the light emission is similar from both light sources and the transition can be made more smoothly. Monochromators are used to separate light into a narrow band of wavelengths, which then passes through a sample.

For all analyses, measuring a reference (or blank) sample, such as a cuvette filled with a similar solvent used to prepare the sample, is imperative. If an aqueous buffered solution containing the sample is used for measurements, then the aqueous buffered solution without the substance of interest is used as the reference. It is important to be aware of the materials and conditions used in UV-Vis spectroscopy experiments: most plastic cuvettes are inappropriate for UV absorption studies because plastic generally absorbs UV light; glass can act as a filter, often absorbing the majority of UVC (100-280 nm) and UVB (280-315 nm) but allowing some UVA (315-400 nm) to pass through. Therefore, quartz sample holders are required for UV examination because quartz is transparent to the majority of UV light.

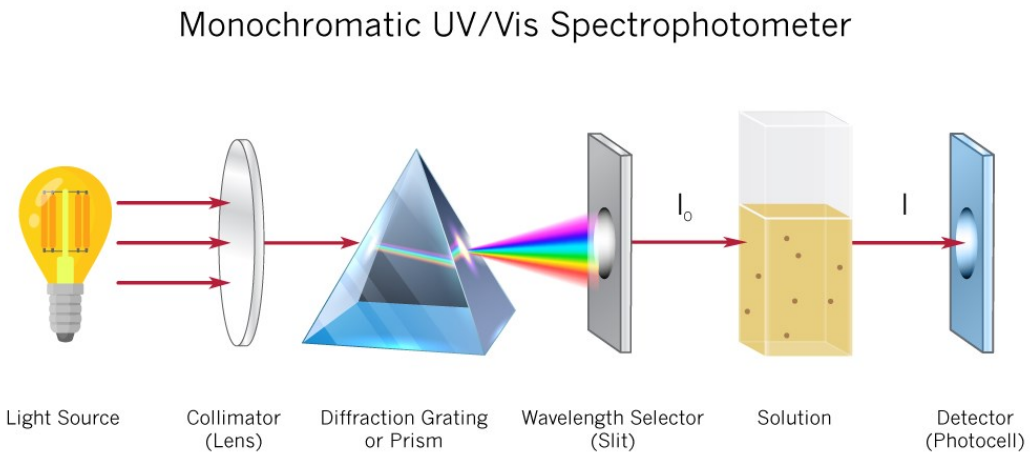

Figure 22 Working principle of UV-Vis spectrometer.

Based on the UV-Vis spectrophotometer, the intensity of light can be reasonably expected to be quantitatively related to the amount of light absorbed by the sample. The absorbance (*A*) is equal to the logarithm of a fraction involving the intensity of light before passing through the sample (I_o) divided by the intensity of light after passing through the sample (*I*). The fraction I divided by I_o is also called transmittance (*T*), which expresses how much light has passed through a sample. However, Beer–Lambert's law is often applied to obtain the concentration of the sample (*c*) after measuring the absorbance (*A*) when the molar absorptivity (ε) and the path length (*L*) are known. Typically, ε is expressed with units of L $mol^{-1}cm^{-1}$, *L* has units of cm, and *c* is expressed with units of mol L^{-1}. As a consequence, *A* has no units.

Beer–Lambert's law is especially useful for obtaining the concentration of a substance if a linear relationship exists using a measured set of standard solutions containing the same substance:

$$A = \varepsilon\, L\, C = log_{10}\left(\frac{I_0}{I}\right) = log_{10}\left(\frac{1}{T}\right) = -log_{10}(T)$$

Chapter 2
“Greenhouse Gases and their use at CERN”

2.1 Greenhouse Gases and Global Warming Potential

A Greenhouse gas (GHG) is defined as a gas that, when in atmosphere, absorbs and emits radiation within the thermal infrared range [12]. A measure of how much heat a GHG traps in the atmosphere in a fixed time span is called Global Warming Potential (GWP) index. The GWP defines how much energy the emission of 1×10^3 kg of a gas would absorb over a period of time, relative to the emission of 1×10^3 kg of CO_2. The GWP index strongly depends on his radiation absorption spectrum in the infrared (radiative activity), on lifetime of the gas in the atmosphere and on the possible high-GWP byproduct of the compound. Carbon dioxide, methane, water vapor and nitrous oxide are the most powerful long lived greenhouse gases in the atmosphere.

GHGs occur naturally in the Earth’s atmosphere, but human activities, such as the burning of fossil fuels, contribute to increase their levels, causing global warming and climate change.

The effect of each greenhouse gas on Earth’s climate depends on its chemical nature and its relative abundance in the atmosphere. As shown in Table 3, some gases have a high capacity of absorbing infrared radiation, whereas others have considerably lower capacities for absorption.

“Carbon dioxide equivalent” or “CO_2e” is a term for describing different greenhouse gases in a common unit. For any quantity and type of greenhouse gas, CO_2e signifies the amount of CO_2 which would have the equivalent global warming impact. The GWP of a gas strongly depends both on its radiation absorption in the infrared spectra (also known as radiative activity) and on the atmospheric lifetime of the gas. In particular, hydrofluorocarbons (HFCs) and hydrochlorofluorocarbons (HCFCs) are called high-GWP gases because, for a given amount of mass, they trap substantially more heat than CO_2. Since there are no significant natural sources of these compounds, they were not present in the preindustrial atmosphere and their presence in the contemporary air reflects emissions associated with industrial activities.

Their high heat-absorption capacity is due to the carbon-halogen bonds (e.g. C-F, C-Cl, C-Br), able to strongly absorb at infrared wavelengths. The effectiveness of these compounds as GHGs depends on both:

1) number of C-X (where X is the halogen atom) bonds in the molecules.
2) atmospheric lifetime of the molecule.

In addition to HFC and HCFC, sulphur hexafluoride (SF_6) is one of the most harmful greenhouse gases known so far. It has an intense absorption at 10.3 μm in the atmospheric window region and a long atmospheric lifetime of 3200 years. Fluorites minerals are a natural source of this compound that is present in a small amount, resulting in a natural background concentration of 0.01 ppt. As a result of anthropogenic emissions the current level of SF_6 in the atmosphere is 400 times higher than the natural background, with an increasing rate of 0.2 ppt/year.

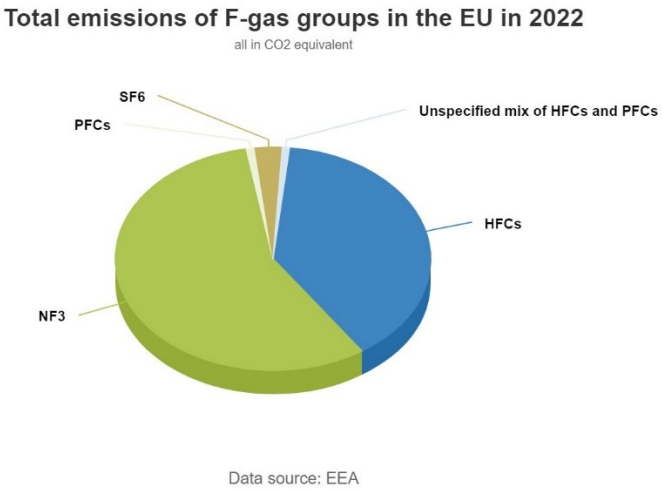

Figure 23 Total emissions of F^- gas groups in the EU in 2022: NF_3 88.51, HFCs 60.41, SF_6 4.31, PFCs 1.39, Unspecified Mix of HFCs & PFCs 1.13.

Due to their harmfulness, the use of fluorinated compounds has been regulated worldwide. The Kyoto Protocol was adopted as the first addition to the United Nations Framework Convention on Climate Change (UNFCCC), an international treaty that committed its signatories to develop national programs to reduce their emissions of greenhouse gases, and the GHGs controlled under the treaty are shown in Table 1 below. Often these GHGs are referred to as the "Kyoto gases".

	Greenhouse Gas	Global Warming Potential (GWP)
1.	Carbon dioxide (CO_2)	1
2.	Methane (CH_4)	25
3.	Nitrous oxide(N_2O)	298
4.	Hydrofluorocarbons (HFCs)	124 – 14,800
5.	Perfluorocarbons (PFCs)	7,390 – 12,200
6.	Sulfur hexafluoride (SF_6)	22,800
7.	Nitrogen trifluoride (NF_3)[3]	17,200

Table 3. List of Kyoto Gases.

As concerns the EU, since 2015, it has been very efficient in reducing F^- gas emissions thanks to the 2014 F^- gas Regulation.

The regulation mentioned above introduced a quota system to phase down the most common F^- gases, saturated HFCs with a Global Warming Potential several orders of magnitude higher than carbon dioxide, in favour of low-GWP unsaturated HFCs, otherwise known as hydrofluoroolefin (HFOs).

In 2024, only one-third of the 2015 amount of HFCs was placed on the EU market. In addition to this quota system, the EU has implemented complementary measures to lower the leakage of F^- gases, encourage the switch to climate-friendly alternative substances, and stimulate innovation and the development of green technologies.

With the rules established by the new F^- gas Regulation, HFCs sold on the EU market should be zero by 2050. This goal serves the EU's objective of achieving climate neutrality by that year. The key measures of the new F^- gas Regulation are summarized in Figure 24.

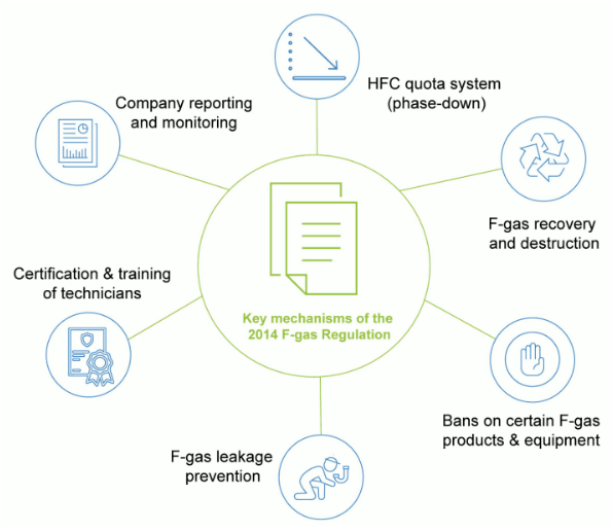

Figure 24 Key points of the 2014 F- gas Regulation.

1. *Reducing hydrofluorocarbons* → The quota system generates a steeper reduction in the amounts that importers and producers may place on the EU market, and in 2050, HFCs will be phased out in the EU.
2. *Expanding the quota system* → HFCs used in metered dose inhalers have been integrated into the quota system. Additional prohibitions on F-gas equipment, products and use of F-gases will apply in the future.
3. *Stricter rules to prevent emissions* → The Regulation covers additional equipment and gases, expanding measures to prevent leakage during transportation, installation, servicing, and disposal of equipment and products.
4. *Facilitating better monitoring* → More digitalization and electronic automation of custom control will allow enhanced enforcement and monitoring in the Member States and combat illegal trade.
5. *Capping EU production of HFCs* → Starting in 2025, producers will receive rights equivalent to 60% of their average annual production from 2011 to 2013. This rate will decline to 15% by 2036.
6. *Certification and training* → Individuals working with these gases were professionally trained. This included certifying technical personnel and companies involved in installing,

servicing, and maintaining F-gases, ensuring that the equipment was managed safely and efficiently [14].

2.2 Decomposition processes of fluorinated compounds

Another issue with the use of fluorinated compounds is the radicalization and breakdown processes which can lead to the formation of equally polluting compounds or, in the worst case, to compounds with GWP even higher than the original ones.

The two main atmospheric pathways are described below.

Photolysis:

HFCs can absorb UV radiation from the sun, which causes the molecules to break down. This process primarily affects HFCs in the upper atmosphere, where UV radiation is more intense and less shielded. The absorption of UV radiation leads to the formation of radicals, which are highly reactive species that can further participate in chemical reactions, e.g. formation of HF (Figure 25).

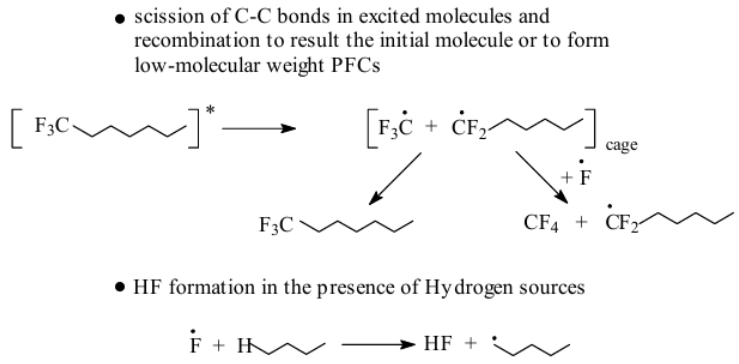

Figure 25 Possible pathway for the formation of HF starting from fluorinated compounds.

Reaction with Hydroxyl Radicals (OH):

The primary sink for HFCs in the atmosphere is their reaction with hydroxyl radicals (OH) in the troposphere. The reaction with OH radicals initiates the breakdown of HFC molecules, leading to the formation of other chemical species. This reaction typically produces a series of intermediate

compounds, such as peroxy-radicals (RO_2) and hydroperoxyl-radicals (HO_2), which further react to produce carbon dioxide (CO_2), water (H_2O), and other stable end-products (Figure 26).

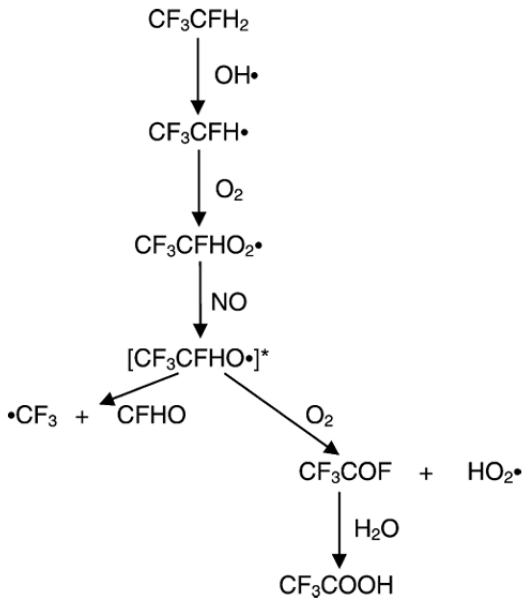

Figure 26 Degradation pathway of HFC after reaction with OH specie.

The final product of many HFCs and HFOs is the trifluoroacetic acid (TFA),as shown in Figure 26 and Figure 27. The formation and accumulation of this compound in the environment raise several concerns, such as:

- *environmental persistence* (some decades) due to its high resistance to further chemical degradation thanks to the presence of strong carbon-fluorine bonds.
- *water solubility* which allows it to be transported easily through the hydrological cycle.
- *potential toxicity* since some studies have indicated that TFA can have adverse effects on certain aquatic organisms, particularly at higher concentrations.

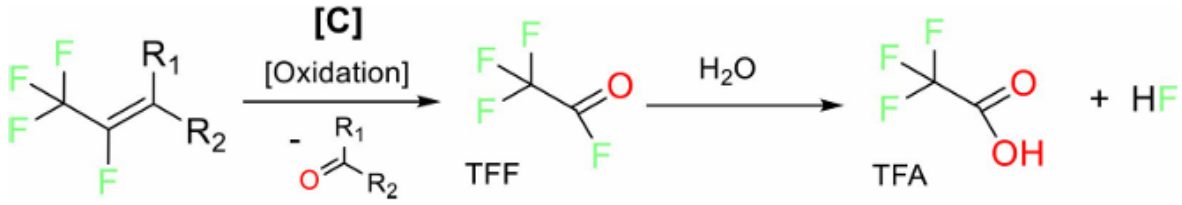

Figure 27 HFO molecules leading to TFA through atmospheric oxidation and hydrolysis [15].

Although HFCs do not directly deplete the ozone layer, their breakdown products can influence stratospheric chemistry, potentially affecting the concentrations of other compounds involved in ozone depletion, e.g. HFC-23 [15].

2.3 Use of GHGs at the LHC facilities

Over the 4 experiments (ALICE, ATLAS, CMS and LHCb) taking data at the CERN Large Hadron Collider (LHC) more than 28 gas systems are delivering the proper gas mixture to the corresponding detectors. In some cases, the use of expensive and greenhouse gases cannot be avoided because of physics requirements that dictate specific choices in the gas mixture, as shown in Table 4.

Gas	GWP	Experiment and detector type
C2H2F4	1430.0	ALICE RPC; ATLAS RPC; CMS RPC
SF6	22800.0	ALICE RPC; ATLAS RPC; CMS RPC
CF4	7300.0	CMS CSC; LHCb GEM, RICH2, MWPC
C4F10	9200.0	LHCb RICH1
iC4H10	3.3	ALICE RPC; ATLAS RPC; CMS RPC
nC5H12	11.0	ATLAS TGC

Table 4 Summary of GHGs used at the LHC Experiments and related GWP values.

If the detector type is considered, the RPC detectors are the main contributors due to leaks at detector level while CMS CSC, LHCb RICH 2 and LHCb MWPC account for about 20% of the total GHG emission, due to the use of CF_4.

Reducing the use of GHGs is a worldwide objective to which CERN wants to contribute. Thanks to the strategies adopted to reduce GHG emissions due to particle detection, the tCO_2e emitted at the beginning of LHC RUN3 have been decreased compared to those of LHC RUN2, as show in Figure 28.

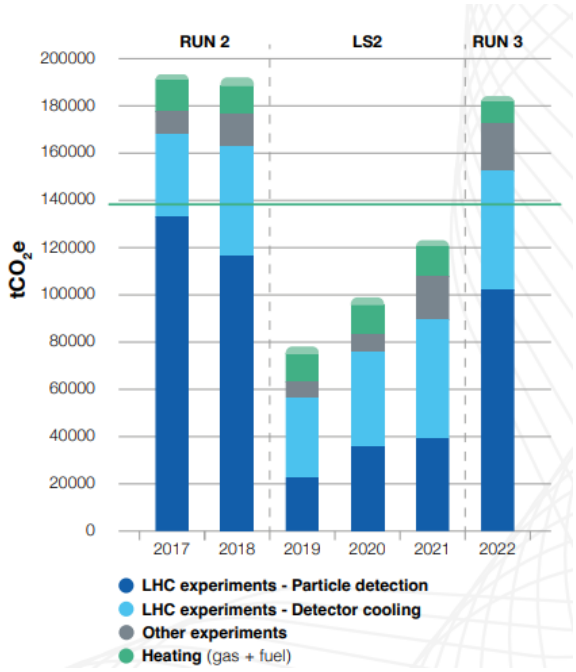

Figure 28 GHG emissions at CERN according to its last environmental report [16].

The plot displayed above illustrates the Organization's greenhouse gas (GHG) emissions in relation to their usage. The blue bars represent GHG emissions from the large LHC experiments, which increased with the gradual restart of the accelerator complex in 2021 and the launch of RUN3 of the LHC in mid-2022. Generally, this contribution is higher during the run periods because the experiments increase the flow rate of the detectors for data collection, which is paused during long shutdowns.

Several approach with different level of complexity can be adopted to control the gas consumption and emission. In particular, EP-DT-FS Gas group identified different categories or level of intervention, which will be described in the following [17].

2.4 CERN strategies to reduce its emissions of GHGs from particle detection

In a very basic gas system, the gas mixture is prepared, it is sent to the detector and is then vented to atmosphere. This type of gas system is characterized by easy-of-use and standard monitoring system is required. However, this approach is not sustainable due to the very high GHG emission to atmosphere.

Four different strategies have been identified to optimize the gas usage at CERN [16]:

- Gas recirculation systems
- Gas recuperation systems
- Search for new environmentally friendly gases for particle detectors
- Plants for the disposal of greenhouse gases by decomposition in harmless compounds.

The first three approaches in the list will be briefly described and their application on LHC experiments will be explained while the last option, has been nowadays discarded. Indeed, systems for the disposal of GHG have been developed by industry, but GHGs are usually very stable compounds hence very difficult to treat. This option would come with significant infrastructure costs and complexity, and it would also fail to address the issue of GHGs unavailability and price increases.

- ***Gas recirculation system***

In the initial phases design of LHC gas systems, the possibility of re-using the gas mixture multiple times was considered in case of large detector volumes or usage of expensive gases, in order to limit their consumption. When a gas system is operated in recirculation mode, the gas mixture is collected after being used in the detector, passed through the Purifier module to undergo purification processes, and re-injected in the system (Figure 29). The maximum recirculation rate, usually between 85% and 99%, is determined by detector leak or impurities levels that cannot be filtered (i.e. N_2).

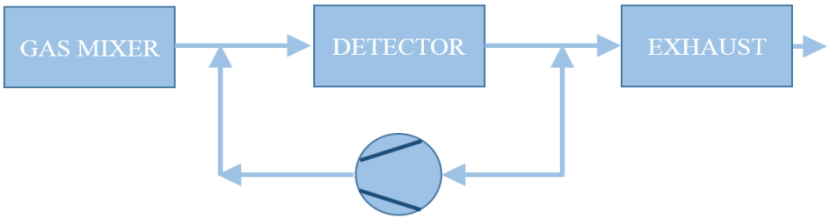

Figure 29 Schematic view of the gas recirculation system.

The advantage of using this gas system is the drastic reduction of gas consumption since the fraction of recirculated gas can be above the 99%.

During the LHC RUN1, the total gas emission from gas recirculation systems accounts for about 85% of the total CO_2 equivalent. Gas recirculation systems allowed reducing operational costs and emissions by 90% or more (depending on the recirculation fraction). Given the high recirculation rate, only 10% of fresh gas had to be injected, reducing significantly both the gas consumption and overall emissions. Nevertheless, 75% of these emissions were due to leaks in the detectors and, therefore, cannot be easily repaired [17].

Although it is mandatory to employ gas recirculation systems when GHGs are used, the disadvantages of these systems stem for their complexity. A constant monitoring of the mixture composition and of the presence of impurities is mandatory. Additionally the detector pressure regulation and the gas system in general are much more complex with respect to a basic open mode gas system.

- ***Gas recuperation system***

When pollutant gases with very high GWPs are used, the recirculation systems are not enough to limit the GHG emissions. For CMS-CSC, CMS-RPC, LHCb-RICH1 and LHCb-RICH2, the gas mixture is recovered from the exhaust module of the gas system and sent to dedicated separation units able to extract selectively a mixture component (Figure 30). Thanks to this approach, it is possible to achieve a further reduction in gas emissions, but it introduces a second level of complexity in addition to the gas recirculation system; due to the uncommon gas mixture

composition used at CERN, which makes it a unique case study, this step requires a dedicated R&D work, targeted on the specific component to separate.

For example, CMS-CSC muon detectors use a gas mixture of $Ar/CO_2/CF_4$ mixed in a ratio 40/50/10 and, despite the detector is tight, the gas mixture is contaminated by air due to gas diffusion mechanism. Whilst some contaminants, as H_2O or O_2, can be removed by the purifier modules, unfortunately N_2 cannot, and it tends to accumulate. In order to overcome this issue without compromising the gas mixture quality, a CF_4 recuperation plant has been developed. It is operational since June 2012 and contributed to further reduction in the GHG emission.

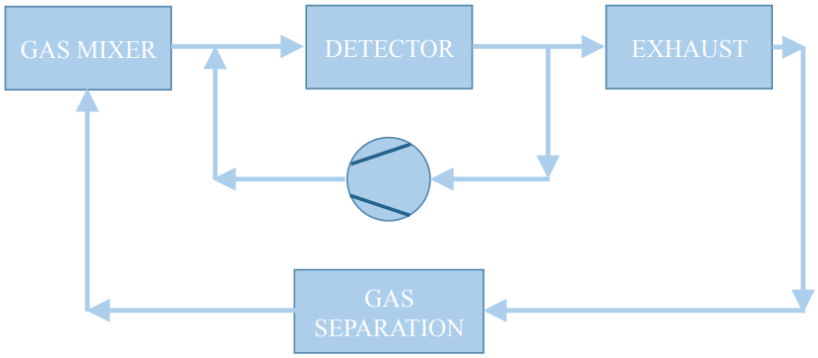

Figure 30 Schematic view of the gas recirculation system with the addition of recuperation system.

All the R&D activities on the LHC gas recuperation systems will be deeply discussed in the next chapter as they represent the main topic of this PhD project.

- ***Search for new environmentally friendly gases for particle detectors***

A third field of research is focused on the replacement of the current GHGs used in gaseous detectors. Due to the recent EU F^- gas regulation, the prices of GHGs could raise, thus possibly making gas detectors operation very costly. Environmentally friendly alternatives to R134a, SF_6 and CF_4, are being searched. In particular, as different compounds have been already developed in industry to replace R134a as refrigerant, these candidates are being looked into as possible replacements in the RPCs gas mixture. The aim is to find a new eco-friendly mixture that is able to reproduce the same detector performance as it is observed with the current gas mixture. Good

results have been obtained with the use of mixture containing HFO-1234ze ($C_3H_2F_4$), that is a hydrofluoroolefin with a GWP < 1 for 100-year time horizon, and a neutral gas.

A definitive solution is not still achieved, and further R&D studies will be needed.

Chapter 3
“LHC Gas Recuperation systems”

As shown in the previous chapters, some of the LHC gas detectors need to be filled with GHGs to properly operate. The first adopted strategy to reduce the emissions of these gases in the atmosphere, considering also the huge volume of gaseous detectors, was the gas recirculation, thanks to which a fraction between 80% and 98% is reinjected in the detectors after passing through one or more modules dedicated for the purification of the gas mixture. In most cases recirculating 100% of the gas is not reasonable due to the presence of impurities, such as nitrogen, that cannot be removed by physical separation processes. For this reason, many gaseous detectors are currently working at a recirculation fraction between 90% and 99%. For those working at 90%, the remaining 10% of the mixture is sent to the atmosphere after passing through the detector and the same amount of fresh gas mixture is continuously injected into the system to compensate the gas exhausted and the detector leaks. In some cases, more gas happens to be released into the atmosphere, for example during maintenance periods or for modifying the gas mixture composition.

To overcome this problem, some recovery systems were designed and installed at CERN for the recuperation of gas mixture component which contributes more to the GHGs emissions. The recuperation process is based on the extraction and purification of the fluorinated compound at high purity level from the detector gas mixture. The compound is then stored and reused in the gas system; this allows to decrease both emissions and consumption of fresh gas, and to overcome availability and increasing prices issues.

On the other side, recuperation plants added complexity to gas systems and need continuous monitoring of gas mixtures. Dedicated R&D studies are thus essential to optimize recuperation plants for the diverse gas mixtures used in LHC gaseous detectors. This thesis predominantly focuses on the recuperation of Tetrafluoromethane (CF_4 or R14), 1,1,1,2-Tetrafluoroethane ($C_2H_2F_4$ or R134a) and Perfluorobutane (C_4F_{10}), which have Global Warming Potentials of 7390, 1430 and 8860, respectively.

CF_4 is utilized in various LHC Experiment gaseous detectors for cleaning wires and preventing ageing and improving time resolution. Additionally, CF_4 is a major component in the gas mixture of a Ring Imaging CHerenkov (RICH) detector in the LHCb experiment due to its low dispersion

and refractive index. Despite operating with gas recirculation, the recuperation of CF_4 is a critical step to minimize its release into the atmosphere.

The chapter delves into the application of selective membranes for the isolation and recovery of CF_4 from gas mixtures. It delineates the utilization of this technique in the LHCb RICH2 detector and the CSC detectors system of the CMS Experiment to separate CF_4 from other gas components.

The LHCb RICH2 detector operates during physics runs with a gas mixture consisting of 92% CF_4 and 8% CO_2, filling a 100 m^3 detector volume. Emissions only occur during the purifier module's regeneration procedure and detector pressure adjusting. During the LHC LS2, a significant gas emission event was scheduled, due to filling the detector volume entirely with CO_2 for maintenance purposes. Afterward, the volume was to be refilled with a gas mixture of CF_4/CO_2 in a 92/8 ratio for the LHC RUN3. The RICH2 gas system originally included a separation membrane module for N_2 separation, then it was repurposed as a CF_4 recuperation plant during the LHC LS2. A brief overview on the characterization and optimization of the recuperation process carried out during the LS2 (2018-2021) when all CF_4 content was replaced by CO_2 is given in this chapter. Additionally, a detailed description of the plant and of the CF_4 filling procedure performed before RUN3 will be given.

The CMS CSC recovery system for the CF_4 involves the use of selective membranes in the first part of the recuperation process of the CF_4 too, this time from a gas mixture of $Ar/CF_4/CO_2$ in a ratio 40%/10%/50%. CSC gas system has a total volume of 90 m^3 and a total flow of 700 l/h are continuously injected to compensate the gas mixture exhausted to keep a stable N_2 concentration of 1% in the detectors. Recuperation system is operational since 2012 and it is made of four modules thanks to which the CF_4 is recovered with a purity of 90% and an efficiency of 70%. Significant progress was made starting in 2018 with the continuous reinjection of CF_4 into the system. Particularly, from 2021, it became possible to not only inject a 50/50 mix of fresh and recuperated CF_4, but also to increase the proportion of recuperated CF_4 to 70%. The quality check of recuperated CF_4 is performed via Gas Chromatograph and Single Wire Proportional Chambers (SWPCs) monitoring system.

$C_2H_2F_4$, to which we will often refer in this thesis with the name R134a, is used as main gas mixture component for Resistive Plate Chambers (RPCs) that are installed in three out of the four main LHC experiments, ALICE, ATLAS and CMS, and they are fundamental for their Muon Systems

since LHC RUN1. In each experiment, the R134a is used in combination with iC_4H_{10} and SF_6 and it represents at least the 90% of the mixture. The RPCs have a big volume between 8 and 13 m^3, depending on the experiment, and work at a recirculation fraction of around 90%.Given this information, it is easy to understand the importance of recovering R134a, a project that began research and development in 2019. The chapter will examine the design, operational principles, and advancements of the final R134a recovery plant installed at CMS in 2023. First, it will describe the characteristics of the R134a/iC_4H_{10} mixture, highlighting the significant challenges posed by the formation of a minimum boiling point azeotrope in its vapor-liquid phase transition; then it will show the tests performed which led to achieve a stable co-injection of the recovered R134a in a ratio 50/50 with the fresh one.

The last recovery system mentioned in this chapter concerns the molecule C_4F_{10}, which is used to fill the LHCb RICH1 detector. Unlike other detectors discussed earlier, RICH1 specifically works with pure perfluorobutane. However, due to the limited availability and high price of this gas, the detector is usually filled with C_4F_{10} just from February to October, according the LHC operation schedule. Afterward, it is emptied and refilled with pure CO_2 during the LHC's maintenance pauses to minimize the risk of gas loss in the LHCb cavern. Since the detector is permeable to water and air, a cleaning of the gas mixture is also carried out when the concentration of these compounds exceeds 1% of the total mixture. Filling, emptying, and cleaning are accomplished using the recovery system, which is based on a one-stage distillation process. In this process, the C_4F_{10} is condensed while air and CO_2 are removed. The separation process and the results obtained in the past three years will be further discussed.

3.1 Gas separation techniques for LHC recovery systems

Each recovery system installed at the LHC experiments required intense R&D activity and expertise in different topics, to deal with:

- the use of uncommon gas mixtures not employed in other industrial systems and the consequent lack of information in the literature
- the selection of separation processes that did not cause the formation of undesirable reaction by-products, in order not to contaminate the detectors
- the study of the costs and emissions of the plant in relation to the initial gas mixture

After evaluating all these factors, it was concluded that the most effective method for recovering CF_4 is to use selective membranes for separation, along with zeolites for pressure and temperature swing absorption (PSA and TSA) processes, especially for complex mixtures such as those found in the CSC. However, for separating R134a and C_4F_{10}, distillation was identified as the best method. Each separation technique will be described in more detail.

3.1.1 Selective membranes separation

Separating two substances that would normally mix requires energy and can be done using various methods and devices. Different techniques may require varying amounts of energy. Membrane processes, like reverse osmosis and electrodialysis, require less energy compared to processes involving phase transitions. Membrane technology offers continuous operation and scalability but may have limitations in terms of lifespan and scaling up the process and they can be classified based on their structure, such as their thickness, which determines their resistance to mass transfer.

When the feed inlet stream enters the module, its composition and flow rate change as it travels through the membrane due to interactions such as sorption, diffusivity, and kinetic diameter of the molecules. The feed is separated into permeate stream and retentate stream, as shown in Figure 31, with the retentate being the final product of interest in the case of CF_4 separation process in the CMS CSC and LHCb RICH2 recuperation systems.

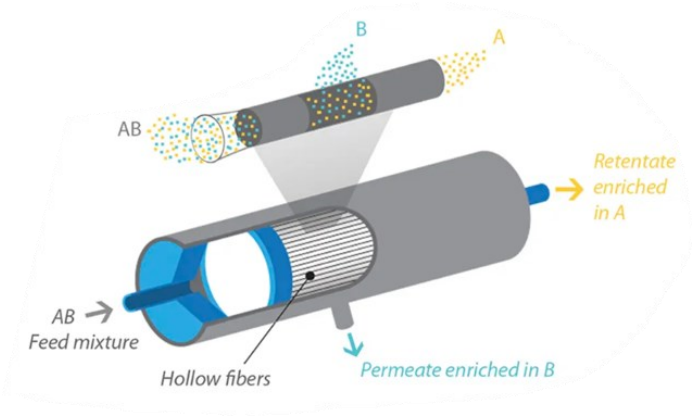

Figure 31 Working principle of a separation process using membranes.

Research in membrane technology focuses on developing new membranes that increase permeability and selectivity or enhance selectivity without compromising permeability. The driving force for gas separation is the partial pressure gradient, and the membrane itself is critical in determining the selectivity and flux.

Membranes are made from various polymers such as polycarbonates, polyimides, polyamides, polyetherimides, or polysulfones. Most membranes used for gas separation are non-porous and gas transport through these membranes is usually described by a solution-diffusion mechanism.

To understand the fundamentals of gas separation, factors related to the polymer's nature, such as chemical structure, must be considered. Two important parameters in this context are the glass transition temperature and the crystallinity. The glass transition temperature determines whether a polymer is in a glassy or rubbery state and is influenced by chain flexibility and chain interaction. Generally, rubbery materials (elastomers) have higher permeability while glassy polymers have higher selectivity. For example, elastomers exhibit high permeabilities and low selectivity for CO_2, whereas glassy polymers show much lower permeabilities but generally high selectivity.

The fundamental principle of gas separation relies on the permeability coefficient (P), which signifies a membrane's ability to allow gas molecules to pass through. This coefficient can be expressed using the equation:

$$P = Diffusivity\ (D) \times Solubility\ (S)$$

Solubility is a thermodynamic parameter that quantifies the amount of a substance absorbed by the membrane under equilibrium conditions, while diffusivity is influenced by the size of the gas molecules - larger molecules have lower diffusion coefficients.

The measurement of permeability coefficient is commonly expressed in Barrer units (1 Barrer equivalent to 10^{-10} $cm^3_{STP} \cdot cm \cdot cm^{-2} \cdot s^{-1} \cdot cmHg^{-1}$). It's important to note that gas solubility generally increases with higher gas condensability, such as critical temperature. For example, in most polymers, CO_2 exhibits higher solubility compared to CH_4, O_2, and N_2. The membrane selectivity, which represents the ability of a membrane to separate two molecules (A to B), is determined by their permeability ratio:

$$\alpha = {}^{P_A}/_{P_B}$$

Additionally, the selectivity for a binary gas mixture can be calculated using the molar concentration of the two gases in feed and permeate:

$$\alpha = {}^{y\,(1-x)}/_{x(1-y)}$$

where *y* is the permeate concentration of the fast-permeating gas and *x* is its feed concentration.

The membranes chosen for the CF_4 recovery systems are the hollow fiber membranes (HFM) developed by UBE industries. HFM of polyimide Matrimid®5218 (Figure 32, UBE Ind.), characterized by high gas selectivity, are specifically designed for CO_2 separation and they are suitable for the extraction of CF_4.

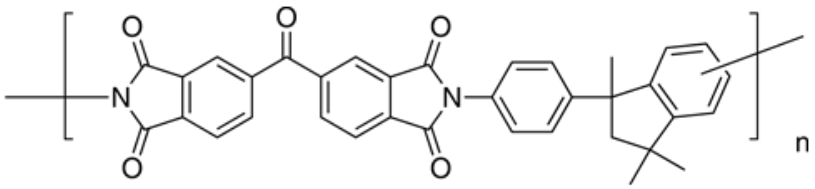

Figure 32 Polyimide Matrimid®5218 chemical structure.

The UBE membrane effectively segregates CO_2 within the permeate stream, allowing the remaining components to pass through the retentate stream at a high purity level. Developed by

UBE Industries, the HFM membrane comprises capillaries constructed from aromatic polyamide. The older membrane features a symmetrical dense-porous structure, whereas the latest version exhibits an asymmetrical dense-porous structure attained through varied polymer chain lengths, resulting in variable porosity across the capillary's cross-section. The uniform composition and structure of the initial membrane type determine the flux and are referred to as homogeneous (dense) membranes. In dense membranes, molecules of different compounds dissolve into the membrane matrix and then diffuse through the membrane driven by a concentration gradient. The permeability of each species is influenced by the solubility of each compound into the membrane material (thermodynamic aspect) and by the rate at which each component diffuses through the membrane (kinetics aspect) [18]. The average pore diameter in dense polymer membranes lies within the thermal motion of the polymer chains from which the membrane is formed. The asymmetric membrane comprises a thin, dense selective layer (skin) supported by a much thicker microporous support layer, supplying mechanical reinforcement. The unique structure of the asymmetric membrane arises from varying the length of the polymer chain, creating variable porosity in the cross-section [19]. It combines the high selectivity of a dense membrane with the high permeability of a very thin membrane. Asymmetric dense/porous membranes are obtained through phase inversion, during which the polymer is transformed from a solution to a solid state in a regulated manner, often by precipitation upon immersion. The industrial production of asymmetric membranes has significantly advanced in recent years [28]. It has been observed that polymers with high chain stiffness, weak interchain interaction, and loose chain packing tend to exhibit high gas permeability, indicating that both dianhydrides and diamines components of the polymer should not contain flexible links. Owing to the glassy nature of these polymers, they tend to thermodynamically rearrange their chains, reducing the number and sizes of free volume contributing to gas permeability [20]. The module is housed in a high-pressure steel housing designed for counter-current stream flows.

In an ideal separation process, all the CO_2 molecules present in the feed mixture would permeate the membrane walls, while all the CF_4 molecules would flow at the retentate output of the membrane. Given the non-ideal nature of the separation process, separation membranes have limitations in their performance, which can be tuned through the accessible parameters depending on the requirements on the separation product. For this specific case, while on one hand it is crucial that the retained gas contains the highest possible CF_4 fraction, it is also fundamental that the fewer possible CF_4 volume leaves the membrane through the permeated

flow. For example, one could have very pure CF_4 in the retentate gas fraction, but then such fraction could contain only half of the total CF_4 present in the input, while the other half would be lost in the permeate stream. Therefore, a balance should be found between having very pure recuperated CF_4 and recuperating a gas volume that is high enough to make the process worth the costs and efforts. To tune the balance of the process requirements, membrane performance is evaluated with two parameters: recovered gas quality and CF_4 separation efficiency. The recuperated gas quality is simply expressed with the CF_4 concentration in the gas volume of the retentate stream. The CF_4 separation efficiency is defined as follows:

$$\epsilon(CF4) = {volume\ (CF4^{output})}\Big/{volume\ (CF4^{input})}$$

where the output is the retentate gas stream. It should be considered that CF_4 separation efficiency depends on different factors, such as the input gas pressure, the feed flow rate and mixture composition. For example, for the same type of membrane different versions are produced, each specifically developed to work with a given input flow rate, in way to optimize the separation for such flow range. For this reason, different studies were realized to characterize the UBE membranes to maximize their performance in the LHC CF_4 recuperation plants. The results of the studies performed on these modules for the separation of CF_4 will be discussed later.

3.1.2 Thermal and Pressure Swing Adsorption (TSA & PSA)

Molecular sieve adsorbents are powerful crystalline aluminosilicates that have the remarkable ability to selectively adsorb molecules based on their size and polarity. These adsorbents, represented by the stoichiometry $M_{x/n}[(AlO_2)_x(SiO_2)y]_zH_2O$, offer a regulated structure of cages connected by windows, allowing for precise control of pore size from 3Å to 10Å, and are highly effective at re-adsorbing water and other polar molecules.

Zeolites, comprised of tetrahedra of silicon and aluminium, are assembled into a three-dimensional crystalline framework, characterized by a variety of window sizes based on the number of oxygen atoms in the ring – four, five, six, eight, ten or twelve. This unique feature allows for selective adsorption of specific molecules, making zeolites an ideal choice for various industrial applications. Aided by strong ionic forces (electrostatic fields) due to the presence of cations and by the enormous internal surface area of up to 1,000 m^2/g, molecular sieves will adsorb a considerable amount of water or other fluids. If the fluid to be adsorbed is a polar

compound, it can be adsorbed with high loading, even at very low concentrations of the fluid. Molecular sieves will, therefore, remove gas or liquid impurities to very low levels (ppm or less). Another feature of molecular sieve adsorbents is their ability to separate gases or liquids by molecular size or polarity. The pore, or cage, openings are the same size as many molecules, e.g., in the case of hydrocarbon paraffins, straight-chained molecules can fit into the pores and be adsorbed, while the branched-chain molecules cannot enter the pores and pass through the molecular sieve bed unabsorbed.

These materials are used in the LHC gas systems in two separate separation processes: Pressure swing adsorption (PSA) and Thermal swing adsorption (TSA) (Figure 33).

The temperature fluctuation of an adsorbent bed on a periodic basis forms the basis of TSA processes. Adsorption takes place at low temperatures, and the bed regenerates at high temperatures. Hot gas or steam is frequently utilized during this phase, and the bed must cool down before it can be used again.

Two disadvantages of the procedure are its lengthy duration (typically many hours to several days) and its high energy consumption and big absorbent inventory.

In the PSA, a gas stream enriched in the less strongly adsorbed components of the feed gas is produced by selectively adsorbing certain components of a gas mixture at a relatively high pressure through gas-solid interaction within a densely packed column of the adsorbent. For desorption, no external heat is typically utilized.

The vacuum swing adsorption (VSA) procedure is more frequently utilized. In this process, desorption is accomplished under vacuum while the adsorption stage is carried out at a pressure level close to ambient. Both ideas are combined in a pressure-vacuum swing adsorption (PVSA) process.

Although simple in concept, a practical PSA/VSA process can be quite complex since it employs a multicolumn design with adsorbers operating in a cyclic steady state via a series of successive non-isothermal, non-isobaric, and non-steady-state phases. Adsorption, desorption, and several other complementary processes are among them; their goal is to maximize the performance of the separation process while maintaining control over the purity and recovery of the product gas.

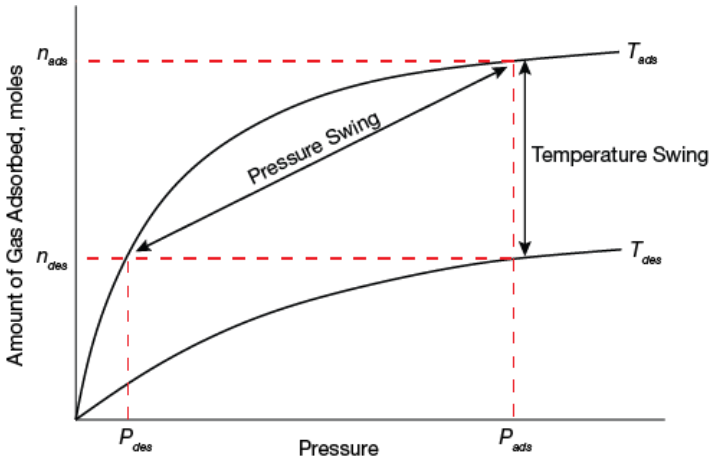

Figure 33 Comparison between pressure and thermal swing adsorption.

3.1.3 Distillation

When components of a combination have noticeably different boiling points, distillation, a liquid purification technique, can be used to separate the components. The process of distillation involves boiling a liquid in a "distilling flask," after which the vapours go to another part of the device and encounter a cool surface. On this cool surface, the vapours condense, and the condensed liquid—referred to as the "distillate"—drips into a reservoir apart from the original liquid. Distillation is the process of boiling a liquid, condensing the gas, and then gathering the liquid in another location.

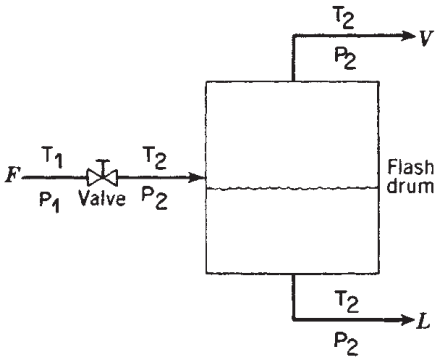

Figure 34 Example of a single stage equilibrium-flash process.

The single stage equilibrium-flash process depicted in Figure 34, which can be adiabatic and isothermal, is the most basic continuous distillation method. A choke valve causes a partial phase change in an adiabatic flash process because of a sudden pressure change at that valve. A choke valve is not required in an isothermal process since phase change takes place at the heat exchanger that is situated prior to the flash drum. Both types of flash have two phases that form before the flash drum and two streams that exit it: liquid at the bottom of the drum and vapor at the head. Thus, the flash drum's sole purpose is to enable the two phases' physical separation. This type of separation process is used for the separation of C_4F_{10} from N_2 and CO_2 in the LHCb RICH1 detector.

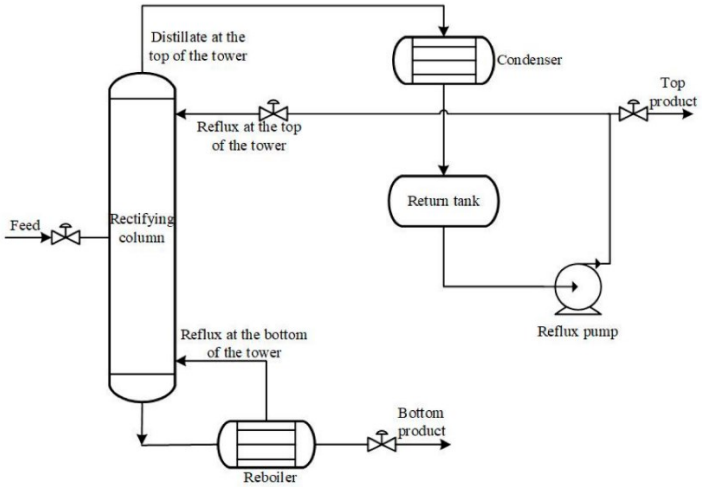

Figure 35 Example of a standard distillation column.

The equilibrium liquid and vapor compositions of a binary mixture are determined by temperature and pressure. Thus, it is usual practice to display experimental results using tables of vapor mole fraction y and liquid mole fraction x for a single ingredient over a range of temperature T (Figure 35) for a fixed pressure P or over a range of pressure for a fixed temperature.

The basic composition relationship between the vapor and liquid phases in equilibrium can be expressed as a function of the total system pressure, the vapor pressure of each pure component, and the liquid-phase activity coefficient of each component *i* in the mixture at low-to-moderate pressure ranges typical of most industrial applications:

$$y_i P = x_i \gamma_i P_i^{sat}$$

When systems display perfect liquid-phase behaviour, Equation 5 reduces to Raoult's law and the activity coefficients, γ_i, equal unity. A system is considered to exhibit positive deviations from Raoult's law if $\gamma_i > 1$, and negative departures from the law if $\gamma_i < 1$ for nonideal liquid-phase behavior. When systems are sufficiently nonideal, deviations can occur to the point where temperature-composition phase diagrams show extrema where the compositions of the liquid and vapor in equilibrium are equal. The system is said to create an azeotrope when this occurs.

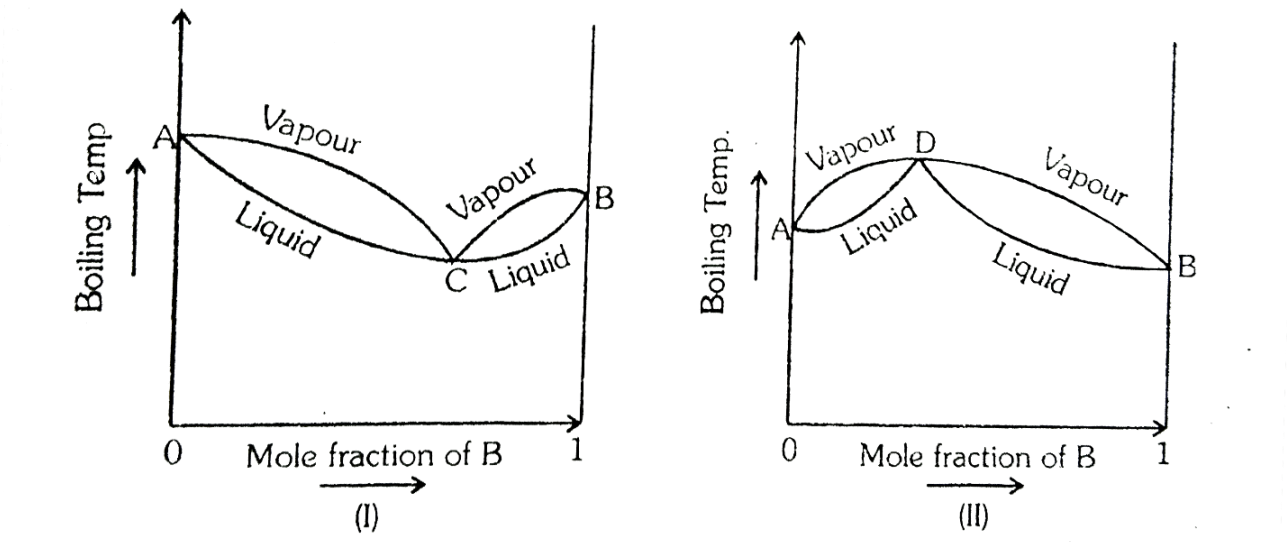

Figure 36 Plots of minimum (I) and maximum (II) boiling point azeotropes.

Azeotropic systems show a minimum in the T-x,y diagram when the deviations from Raoult's law are positive [Figure 36 (I)] and a maximum in the T-x,y diagram when the deviations from Raoult's law are negative [Figure 36 (II)].

The composition of the azeotrope moves toward one of the pure components (toward the higher-boiling pure component for maximum-boiling azeotropes, and toward the lower-boiling pure component for minimum-boiling azeotropes) when the difference in boiling points between the components grows. Even when there are significant departures from Raoult's law, mixtures of components whose boiling points differ by more than roughly 30°C typically do not display azeotropes identifiable from the pure components.

For the LHCb RICH1 C_4F_{10} recovery system it currently uses an isothermal single stage equilibrium-flash process. The presence of compounds with very different boiling points (CO_2, C_4F_{10}, air) doesn't require to perform more distillation steps to obtain pure C_4F_{10}. For the R134a, the presence of a minimum boiling point azeotrope requires a more complex apparatus in which more than one flash vaporization unit is series connected to improve the separation process with respect to the single flash operation, that tends to a differential distillation (Figure 37) [21]. The two processes will be detailed discussed in the dedicated paragraphs.

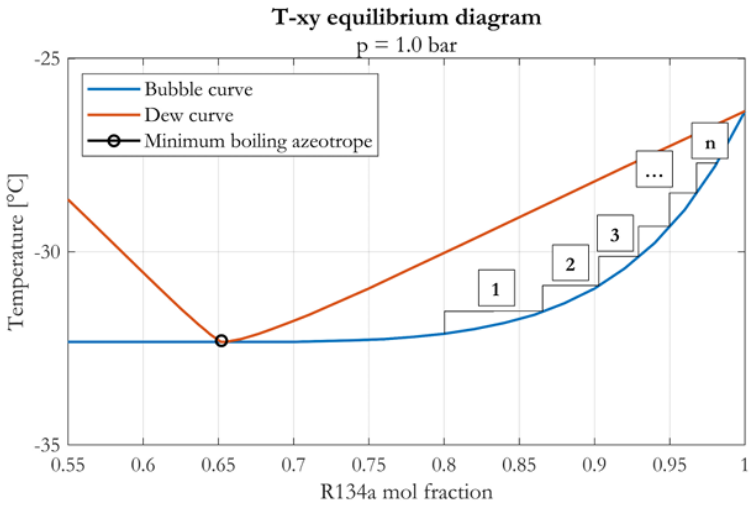

Figure 37 T-xy equilibrium diagram for the R134a-iC_4H_{10} minimum boiling point azeotrope.

3.2 LHCb RICH2 CF_4 Recuperation system

The RICH2 detector in the LHCb experiment uses CF_4 as the main component of its gas mixture due to its low dispersion and refractive index. To mitigate potential scintillation, about 8% of CO_2 is added to CF_4. However, CF_4 has a high GWP of 7390 and is relatively costly. As a result, the gas mixture is recycled in a Closed Loop system with a gas recirculating fraction of around 100%. To keep the photon absorption at an acceptable level, the H_2O and O_2 impurities are limited to about 100-200 ppm thanks to the purifier module.

During maintenance operations in the LHC LS2, the 100 m^3 of the RICH2 volume was filled with 100% CO_2 to prevent the waste of CF_4. Before RUN3, the detector was emptied of CF_4 mixture and refilled. To ensure the correct concentration of gas components in the detector volume, a thorough flushing of the gas system, equivalent to at least four volume changes, is necessary. This process would result in a large quantity of gas, mostly CF_4, being exhausted into the atmosphere. The aim of the recovery plant is to extract high-quality CF_4 from the exhaust gas mixture for storage and future use.

3.2.1 Recuperation plant

The recuperation plant was already planned in the original design of the RICH2 gas system, but it has been physically introduced only in 2018. It is made of a sequential membrane module, standard purifier module and a compressor module with a battery for the storage of the recovered gas, as show in Figure 38.

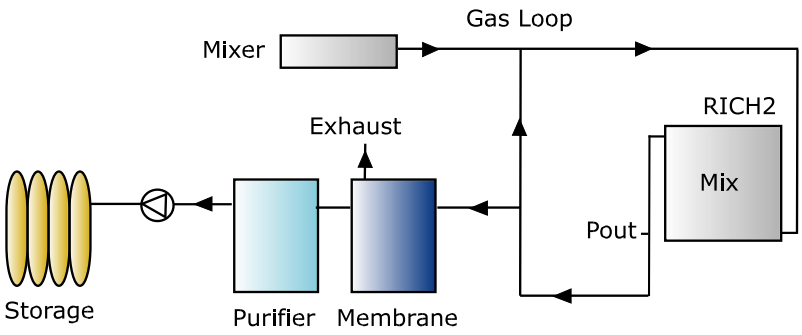

Figure 38 Scheme of the LHCb RICH2 gas system.

In the first module of the recuperation plant, the membranes one, the separation of the CF_4 from most of the CO_2 and N_2 takes place. The module is made of two separation membranes (hereafter called M1 and M2).

The module can be operated in the following configurations (Figure 39):

- Single membrane: the gas is sent only through M1, then the retained fraction is collected to storage (CF_4 enriched) while the permeate is sent to exhaust (CO_2 enriched) (I);
- Double membrane simple: the permeate fraction coming from M1 is used as input to M2, whose permeate is sent to exhaust while the retained fraction is co-fed with the retained from M1 to storage (II);
- Double membrane with reinjection: the permeates fraction from M1 is used as input to M2, whose permeate is sent to exhaust while the retained fraction is injected back as input of M1 for a further grade of purification (III).

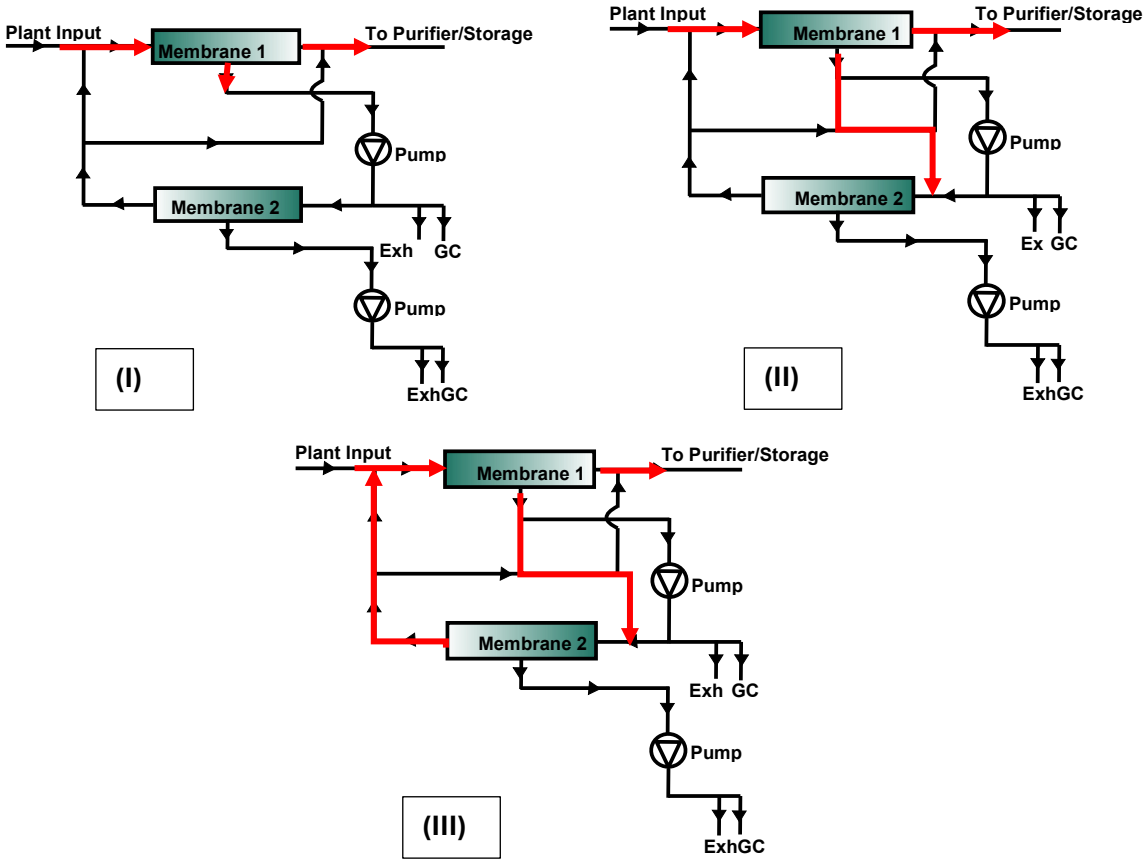

Figure 39 Possible membrane module configurations: (I) single membrane, (II) double membrane simple and (III) double membrane with reinjection.

The module uses the optimal configuration depending on the requirements in gas purification grade. Each of the two membranes is equipped with a pump to extract the permeate gas flow. The output from the membrane module, whether from M1 alone or from M1+M2, can then be sent to the subsequent stages of recuperation. To check operational efficiency, gas sampling points are located at relevant positions throughout the module. The collected gas sample is directed to a Gas-Chromatograph (Agilent µGC 3000) to measure the concentration of each gas component in the mixture.

The purifier module plays a crucial role in the gas recirculation system by quantitatively removing impurities like H_2O from the gas mixture before it is reintroduced into the system. The purifier cartridges, specifically designed for H_2O adsorption, also have the capability to trap CO_2 molecules, providing an additional purification level for extracted CF_4 when placed after the membrane separation. As the final stage, the compressor module compresses and stores the recaptured gas; it has been modified to include a loop with a buffer volume. This modification allows the compressor to operate within a specific range of input gas.

The setup is equipped by a set of sensors, enabling continuous remote monitoring of operation. Four Mass Flow Meters (MFMs) are strategically installed at the input and output (retentates) of M1 and M2 to accurately measure the gas flow rate. Additionally, pressure sensors are strategically positioned at various points within the setup, including membranes input/output, before the pump, at the purifier, compressor input/output, and the storage battery.

3.2.1 Characterization of the membranes

Before designing the final recuperation plant, the efficiency of the membranes was tested in order to understand the best configuration and the optimal operation parameters for the module. The studies were carried out using the µGC to monitor the composition of the gas mixture at the different stages of the separation.

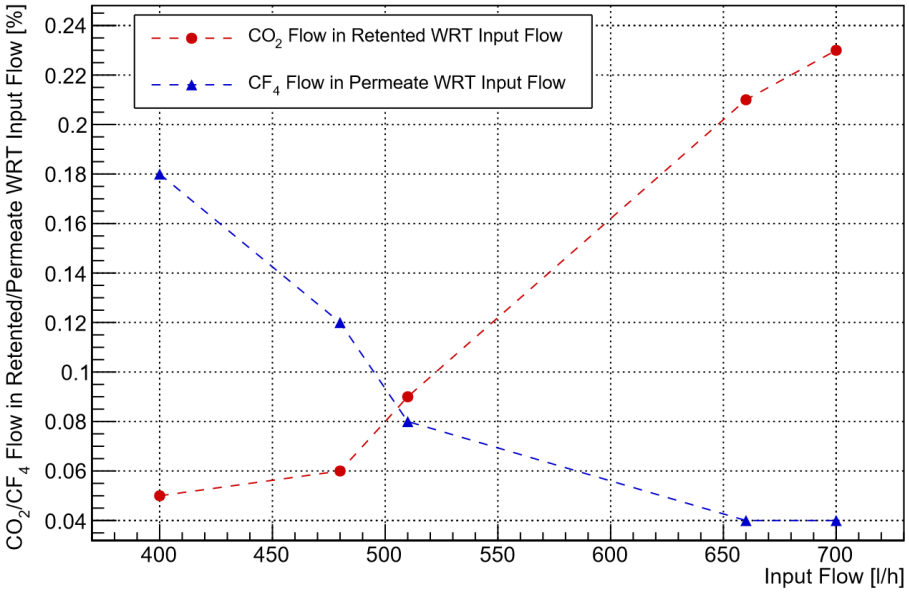

Figure 40 Gas composition in terms of CO_2 and CF_4 fractions at both retentate and permeate side VS membrane input flow.

Preliminary studies showed a dependence of membrane operation on the membrane input gas flow rate, as shown in Figure 40. The membrane module was therefore tested using M1 only (single membrane configuration) with different input flow rates. Lower flows (400-450 l/h) showed a lower CO_2 concentration in the recuperated gas (retentate side), but a higher concentration of CF_4 in the permeate gas fraction, therefore a lower CF_4 separation efficiency. At higher flow rates, such as 700 l/h, the CO_2 concentration on the retentate side of the membrane is too high for the recuperated gas quality to be considered acceptable. The optimal input operation flow for CF_4/CO_2 92/8 gas mixture is achieved by flushing around 500 l/h, which allows to reach high CF_4 separation efficiency (>95%) keeping low the CF_4 loss.

For a working flow of 500 l/h, the CO_2 concentration at the retentate side was measured to be between 2% and 5% and given the fact that purifier material (MolSieve 5Å) designed for H_2O adsorption can also trap CO_2 molecules when in low concentration, the purifier was confirmed to be a good solution to absorb it without saturating. The CO_2 concentration after this module was measured to be around 0.02% guaranteeing a good purity of the CF_4 sent to storage.

3.2.2 CF_4 Recuperation Process

In this section the results of the emptying procedure of the RICH2 detector performed before the LHC LS2 will be briefly described since it was realized before the starting of this PhD. The filling procedure will be described in detail instead. The performance of the recuperation system is reported in terms of its efficiency in separating and re-using CF_4 for detector operation.

3.2.2.1 RICH2 Emptying Procedure

The CF_4 recuperation plant is used during the phases of transition between nominal gas mixture (CF_4/CO_2 92/8) and 100% CO_2 and vice versa. The first phase of the CF_4 recuperation foreseen for the beginning of LS2 consisted in emptying the RICH2 volume containing the gas mixture used during the run to replace it first with pure CO_2 only, and subsequently with Air. With the presence of Air allows indeed to perform maintenance by physically accessing the detector, in absence of CF_4 and CO_2 in the experimental cavern. The aim of this phase of the recuperation is to avoid the loss of large volume of CF_4 originally in the detector into the exhaust during the injection of CO_2 and to extract it from the gas with high grade to be reused in the future.

The CF_4 recuperation has been operational since June 2019 for five months, after the studies on the membranes described previously. During this period, the recuperation plant has been working for about 500 hours. The plant could not indeed work in a continuous mode, given the need of attentive monitoring of operation parameters and recuperation efficiency at each stage.

The effective recuperated CF_4 available for further use is the one accumulated in the storage battery volume, for a total of 28.5 m^3 at the end of operation (Figure 41).

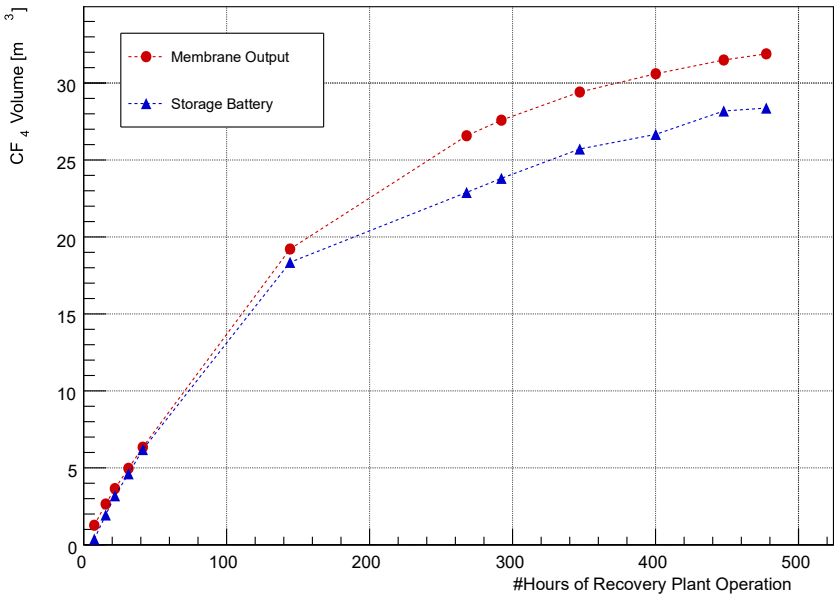

Figure 41 CF_4 integrated volume at the output of the membranes (red) and in the storage module (blue).

The recuperation process was stopped when the CF_4 concentration in the detector was around 7%, since below such concentration the gain in separation efficiency is negligible, and the balance between recuperated and exhaust gas is no more convenient, as shown in Figure 42. Considering the initial gas loss of 25 m^3 due to oscillation of atmospheric pressure and the one of 15m^3 due to detector maintenance in the LHCb cavern, the overall plant efficiency was calculated to be around 65%.

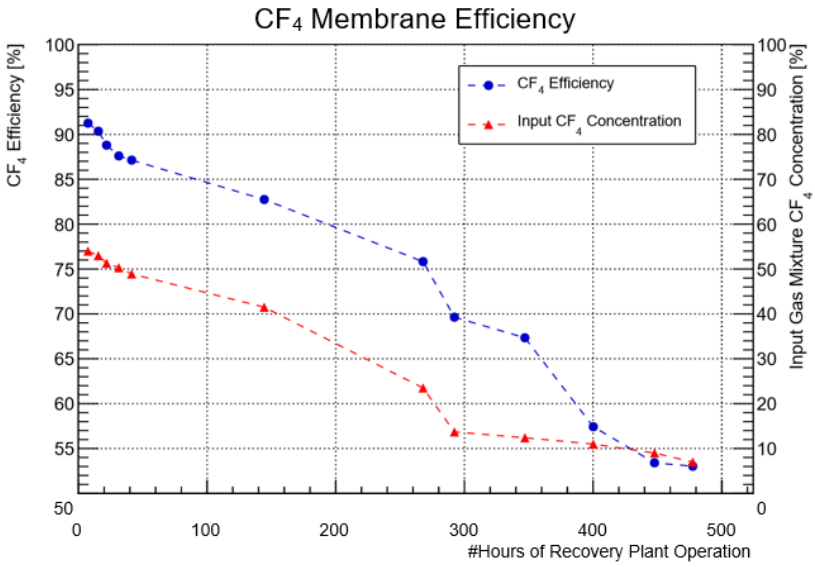

Figure 42 CF_4 separation efficiency and CF_4 concentration at the input of the module during emptying procedure.

What can be concluded from the last graph is that, considering that the recovery operation started with an input gas mixture of CF_4/CO_2 60/40, the gas fraction lost during the end-of year stop would have been recuperated with very high efficiency (<90%), increasing the overall operation efficiency [12].

3.2.2.2 RICH2 Filling Procedure

Six months before the launch of the LHC RUN3, the filling procedure started. The first step was to fill the detector with pure CO_2 to avoid too much air in the system during the recuperation process, which should not exceed the 1% of the detector volume. When this phase was completed, the filling started. According to the results obtained during the studies for the characterization of the membranes in 2019, it was deemed more convenient to split the overall process in two parts, one operating in Open Mode and the other using the recuperation system.

In the first phase, CF_4 was injected from the mixer setting the system in Open Mode, that means all the gas was exhausted to atmosphere. The detector is designed for both filling and emptying through its upper and lower sections, respectively, which are positioned opposite each other. The

selection of these sections is based on the specific gas being introduced into or removed from the detector. Since the CF_4 is heavier than CO_2, the choice is to fill the detector with CF_4 from the bottom of the chamber so that only CO_2 evacuates from the upper chamber output and moves to the exhaust. Moreover, among the total 40 m^3 of CF_4 that were injected in the system in this phase, about 25 m^3 came from the storage battery filled with the CF_4 recuperated during the emptying procedure realized in 2019. The schematics of the gas system configuration used in the Open Mode phase is showed in Figure 43.

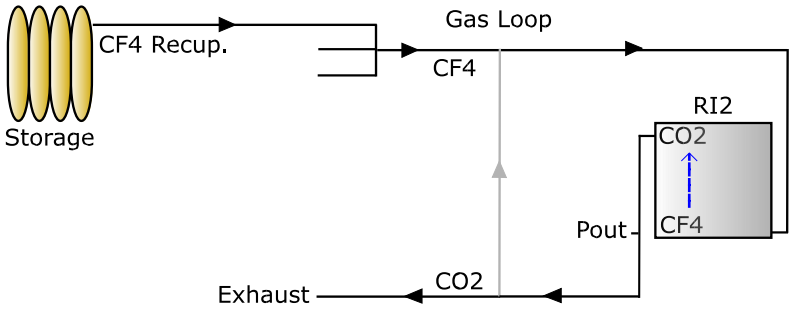

Figure 43 Scheme of the gas system configuration during filling procedure without the recuperation plant.

The exhaust mixture composition was continuously monitored with the Gas Chromatograph to be sure that in this phase only CO_2 was sent to exhaust and no CF_4 was wasted. Another parameter that allowed to monitor the composition of the exhaust gas was the chamber output pressure: given the different density of the two gases, the pressure measured at the output of the chamber is affected by the hydrostatic pressure exerted by the gas column as tall as the chamber volume. When such column is fully filled by CO_2, the output pressure is around 1.5 mbar, while when CF_4 is predominant, it reaches around 4.2 mbar. The transition between these two values gives indication of the gas mixture composition variation. By merging the values of output pressure and CF_4 concentration from GC measurements during the filling procedure (Figure 44) are reported in Figure 44 in which in the first phase just described, the output pressure was stable around 1.5 mbar and no CF_4 was detected in the analysis.

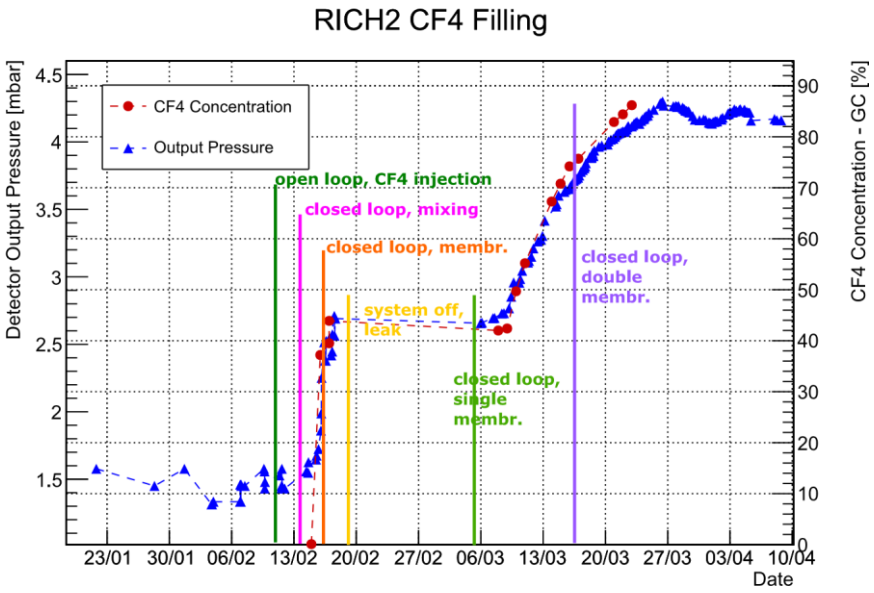

Figure 44 Detector output pressure and CF_4 concentration (from GC analysis) upon time during filling procedure.

When the CF_4 concentration at the Exhaust module of the gas system reached a value around 37%, the filling procedure passed to the second phase in which the gas system was put in Closed Loop without mixer injection, in order to ensure a homogeneous composition of the mixture. As shown in Figure 44, during these hours (between pink and orange line in the plot) the output pressure of the chamber rapidly increased meaning that all the CF_4 was accumulated in the bottom part of the detector.

At that point, the recuperation plant was put in the Loop and the injection of CF_4 restarted from mixer module, as shown in Figure 45. With such configuration, all the gas coming out from the chamber was sent to the membrane module with a flow set around at 500 l/h; then the gas from retentate side of the membrane was sent again to the chamber, while the gas belonging to permeates side enriched in CO_2 was exhausted to air. The mixer was used to compensate for the fraction of gas exhausted through the membrane module.

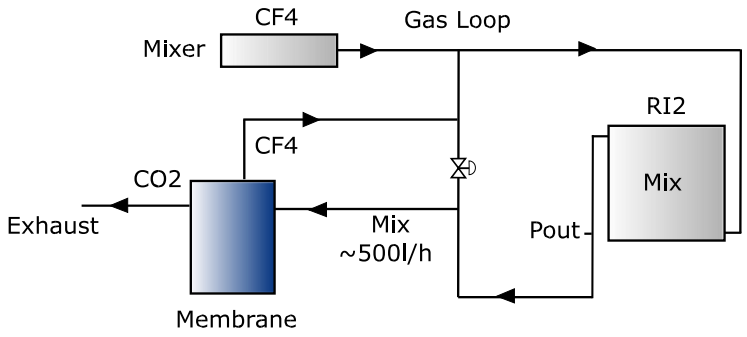

Figure 45 Scheme of the gas system configuration during filling procedure, by integrating the recuperation plant.

In the configuration of the Membrane module, we utilized two out of the three possible configurations detailed on page 71. We began by operating in Single Membrane mode and then transitioned to Double Membrane (simple) operation mode. Our observations during the emptying procedure revealed that as the CF_4 concentration at the module input decreased, the separation efficiency experienced a notable decline (Figure 42). Specifically, this reduction in efficiency corresponded to an increase in the CF_4 lost to exhaust on the Permeate side. Even though the composition at the Retentate (98/2 CF_4/CO_2) and Permeate (5/95 CF_4/CO_2) outputs remained largely unchanged, the volume at the Permeate side expanded, resulting in a significantly higher absolute value of lost CF_4 volume. Consequently, we retained the Single Membrane configuration until the CF_4 concentration reached approximately 70%, after which we transitioned to Double Membrane to redirect the Permeate flow to the second membrane for further separation. This strategy allowed us to recover a portion of the CF_4 that would have otherwise been lost to the exhaust.

The Closed Loop with Membrane module operated until the gas mixture at the membrane input reached about 90% of the final concentration required for the experiment (92% CF_4 and 8% CO_2). The increase in CF_4 in the output gas mixture was closely monitored along with the chamber output pressure, which stabilized at around 4.2 mbar. (Figure 44).

In this case, the efficiency of the gas recuperation process was calculated by considering the input and output gas volume flows of the membrane module, as well as the relative measurements of gas mixture composition. Figure 46 illustrates the trend of recuperation efficiency for both the emptying and filling procedures. It reveals that both trends are compatible

with each other, despite measurements being taken over a different range of input concentration. The figures demonstrate that an increase in CF_4 concentration at the input of the membrane module results in improved recuperation efficiency, as less CF_4 is lost in the Permeate side. However, separation efficiency significantly drops to below 80% for CF_4 concentrations below 50-40%. Additionally, the trend from the filling procedure confirms that efficiency continues to improve with increasing input CF_4 values, and it almost reaches 100% efficiency for concentrations above 80%.

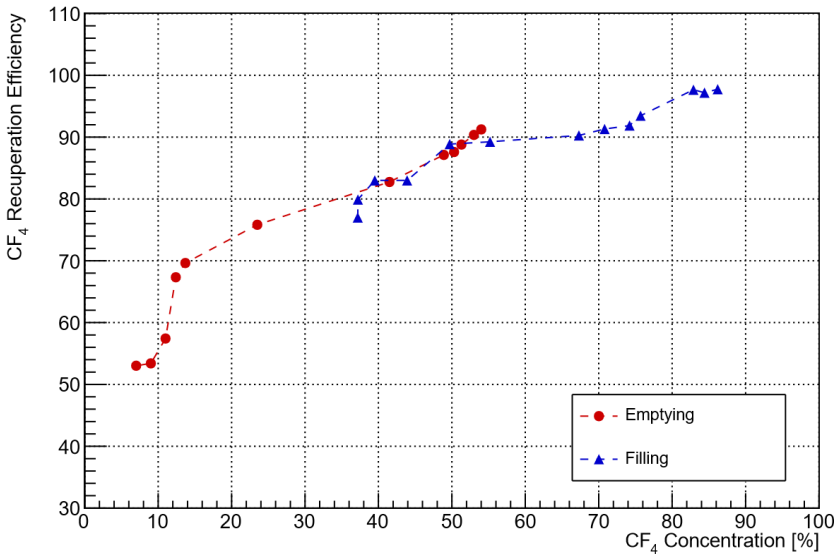

Figure 46 Overlap of CF_4 recuperation efficiency values during emptying (red) and filling procedures (blue).

Finally, the efficiency of the recuperation system can be evaluated by comparing the volume of CF_4 used during the filling procedure with the volume that would have been necessary if the system operated in Open Loop. If the system were to operate in Open Loop, an estimated 250 m^3 of CF_4 would be required to achieve a 92% concentration in a 100 m^3 volume of the detector. In the actual filling procedure, 40 m^3 was injected with the system in Open Loop and 55 m^3 was injected with the system in Closed Loop to achieve the final 90% CF_4 concentration. This resulted in a total usage of 95 m^3 of CF_4, with 30 m^3 sourced from the storage of the previous emptying procedure. Considering both emptying and filling processes, only 65 m^3 of CF_4 was used, resulting in a potential consumption saving of about 75% compared to the Open Loop operation.

3.2.3 Studies for recovering the CF_4 from the Purifier module

The membrane module described above is not designed to operate continuously as it requires monitoring via μGC analysis throughout the entire process. Nevertheless, the Purifier module, as shown in Figure 38, can operate continuously during recuperation and normal run periods.

In the RICH2 gas system, a highly efficient purifier module is utilized, featuring two 24-liter cartridges filled with MolSieve 5Å designed for H_2O adsorption through TSA process. The gas is efficiently purified as it passes through the column at a flow rate of 3.5 Nm^3/h and a pressure equivalent to the gas loop one. Molecular sieve efficiently removes impurities from the gas, while the rest of the gas mixture remains unaffected. When the run volume reaches 500 m^3, the column swap occurs by regenerating the saturated column through a vacuum process and subsequent heating up to 200°C. Notably, all gas inside the column at the time of regeneration was meticulously discarded prior to conducting this test.

This particular material has been found to be able to trap small amounts of CO_2 and CF_4. As a result, conditioning the column with CO_2 before the gas circulation is necessary to prevent any changes in the gas mixture composition and to avoid wasting CF_4. Even with the conditioning, a small portion of the gas mixture gets adsorbed, which can be observed from the slight pressure drop in the detector gas loop.

Since the compressor module was designed to recover the gas also from the Purifier, the goal of the test was to understand if a fraction or all the gas exhausted in the first part of the regeneration process could be recovered in the CF_4 battery storage.

The test was designed to extract gas from the column by starting at the gas loop pressure value of around 600 mbarg, and then filling a small Festo buffer of 0.75 litres or 20 litres, according to the test, until the pressure inside reached 100 mbarg (Figure 47).

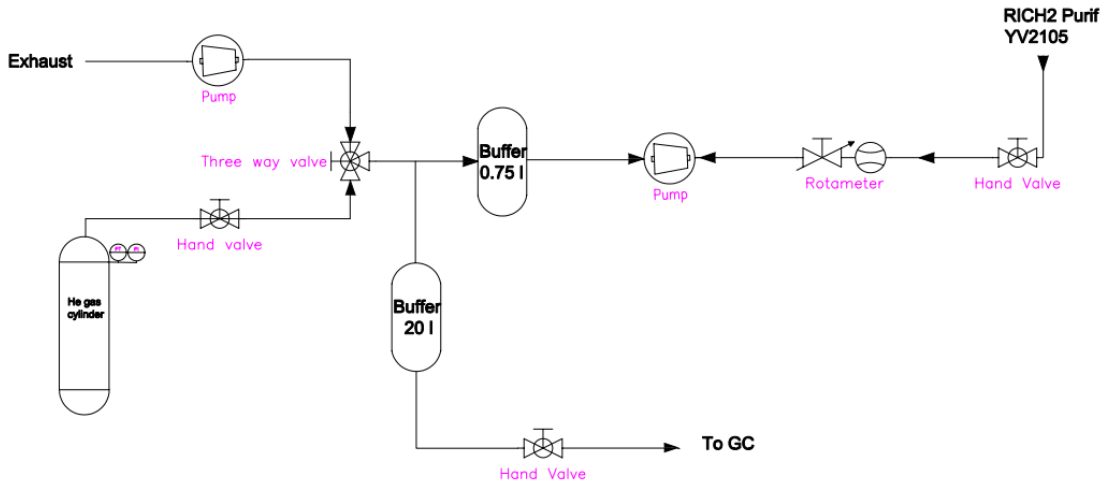

Figure 47 P&ID of the setup used for the RICH2 Purifier module tests.

At that point, the purifier column stopped emptying and around 10 µGC analyses of the gas in the volume were performed. This procedure was repeated until the purifier cartridge reached vacuum. Between each step, all the pipes and the Festo volume were "cleaned" purging them with Helium and then doing vacuum. During the test some parameters were continuously controlled, such as the initial and final pressure of the purifier column at each emptying step, pressure of the buffer before the gas chromatograph and the concentration of CF_4, CO_2 and N_2 at each step.

The last test was performed emptying the cartridge from 600 mbarg to -700 mbarg and sending this gas in the buffer volume in one step. This test was done because in the previous ones some air was found at specific pressure values so the goal was to understand if this was due to a leak in the setup or it came from the cartridge itself.

3.2.3.1 Results

The two tests shown in Figure 48 were performed at the same condition, but with a difference in the original CO_2 concentration, which was higher for the Test 1. For this reason, during Test 1 the

CO_2 had a huge peak in concentration at the very beginning of the emptying phase, between 550 and 500 mbarg, where it arrives at 35% of the total extracted mixture, and between -300 mbarg and -450 mbar, where it arrives at around 20%. Between 500 mbarg and -300 mbarg, its concentration is around 5-10% for both tests, as show in the plot in Figure 48.

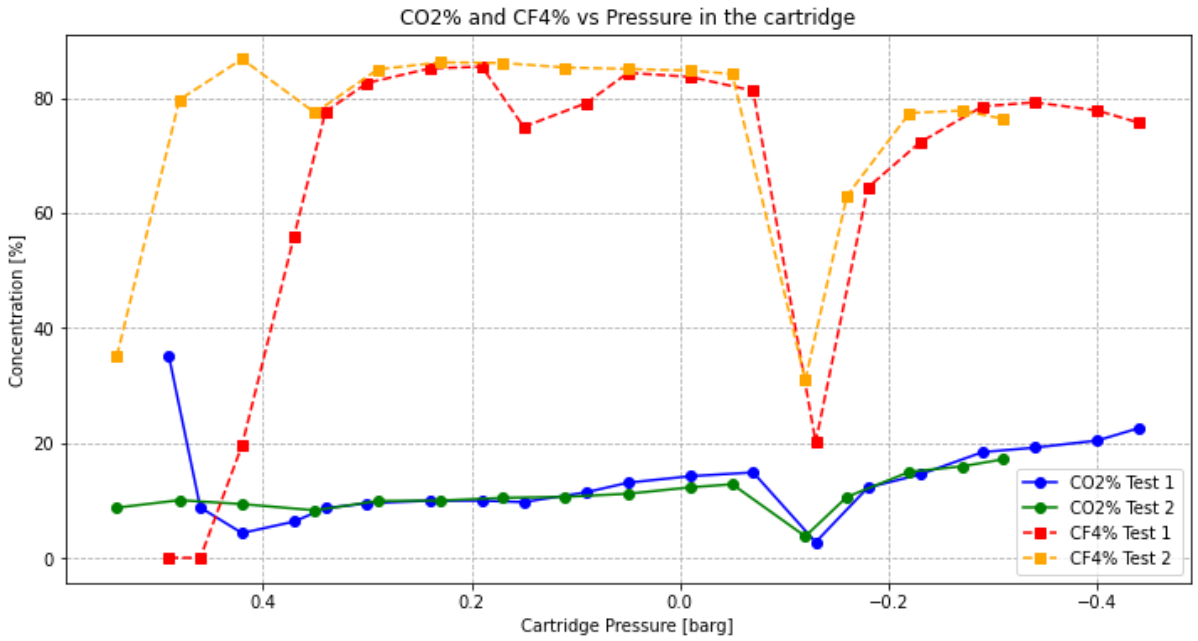

Figure 48 Trend of CO_2 and CF_4 VS pressure in the purifier cartridge during two tests.

At approximately -130 mbarg, the concentrations of CF_4 and CO_2 significantly decreased, favouring air and indicating that most of this gas was desorbed from the purifier's material. The volumes of CO_2, CF_4 and air were integrated over time considering their concentration in order to obtain the total volume for each component and see if it might make sense to recover that gas.

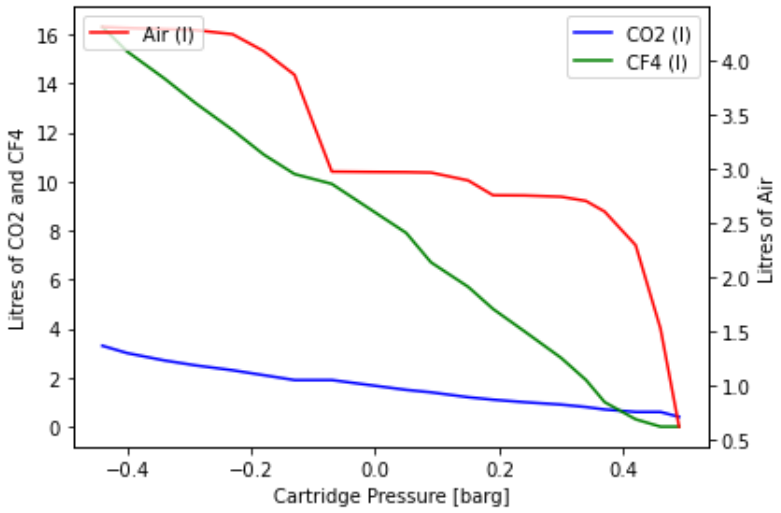

Figure 49 Integrated volumes of CF_4, CO_2 and air extracted from the purifier cartridge.

In Figure 49, the integrated volumes over the pressure in the cartridge for CF_4, CO_2, and air are displayed. This plot confirms previous observations, showing that the air volume increases significantly during the first and last phases of the emptying column, while the trends of CO_2 and CF_4 remain more stable over time.

Considering the initial composition of the CF_4 recovery battery, (94% CF_4, 5% CO_2, 290 ppm O_2, and 4900 ppm N_2), and the total volume extracted from the purifier cartridge of 28 litres, it was decided to send all the gas to the recovery battery.

Indeed, based on the saturation volume set for this purifier module and the flow rate of the gas mixture, the swap of the columns occurs roughly every six days, resulting in the recovery of around 1m^3 of CF_4 from the purifier over a year. It causes a dilution of the CF_4 in the battery with a decrease in its concentration by around 0.7% per year. This is acceptable until the battery reaches the same composition of the detector, 92/8 CF_4/CO_2, that will happen at the end of RUN3.

The latest test results indicate that the gas mixture from the cartridge comprises 84.5% CF_4, 15% CO_2, and 0.5% air. Notably, the concentration of air is lower than in previous tests, potentially due to a minor leak in our testing setup.

3.3 CMS CSC CF_4 Recuperation system

Cathode Strip Chambers (CSC), a part of the CMS Muon System, is another LHC detector using CF_4 in the gas mixture, in a less extent. Indeed, the current CSC gas mixture used is made of 40% Ar, 50% CO_2, and 10% CF_4. In particular, Ar provides the necessary gas gain for desired HV settings, CO_2 is used for quenching of spurious pulse and enhance time response, and CF_4 has anti-aging properties preventing wire etching and polymerization [22].

Because of a very large detector volume of 90 m^3 and the cost of CF_4, the CSC gas system has been designed to operate in a closed-loop mode with less than 5% fresh mixture injected. However, a challenge arose when it was found that air contaminated the mixture back from the detector, belonging to diffusion leaks from detector construction components. To minimize the presence of O_2 and other contaminants, the percentage of fresh mixture injected was increased to 10%, and a gas recuperation system was developed to extract and store CF_4 from the CSC Exhaust module after the Purifier module. This initiative not only mitigates environmental impact but also significantly reduces costs related to CF_4 usage.

3.3.1 Recuperation plant

The recuperation plant (Figure 50) was added as non-standard LHC gas system in 2015 and since then its efficiency has progressively increased from 20% to 70%. The recovery plant is made of four modules in which the CF_4 is separated from the other components of the gas mixture and from impurities accumulated during detector operation (Figure 50). Thery are:

- Membrane module for CO_2 bulk separation
- Molecular sieve 4Å for CO_2 residual removal
- Molecular sieve 13X for CF_4 adsorption and recuperation
- CF_4 compressor and battery storage

a)

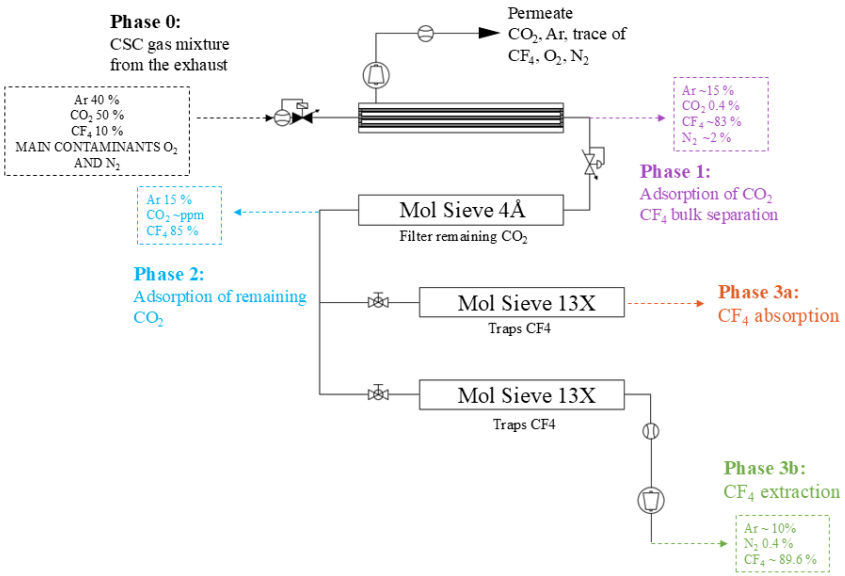

b)

Figure 50 a) Picture of the CF_4 recovery system installed at CMS; b) Schematic view of the CF_4 recuperation process in CMS.

The system and the injection of the CF_4 recuperated at the CSC mixer are designed to work in continuous 24/7.

In the first module, 4 membranes from UBE industries optimized for the separation of CO_2 are installed. Three membranes work with a feed flow up to 300 l/h and the fourth can work with an input flow up to 600 l/h. After the tests performed in 2021, it was found out that four membranes largely supplied for the workflow of the recovery system, so one of the three low flow membranes was placed on standby, maintaining operational 2 low – and the high - flow membranes. The cartridges work in parallel and through the upstream rotameters, flow is split so that each low flow membrane works at $^1/_4$ of the total flow and the high flow membrane manages the remaining half flow.

As seen for the RICH2 CF_4 recovery system, also in this case the CF_4 is collected at the retentate side of the modules with an outlet composition of 82.5% of CF_4, 15% of Ar, 2% of N_2 and 0.5% of CO_2 and a flow rate of ~80l/h.

The gas is then directed to the second module to reduce the CO_2 concentration, as the Molecular Sieve 13X used is able to capture both CF_4 and CO_2. This purifier module for the CF_4 recovery plant comprises two 24-liter columns. During normal operation, one column purifies the gas while the other is on standby or under regeneration mode. Although heating is required due to the strongly binding of CO_2 to the 4Å Molecular Sieve, the comparison between the 90-hour cartridge lifetime and the 12-hour regeneration time illustrates that the system is well-coordinated. The cartridge's lifespan of 90 hours ensures continuous operation over an extended period, while the relatively short 12-hour regeneration time allows for quick recovery and readiness for subsequent cycles. This balance ensures that the system operates efficiently without significant downtime, maintaining a steady progression in its performance.

Finally, the CO_2 free gas containing Ar (15%), CF_4 (85%) and some ppm of N_2 is sent to the second absorber module containing a 13X Molecular Sieve that is characterized by a pore diameter of 10Å. This allows to absorb and extract selectively CF_4 while Ar and N_2 remain in the cartridge's head space and are vented to air as waste stream. The absorption starts from vacuum and stops when the relative pressure inside the cartridge is equal to zero or to the pressure in the supply line to the module. The presence of a central heating bar reduces the time required to reach the nominal regeneration temperature, thereby minimizing downtime when complete thermal regeneration is necessary.

Once the CF_4 desorption from the 13X Molecular Sieve, it is sent to a buffer volume, compressed and stored into cylinders suitable for pressurized gas. Two batteries are installed for a total

volume of 600 litres, which are alternatively used: while one of the batteries is filled with recuperated gas, the other one is used as a CF_4 supply for the CSC mixer. A gas line is used to supply a second CF_4 Mass Flow Controller (MFC) dedicated to the injection of the recuperated gas into the mixture. Thanks to the improvements done on the system, nowadays only 40% of fresh CF_4 is injected, being the rest recovered CF_4.

The status and efficiency of the full recuperation plant is monitored through online μGC analyses. In addition, a dedicated infrared analyser has been installed (continuous monitoring of CO_2 and CF_4) and a gas monitoring system based on single wire detectors (SWPC) has been implemented to check the gas mixture quality.

3.3.2 Characterization of membranes

The efficiency of the membranes was tested in order to understand the best configuration and the optimal operation parameters for the module [23]. The studies were carried out using the μGC and mass flow meters to monitor the composition of the gas mixture at the different stages of the separation and to calculate the separation efficiency. The membranes were tested both individually and in parallel to calculate the overall efficiency of the module. Each test was realized with the membrane installed in a custom-made system where all the parameters could be tuned and measured. In detail, the input gas flow (from the exhaust module) was set by the user through the WinCCOA software, the gas flow rates of permeate and retentate were monitored with Flow Calibrator devices that have a precision of 0.5% of reading (MesaLab DryCal [30]), the pressure at the permeates and retentates sides were kept constant with manometers. The negative gradient of pressure at the permeate side was allowed by a pump. Finally, the gas mixture concentration at the permeate and retentate sides of the membrane was measured using a Gas-Chromatograph (1.5.1 Gas Chromatograph).

Label	Model	Flow rate [l/h]	Characteristics
M1	CO-C10	300	High thickness and gradient of density
M2	CO-C10A	300	High thickness and gradient of density
M3	CO-C10A	300	High thickness and gradient of density
M4	CO-C410A	600	High thickness and gradient of density
C07FS	CO-C07FS	300	Small thickness and gradient of density

Table 5 Membranes tested as part of the R&D activities on the membranes module of the CF_4 recovery plant.

The CO-C10, CO-C10A and CO-C410A membranes are characterized by high thickness of fibers and a gradient of density, preferred to others owing to their low production costs, high surface/volume ratios, reduced overall dimensions of the equipment (footprint) and excellent mechanical strength. The CO-C07FS is an asymmetric hollow fibers membrane and its structure is based on a gradient of density and small thickness of fibers. This membrane configuration consists of an extremely thin, dense layer designed for separation, supported by a porous substrate made from the same material. This design enhances the membrane's mechanical stability to withstand high-pressure feeds while minimizing resistance to mass transport, thereby facilitating high productivity in separation processes [24].

Contrary to the observations in the membranes' tests for the RICH2 recovery, in this case it was important to evaluate the separation efficiency of CF_4 not only from CO_2 but also from Ar, which emerged as the main contaminant at the end of the separation process.

The separation efficiency was calculated as following:

$$\epsilon(CF_4) = {Volume\ CF_4^{Output}} \Big/ {Volume\ CF_4^{Input}}$$

In the equation above, the output volume is the flow measured at the retentates side while the input flow is the feed one.

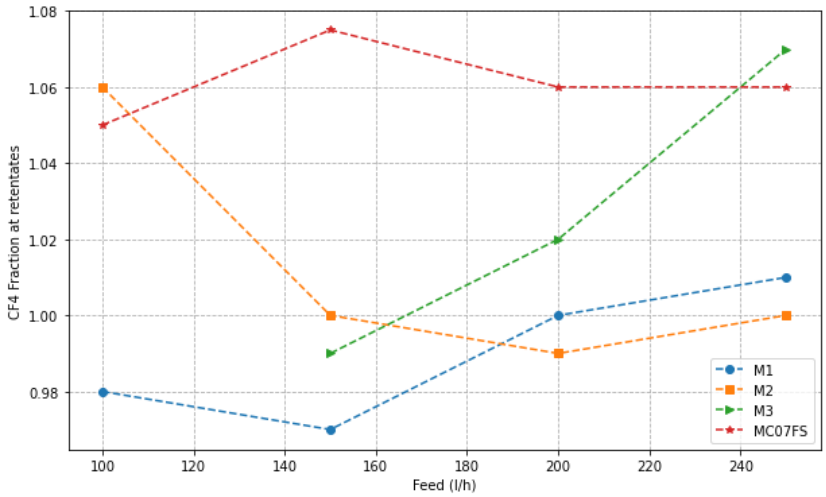

Figure 51 CF_4 fraction at the retentate side VS membrane feed flow.

The plot shown in Figure 51 summarises the results obtained for M1, M2, M3 and MC07FS. It is clearly visible as there isn't any significant difference between the four membranes. All of them show a good separation efficiency of around 100% that slightly increases with the input flow, as seen in the previous paragraph.

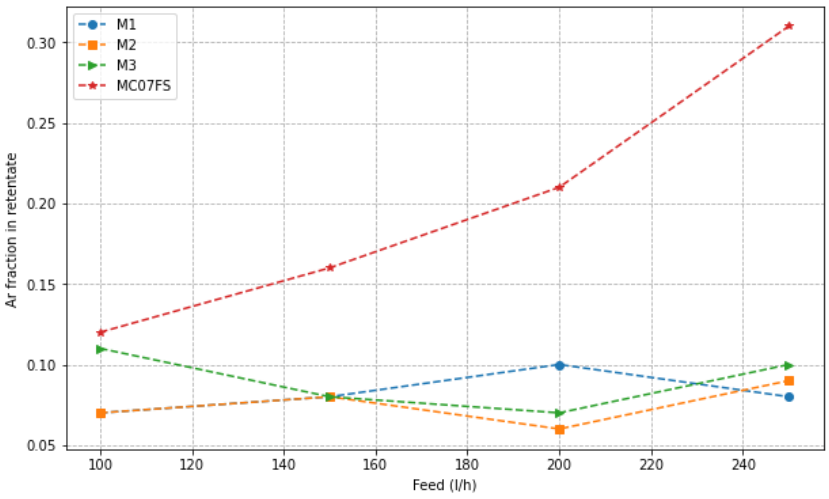

Figure 52 Ar fraction at the retentate side VS feed flow.

During the tests, the second parameter analysed was the concentration of Argon (Ar) at the retentate side, which was considered a contaminant.

$$Ar\ fraction = {Volume\ Ar^{Output}}/{Volume\ Ar^{Input}}$$

Figure 52 illustrates that the membranes exhibit different behaviours towards Ar. Specifically, membranes with high thickness and density gradient (M1, M2, M3) demonstrate greater selectivity towards CF_4, indicating not only to CO_2 but also to most of the Ar is removed through the permeate side.

On the other hand, the MC07FS operates differently, showing reduced selectivity towards CF_4 as the feed flow increases, letting also Ar evacuating through retentate side. This can be explained considering that this module has been optimized for CO_2 separation and that in general, this kind of separation device performs better at higher flows settings. Since our focus was on the recovery of CF_4 rather than CO_2, this membrane is unsuitable for the CSC CF_4 recovery system due to the high contamination of Ar at the retentate side in comparison to the other membranes tested.

M4 was tested as well and showed the same behavior seen for M1, M2 and M3.

Considering the input flow to the recuperation system between 500 and 700 l/h, at the end of the test it was decided to work with 2 membranes “low flow” (M2 and M3) and one membrane “high flow” (M4).

Then the overall efficiency of the module was tested, and the results are shown below in Figure 53.

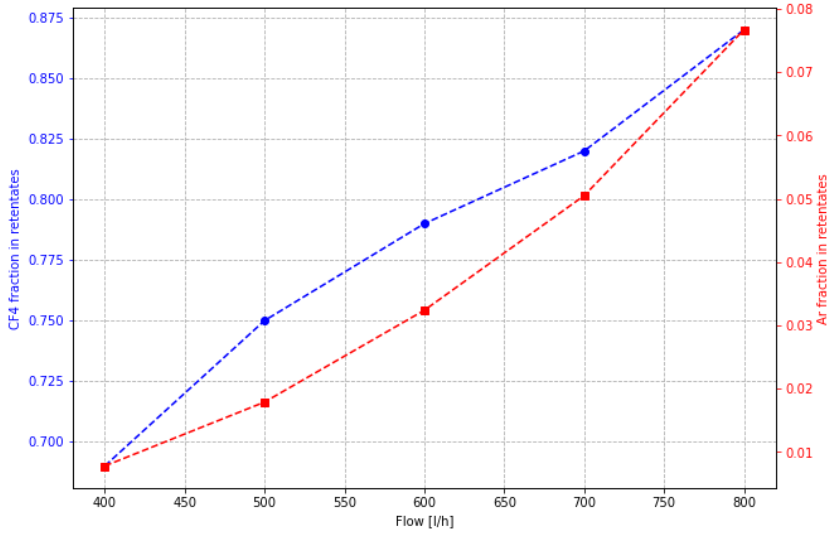

Figure 53 CF_4 and Ar fractions at the retentate side of the membranes module (M1, M2 and M3) of the CF_4 recovery plant VS feed flow.

The data from the plot above clearly demonstrates that the overall efficiency of CF_4 separation is significantly impacted by the feed flow rate compared to the single membrane tested previously. It is evident that as the flow rate increases from 400 l/h to 800 l/h, the CF_4 recuperation efficiency also increases by almost 30%. However, it is important to note that the concentration of Ar also increases at the same time. According to the tests, the tradeoff between quality and efficiency is observed at around 600 l/h, where the CF_4 fraction at the retentate side is approximately 75% and the fraction of Ar stands at around 3%.

The performance of the membrane module is affected by another parameter, which is the permeate pressure. Figure 54 shows that as the pressure difference between permeates and retentates increases, the quality of recuperated gas at the retentates improves. However, more CF_4 is also found at the permeates, leading to a decrease in efficiency. Additionally, increasing the feed flow results in both higher CF_4 recuperation efficiency but increased concentration of contaminants. In this case, the tradeoff between recuperation efficiency and quality of CF_4 recuperated is observed at 600 l/h and a permeate pressure between -0.5 barg and -0.6 barg.

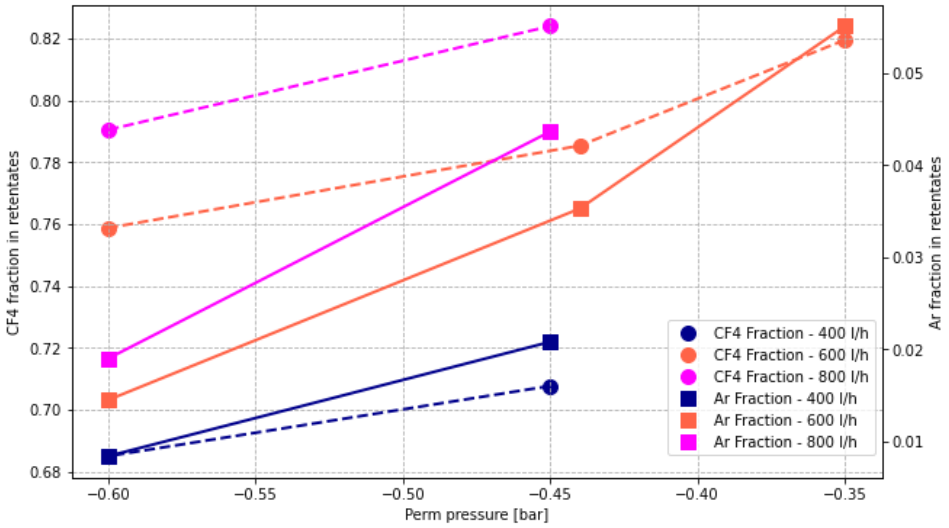

Figure 54 CF_4 and Ar fractions at the retentate side of the membranes module VS permeate pressure.

3.3.3 Characterization of 13X Absorber Module

The first part of the tests on the 13X Absorber Module were focused on finding the best pressure value at which the CF_4 recuperation starts. As anticipated at the beginning of this paragraph, in this module the adsorption process in based on PSA. The process can be summarized as following:

1. The filling procedure starts from vacuum (-0.9 barg) and it ends when the atmospheric pressure is reached.
2. For $P=P_{atm}$, the emptying phase starts.
3. From P_{atm} to -0.45 barg the contaminants not adsorbed by MolSieve are vented to air.
4. From -0.45 barg to -0.9 barg, the CF_4 and some percentages of Ar are desorbed and sent to the storage battery, the MolSieve is regenerated.

Before performing these tests, the pressure (also called "*Argon low limit pressure*") for the recovery of the CF_4 was set at -0.70 barg leading to a very low recuperation efficiency since most of the CF_4 was lost before reaching that pressure inside the column.

The tests were performed increasing step by step the *Ar low limit pressure,* measuring the overall efficiency of the recovery system and monitoring the composition of the CF_4 recuperated at the same time. The results are shown in Figure 55.

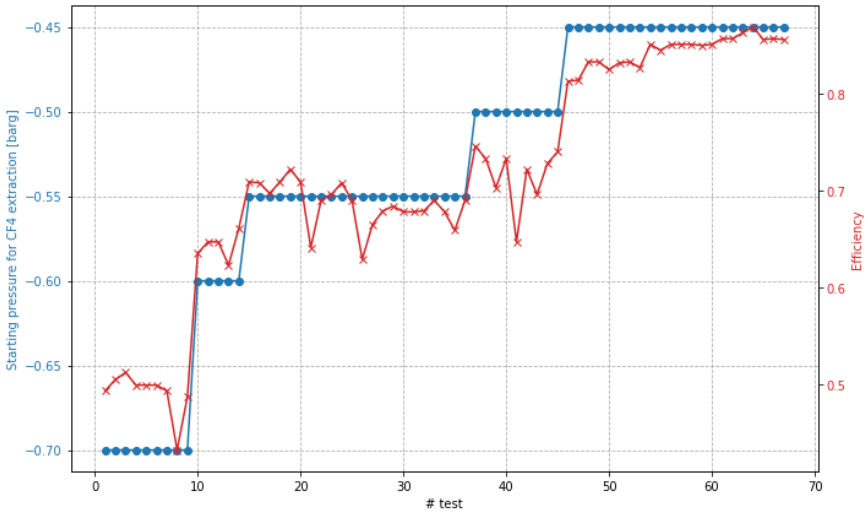

Figure 55 Summary of the tests performed on the 13X absorber module at different extraction pressure and relative efficiency values.

According to the plot, increasing the pressure at which CF_4 is extracted from the column results in a greater quantity of gas, leading to improved separation efficiency. However, the quality of the CF_4 must be controlled to be sure to recover the most of CF_4 and to not contaminate the recuperation battery with other compounds.

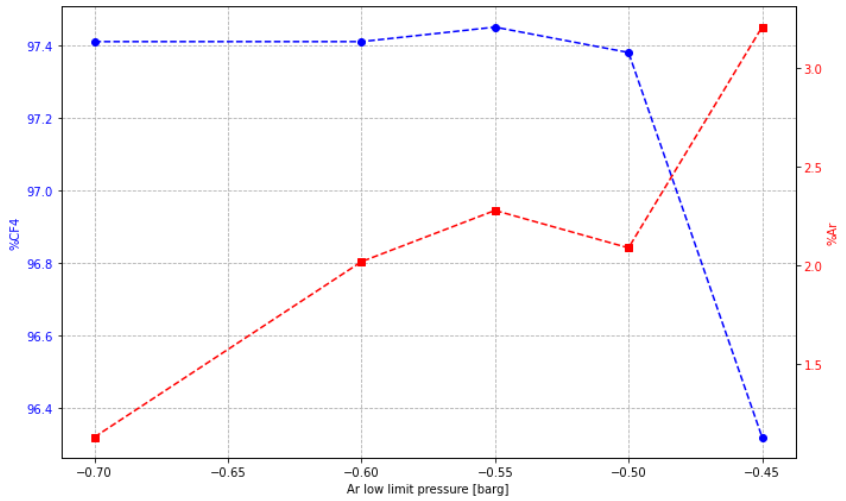

Figure 56 CF_4 and Ar concentrations at different extraction pressure in the 13X absorber module.

In Figure 56 the trends in concentrations of CF_4 and Ar at different Ar low limit pressure values are shown. Despite the significant increase of pressure for the CF_4 extraction, the composition of the recovered gas didn't change, confirming the success of this test.

The tests were performed during the LHC Long Shutdown 2 when the CSC gas mixture was set at $Ar/CO_2/CF_4$ 40/55/5. In contrast, during LHC RUN periods, the CSC detectors operate with a gas mixture of $Ar/CO_2/CF_4$ in a ratio 40/50/10. Indeed, when the CF_4 in the mixture is at 5%, the column requires about 2 hours to fill, while introducing 10% CF_4, the filling time is behalf. The reduction in filling time and contact time between gas and zeolites significantly decreases the amount of CF_4 absorbed, resulting in a final gas composition of approximately 85% CF_4 and 15% Argon.

One possible explanation is that the quantity of material inside the column is not enough to trap that volume of gas. According to data found in literature [25], at 298 K and between -0.9 barg and -0.052 barg the amount of CF_4 absorbed into 13X MolSieve is around 0.1 mol/kg. Considering that the amount of zeolite in the module is 25 kg, the maximum volume of CF_4 that can be adsorbed is ~55 liters, that is lower than the volume ideally arriving at the CF_4 Absorber module when 10% of CF_4 is present in the mixture. Some tests to understand how the contact time influences the separation process will be performed in the next months.

3.3.4 Procedure for the reinjection of the CF_4 recuperated at the CSC mixer

The two main scopes of recovering the CF_4 are the abatement of GHGs emissions and to prevent possible future shortages or unavailability of gas due to the European legislation. The first scope is achieved by reinjecting the recuperated CF_4 at the CSC mixer through a fourth Mass Flow Controller that is exclusively designated for this purpose.

For this purpose, the recovered gas is sent to the storage module made of two batteries of 12 bottle of 50 liters each, one used to recover the gas, and the other one used to reinject the gas to the mixer. The gas is stored in the battery thanks to a compressor specifically designed for freon gases. Even though the recovery system is fully controlled by software, the swap of the battery is done manually every time it is needed. In particular, the swap is required both when the battery used for injection reaches a pressure lower than 5 barg or when the battery used for storage reaches a pressure higher than 40 barg.

This procedure requires a careful monitoring through µGC analyses and the other monitoring systems described before. This is needed since the quality of a battery can be different to the other one and the detectors are very sensitive to change in mixture composition or to the presence of impurities. Analyses of the CSC mixer are usually performed just before and after the battery swap and then the new battery used for the injection of CF_4 recuperated is analyzed. Some results are shown in the plots below.

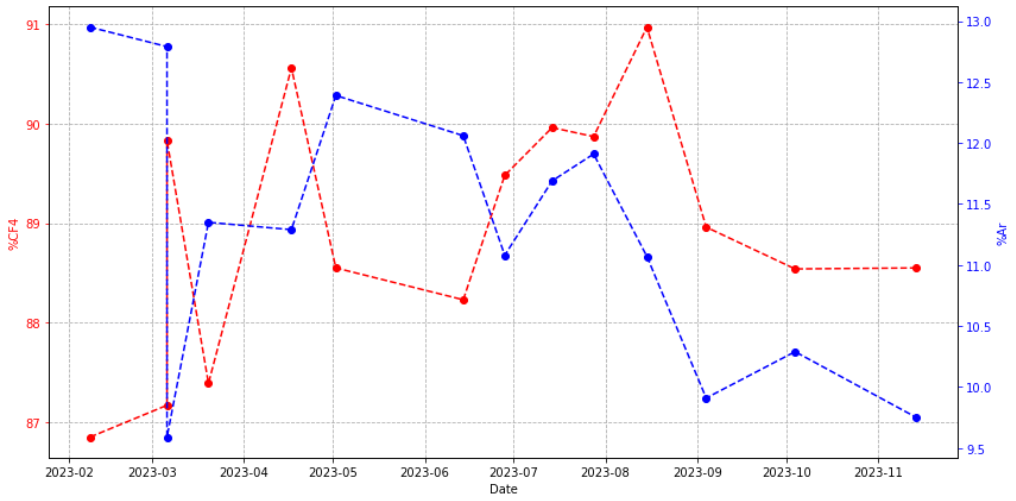

Figure 57 CF_4 and Ar concentrations in the recovery bottle VS time.

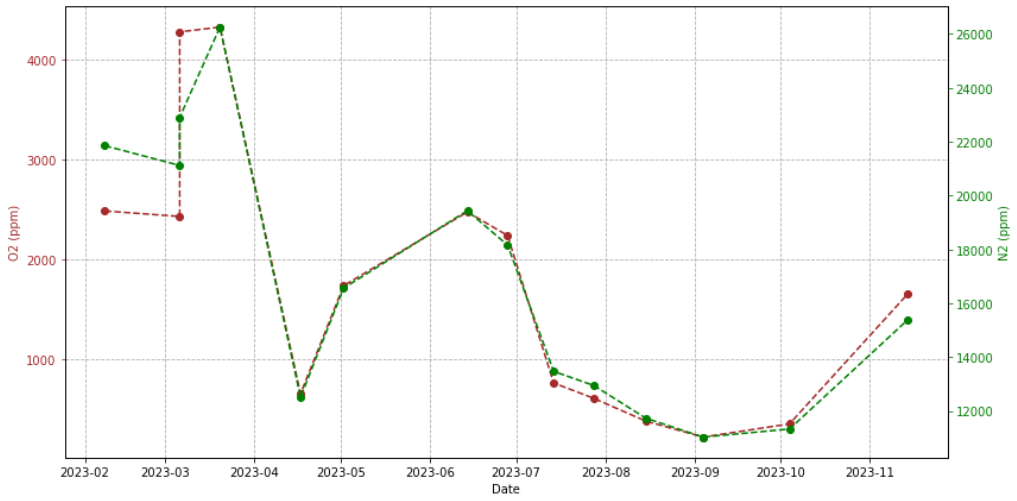

Figure 58 O_2 and N_2 concentrations in the recovery bottle VS time.

In Figure 57 and in Figure 58 some results of the analyses performed for the battery swaps are summarised. During 2023 the compositions of the batteries was almost constant, with the CF_4 oscillating between 87% and 91% and Ar between 9.75% and 13%. As concern the air content, O_2 oscillated between 900 ppm and 4500 ppm while N_2 between 1.2% and 2.6%. Even if O_2 and N_2 pose challenge for the detectors, their concentration are negligible taking into the total volume, so they don't generate any issue for the detector operation. Moreover, it was found out that the amount of N_2 injected at the mixer doesn't influence the concentration of N_2 at the Exhaust module, that is the gas enriched in air after passing through the chambers.

After some software upgrades, it is now possible to adjust the CF_4/Ar ratio in mixer recipes based on analyses. As a result, the software can now automatically fine-tune the flow of recuperated CF_4 to obtain the correct gas mixture for CSCs. Despite issues with the quality of CF_4 recuperated when it accounts for 10% of the original gas mixture, the substantial recovery of CF_4 has necessitated adjusting the ratio of recovered to fresh CF_4 to 60/40.

The initial design of recovery system was made to inject the CF_4 recuperated in a ratio 50/50 with the fresh one. Initially, in 2012, it was not feasible to achieve a recuperation efficiency of 50% for CF_4, as the recuperated amount was below this threshold. From 2020 onwards, intensive research and development efforts enabled the recuperation efficiency to reach and subsequently exceed 50%, as depicted in Figure 59. This rapid increase in efficiency marked a significant advancement in the process.

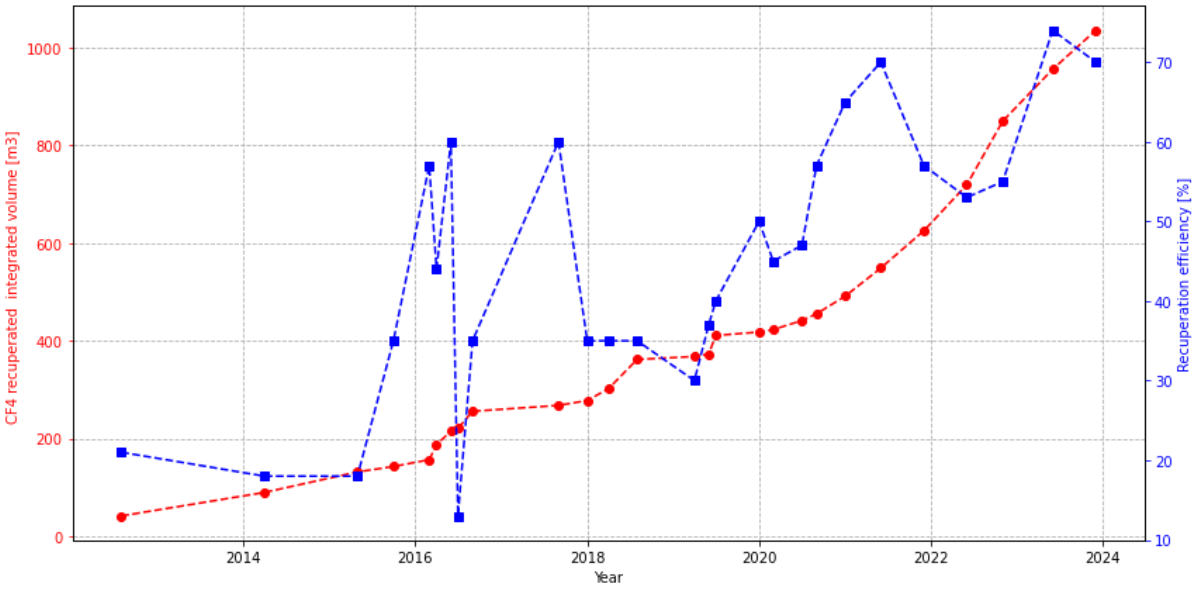

Figure 59 CF_4 integrated volume and recuperation efficiency VS years.

The efficiency reached a peak in 2021 and then it decreased. This was due to change in the gas mixture composition that passed from 5% to 10% of CF_4 with the consequences seen in the previous paragraph. Moreover, at that time only one of the two columns of the CF_4 Absorber module was operational, which slower the entire process and caused also a CF_4 loss. At the end of 2023 the second column was fixed and put in run, leading to a fast increase in the recuperation efficiency that went back to the optimal value of 70%.

3.4 LHCb RICH1 C_4F_{10} Recuperation system

The LHCb RICH1 gas system has a volume of 6 m^3 and the detector works with pure decafluorobutane (C_4F_{10}). After a lot of tests, this gas that belongs to the n-Perfluorocarbon family, satisfies the following requirements for the detector operation:

- High and stable refractive index (up to 200 nm)
- Good transparency
- Long radiation length

The C_4F_{10} gas, like other fluorinated gases, has a high GWP of 9200. To limit emissions, the detector operates in a Closed Loop with a recirculation fraction of 100%. However, due to oscillations in atmospheric pressure, some gas is occasionally exhausted to the air through bubblers mounted in the experimental cavern at the level of the chamber. Consequently, an equivalent amount of gas must be supplied through the mixer to maintain stable the chamber pressure. Similar to RICH2, RICH1 is very sensitive to impurities accumulated in the gas, such as air and water. Their level must not exceed 2% and 0.1%, respectively. Another issue related to the use of C_4F_{10} is its limited availability on the EU market due to recent regulations for the use of fluorinated gases, as discussed in *Chapter 2 "Greenhouse Gases and their use at CERN"*. This underscores the critical need to urgently find a solution to minimize its waste.

The detector is designed with a unique process that involves emptying and refilling it periodically according to the LHC schedule. Before each run, it is filled with pure C_4F_{10}, and before the End of the Year Technical Stop (EYETS) for maintenance and upgrades, the C_4F_{10} is removed from the detector, purified, stored and replaced with pure CO_2. This meticulous process significantly reduces the risk of gas loss due to human error or technical issues. Additionally, once a year, the gas undergoes a thorough purification to eliminate air and water impurities. This ensures the integrity of the gas inside the detector, maintaining its quality and effectiveness.

These procedures are common named *Filling* (from CO_2 to C_4F_{10}), *Emptying* (from C_4F_{10} to CO_2) and *Cleaning* (purification of C_4F_{10}). The gas recovered during these steps is then reinjected into the detector, limiting the consumption of fresh C_4F_{10}.

3.4.1 Recuperation plant

The recuperation plant now used for the C_4F_{10} was not designed for this purpose but it was adapted from an old gas system used for the DELPHI experiment. During each process described above, the gas is firstly sent from the mixer to the detector which is filled from the bottom and emptied from the top. This is done for the same reason as explained previously for the RICH2: as C_4F_{10} is heavier than CO_2 during the first hours of the filling procedure, the mixing of the two gases is forbidden, so that only the CO_2 is exhausted from the detector. When the C_4F_{10} reaches a concentration higher than 40%, it starts to be visible at the exhaust module through μGC analysis and the recovery process starts. The RICH1 gas loop is schematized in Figure 60.

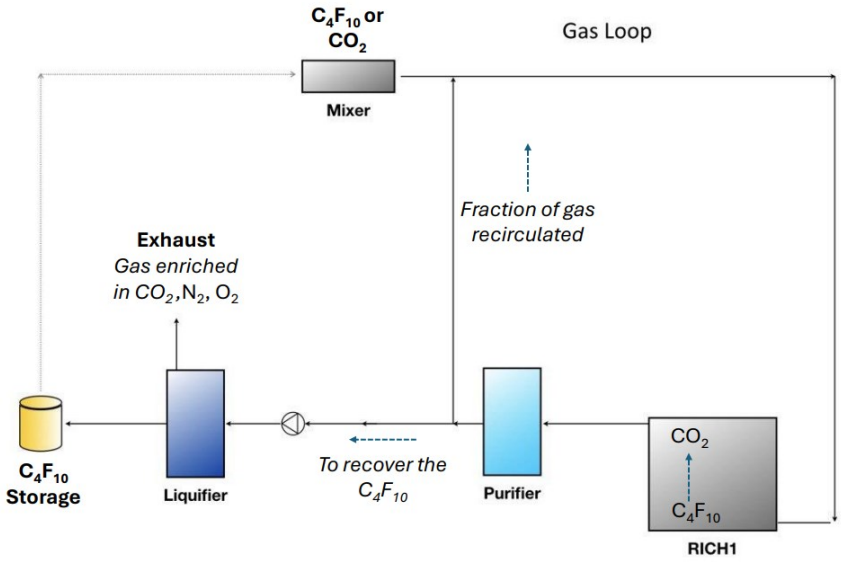

Figure 60 Scheme of the LHCb RICH1 gas system with the recuperation plant.

The recuperation plant is used only during filling, emptying or cleaning procedure and is then switched off and removed from the gas loop. During the recuperation process there are two possible operation modes:

- Open Loop, i.e. all the gas exhausted from the detector is sent to the recovery plant where the impurities are vented to the atmosphere and the C_4F_{10} is recovered in the bottle
- Closed Loop, that means the gas is partially recirculated and only a fraction of the gas exhausted from the detector is sent to the recovery plant.

In the first case the procedure is critical because the use of the recovery system can impact the pressure of the detector that must be kept at around 0.1 mbarg to not damage its mechanical structure. In the second configuration the pressure in the loop is more stable and the gas is also well mixed. Only in the last year the second configuration has been adopted.

The C_4F_{10} recuperation process is very crucial to minimize its environmental impact and for its shortage especially in the European market. On the other hand, the recovery system is the recovery system is not entirely automated, so that valves and rotameters are manually controlled by an operator that must monitor the entire process. This makes this recuperation process more difficult and riskier. For this reason, a new recovery system for the C_4F_{10} have been designed by EP-DT-FS Gas Group at CERN and will be installed and tested in the next months.

In Figure 61, the schematic view of the Liquifier module is depicted, which is used to recover C_4F_{10}. The gas is extracted from the gas loop by a pump and sent to the cold box, set at around -30°C, where flash distillation occurs. The liquefaction temperatures of CO_2 and air differ significantly from those of C_4F_{10}. This temperature difference allows the impurities to remain in the gas phase and be released to the atmosphere, while the perfluorobutane is liquefied and sent to the recovery bottle. The C_4F_{10} in the bottle is in liquid form due to the storage conditions: 2.5 barg and 298 K. The recuperation plant must operate at a higher pressure than the bottle's pressure and it ensures that the recovered C_4F_{10} can be transferred from the plant to the bottle.

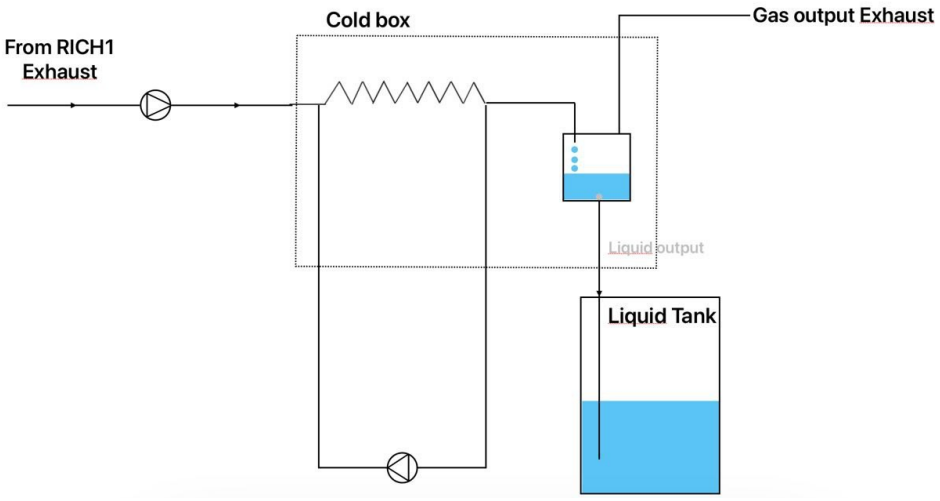

Figure 61 Scheme of the RICH1 C_4F_{10} liquifier module.

When the recovery system started, CO_2 was used to increase the pressure in the recuperation buffer and transfer the liquid into the bottle. However, this procedure caused some CO_2 to dissolve into the liquid C_4F_{10}. As a result, when the liquid was transferred to the bottle, the CO_2 turned into gas, increasing the pressure in the bottle from 2.5 barg to 5 barg. Consequently, the recovery system began working at higher pressures, leading to a higher concentration of CO_2 in the recovered gas. To address this issue, we started cleaning also the bottle. This significantly reduced the amount of CO_2, allowing the recovery system to work at lower pressure.

3.4.2 C_4F_{10} Recuperation Process

In this section the filling, emptying and cleaning procedures of the RICH1 detector will be described. The performance of the recuperation system is reported in terms of its efficiency in separating and re-using C_4F_{10} for detector operation.

3.4.2.1 RICH1 Filling Procedure

The RICH1 is typically filled before LHC collisions resume. To start, the detector is filled with 100% CO_2 and must then reach almost 100% C_4F_{10}, with a tolerance of a few ppm of air and CO_2.

The detector is equipped with four valves: two for filling and two for emptying. It is typically filled from the bottom and emptied from the top, as the different gas densities allow for the extraction of only CO_2 at the beginning of the filling process, thus preventing the waste of C_4F_{10}. This process is illustrated in Figure 58.

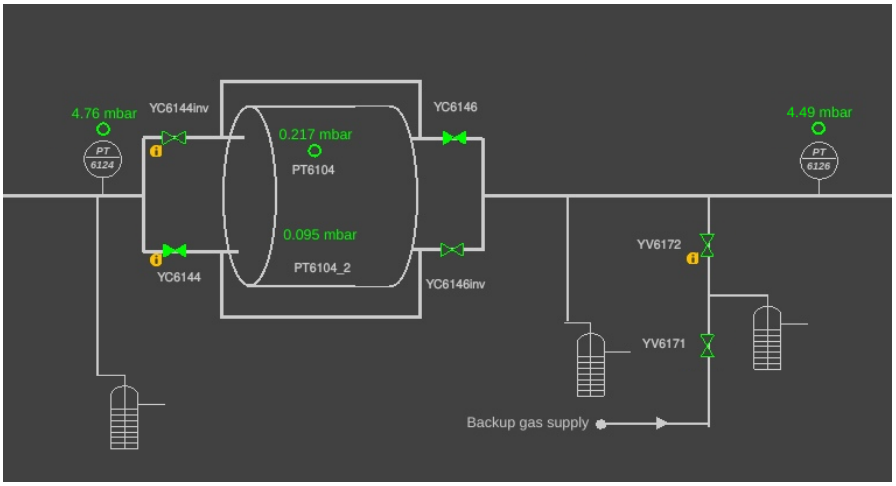

Figure 62 WinCCOA view of the RICH1 detector. YC6144 and YC6146 are ON during the filling of the chamber.

The bottle used for both recovery and injection of C_4F_{10} has two distinct sampling lines. One line is for the liquid phase, which sends gas from the bottle to the mixer, while the shorter line injects gas from the recuperation system to the bottle. Given the CO_2 contamination, it's essential to conduct μGC analyses to determine the liquid phase composition before injecting the gas into the detector. Figure 59 summarizes the analysis results for the liquid phase over the past three years.

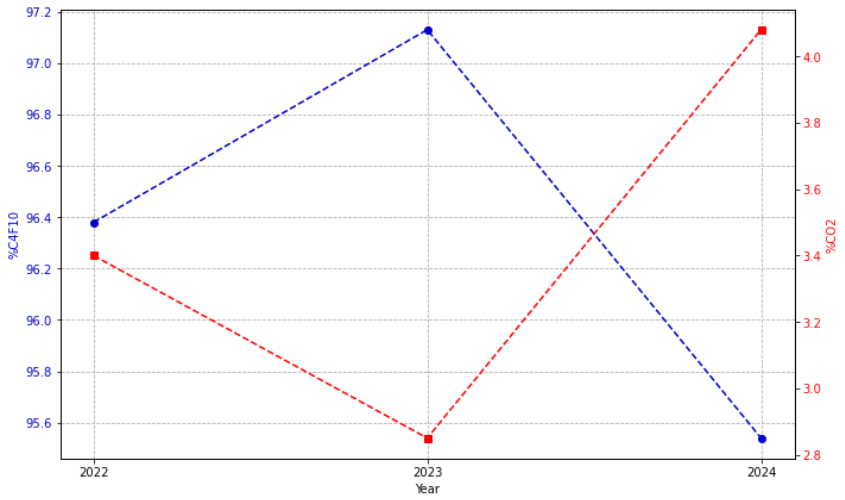

Figure 63 C_4F_{10} and CO_2 concentration in the recovery bottle over the past three years.

The quality of the bottle directly impacts the maximum gas purity achievable in the detector. If the gas mixture changes, the concentration of different compounds and the chamber pressure are the two key parameters monitored. Similar to RICH2, the pressure measured at the chamber's output is influenced by the hydrostatic pressure exerted by the gas column, which is as tall as the chamber volume. Notably, when the column is mostly CO_2, the output pressure is approximately -5 mbar, but when it is primarily C_4F_{10}, it reaches around -75 mbar. This transition between the two values provides a clear indication of the changing gas mixture composition and an example of the results obtained with μGC analysis are shown in Figure 64.

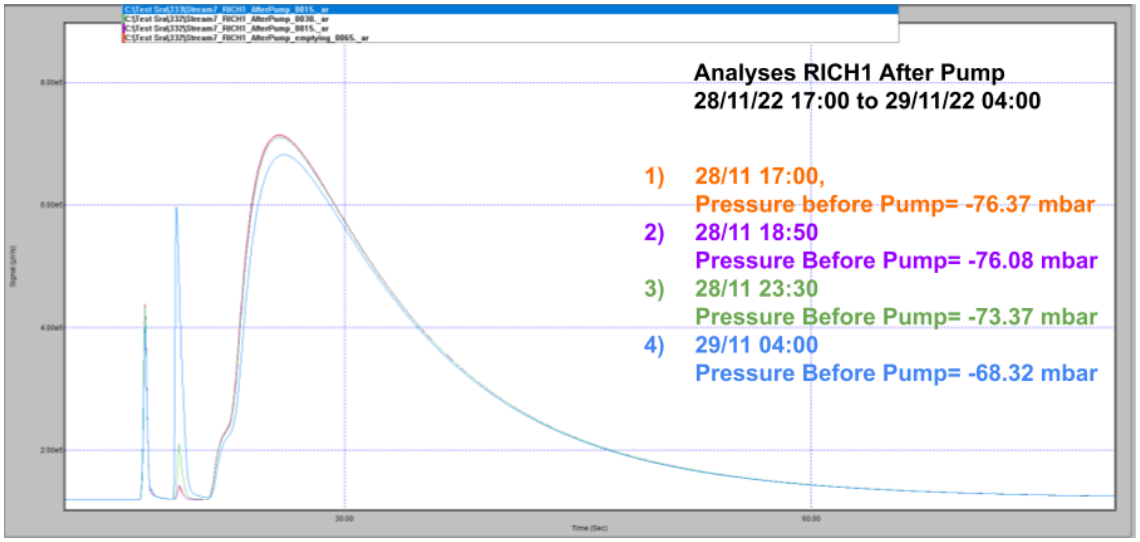

Figure 64 Example of the chromatograms (Signal [mV] VS Time [sec]) performed during the emptying procedure of the RICH1 detector.

The graph in Figure 65 shows the trends of C_4F_{10} and CO_2 concentration during the filling process that took place in March 2022. At the start of the filling, both compounds remained stable for about 9 hours. After that, their concentration changed rapidly until reaching a composition of 90% C_4F_{10} and 10% CO_2. This composition is typically achieved within 48 hours when the mixer is set at 150 l/h. The recovery system kicks in when the concentration of C_4F_{10} at the exhaust of the RICH1 is around 30% and operates continuously until the 80% concentration is reached.

In order to increase the concentration of C_4F_{10} from 80% to 100%, it is necessary to inject C_4F_{10} for around 10 days at 8 hours per day. When the CO_2 concentration exceeds that of C_4F_{10}, the recuperation process is easier. However, when the CO_2 concentration drops below 20%, the recuperation process becomes critical, leading to a high risk of wasting C_4F_{10} at the exhaust due to the high pressure in the recovery plant and the lack of software control. Therefore, continuous operation demands a rigid supervision.

When the gas mixture in the detector matches that of the bottle, there are two possibilities:

- Installing a new bottle of pure C_4F_{10} in the mixer module to increase gas quality in the detector, according to the experiment requirements.
- Using Purifier module to absorb the CO_2 until it is less than 1%. With each purifier cycle, a remarkable 1.2% of CO_2 is absorbed.

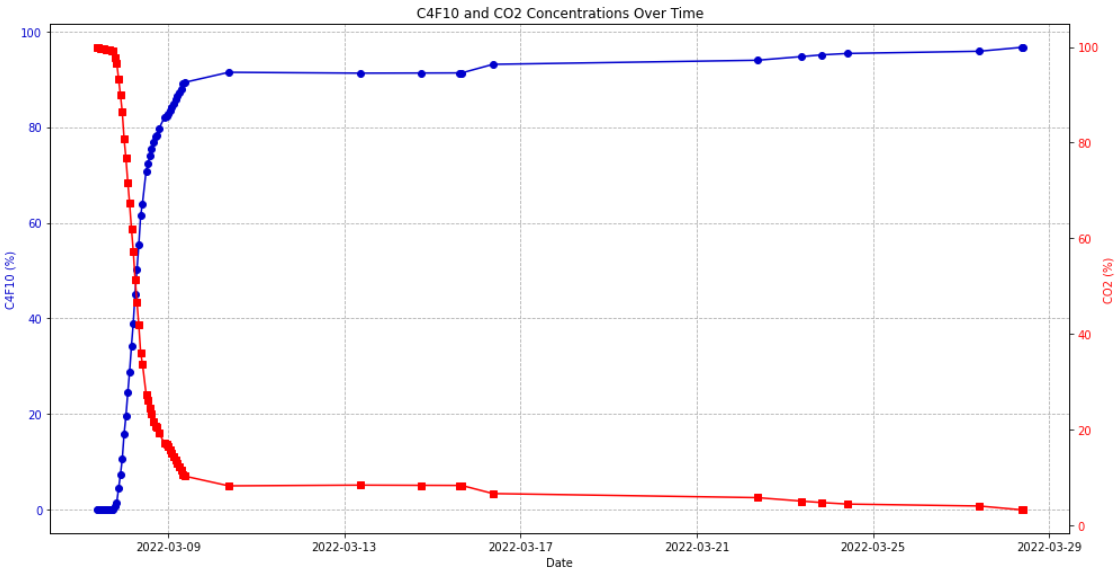

Figure 65 C_4F_{10} and CO_2 concentration during filling procedure.

The efficiency of the recovery system is calculated based on the gas flow injected into the mixer and the difference in weight of the bottle between the beginning and the end of the procedure. With a total gas system volume of 6 m^3, the amount of C_4F_{10} needed to fill is estimated of 60 kg. However, during the filling of the detector, around 110 kg of C_4F_{10} are injected from the mixer,

indicating that at least two volumes are required to achieve the right gas composition in the detector.

In the last three years, more than 150 kg of C_4F_{10} would have been released into the atmosphere without the recovery system. However, only 30 kg are genuinely missing, indicating that the recovery system operated with an 80% efficiency during the filling processes.

3.4.2.2 RICH1 Emptying Procedure

Prior to the start of the LHC maintenance period, typically scheduled at the end of the year, the C_4F_{10} is removed from the RICH1, recovered, and replaced with 100% CO_2. Throughout this process, monitoring is conducted using μGC analyses and by measuring the hydrostatic pressure value.

To empty the detector the mixer is set at 150 l/h in CO_2 and the recovery system is immediately integrated in the gas system loop, to recover the C_4F_{10} exhausted from the chamber. The exhaust of the recovery system is kept closed for the first hours, until the CO_2 concentration is around 20% and the hydrostatic pressure is approximately -50 mbarg. After two days the gas inside the detector passes from 100% of C_4F_{10} to 100% of CO_2. When the pressure before the pump is - 5 mbarg, the injection from the mixer and the recovery plant are stopped and the gas inside the system is left to circulate and homogenize for around 24 hours. Usually during this period, the hydrostatic pressure increases indicating that some C_4F_{10} is still present in the bottom part of the detector. When this occurs, the injection from the mixer and the recovery system are restarted to recover the remaining C_4F_{10} until its real concentration in the detector is below 5%, as depicted in Figure 66. Thanks to the use of the recovery system less than 9 kg were lost per emptying process, resulting in a recuperation efficiency higher than 85%.

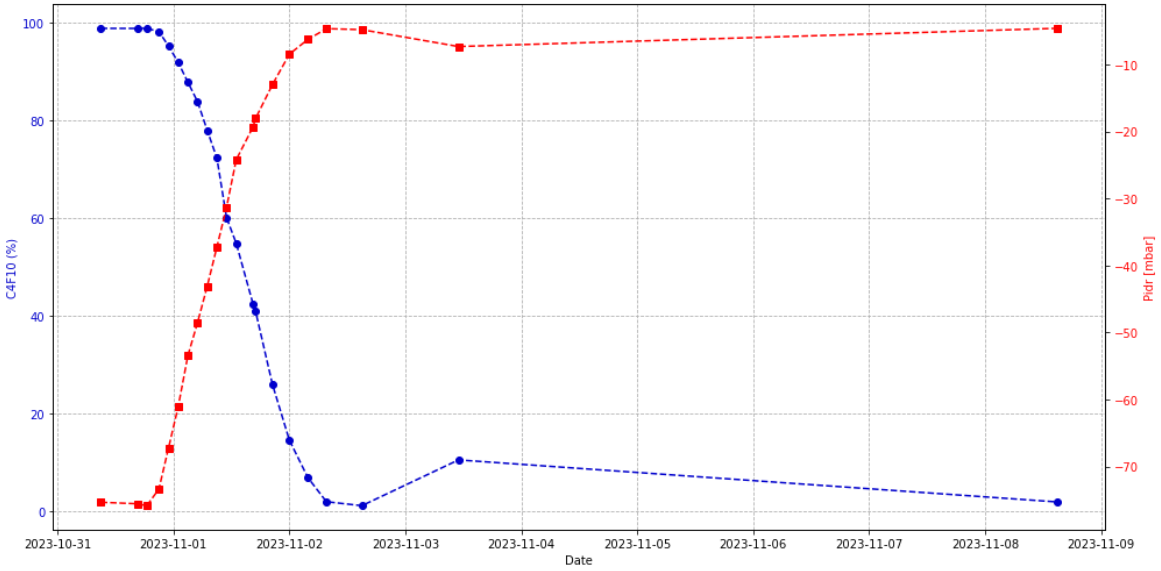

Figure 66 Trends of C_4F_{10} and hydrostatic pressure during emptying procedure.

3.4.2.3 RICH1 Cleaning Procedure

The cleaning procedure is carried out between filling and emptying steps to reduce the concentration of air, which can affect the detector's operation [24]. It is also performed at the end of the filling process to reduce the CO_2 concentration at below 1%. It is often couples with the purifier module. The main difference between the filling and cleaning modes is the setting of the gas loop. In the filling mode, the gas loop is set to open, while in the cleaning mode, it is set to closed, which means that the gas is recirculated and only a fraction is sent to the recovery system. Since the flow to the plant is limited and the concentration of the compounds that need to be vented is very low, this procedure is time consuming, usually around one week, more than the other two procedures previously mentioned. In Figure 67 an example of the chromatograms obtained during the cleaning phase is depicted.

The exhaust line of the recovery system must be manually adjusted using a rotameter and a back pressure regulator to vent only CO_2 and air. However, their concentrations fluctuate rapidly, and sometimes C_4F_{10} is also released into the atmosphere, reducing the overall efficiency of this process to 90%.

Similar to the other recovery systems mentioned earlier, the best configuration for the RICH1 recovery plant is a balance between quality and efficiency, particularly during the cleaning phase.

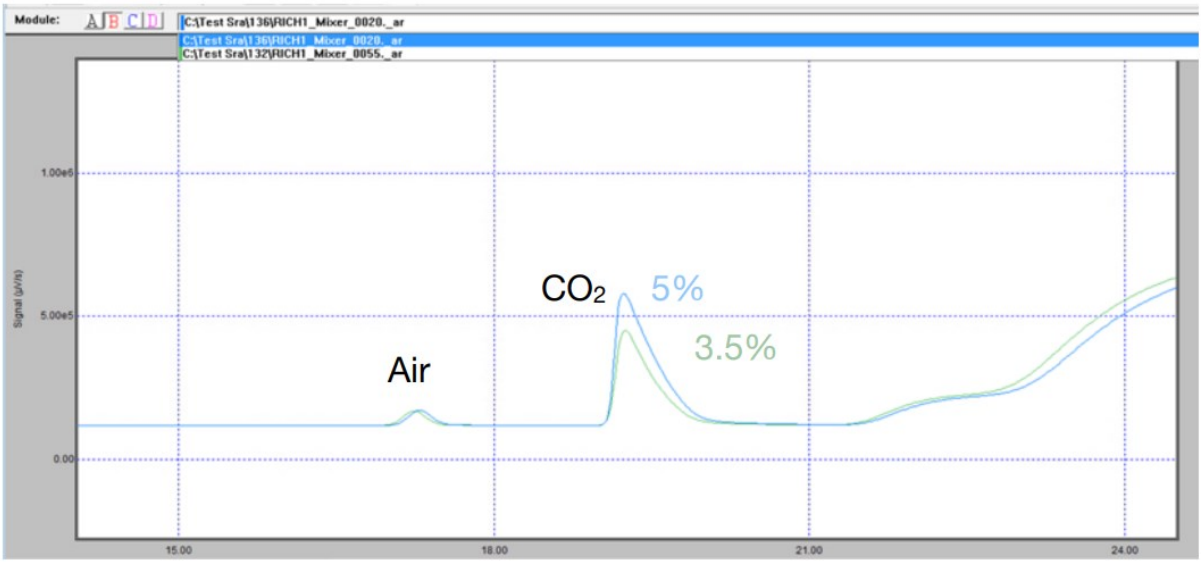

Figure 67 Example of the chromatogram obtained during the cleaning phase.

3.4.3 Research activity on C_4F_{10} recover from the Purifier module

Water is one of the contaminants that affects the RICH1 performances. It can permeate the material of the detector and accumulate within it. To overcome this problem, a purifier module is utilized, featuring two parallel 11 litres cartridges filled with MolSieve 5Å for H_2O adsorption through TSA process. The gas is efficiently purified as it passes through the column at a flow rate of 78 l/h and a pressure equivalent to that of the gas loop. The impurities are quantitively removed from the gas, while the rest of the gas mixture remains unaffected. When the run volume reaches 70 m^3, the column swap occurs by regenerating the saturated column through a vacuum process and subsequent heating up to 200°C.

However, as seen earlier for the RICH2, this type of material is able to trap also small amounts of CO_2 and C_4F_{10}. As a result, conditioning the column before the gas circulation is necessary to prevent any changes in the gas mixture composition or fluctuation of the gas loop pressure. The decrease in the buffer pressure and the consequent injection from the mixer suggested that a not negligible amount of C_4F_{10} was trapped by the MS, so some tests were performed to quantify the C_4F_{10} in the material and to explore the possibility of recovering the gas extracted from the purifier just before the thermal regeneration step.

The initial series of experiments aimed to quantify the alterations in gas composition subsequent to its passage through the purifier. In this purpose, many µGC analyses have been performed: the analysis started 20 minutes before the column entered the gas loop, to have a reference of the gas mixture before interacting with the material just regenerated. The first test lasted 4 hours and the results are shown in Figure 68.

The gas mixture composition before the purifier was measured as C_4F_{10} 87%, CO_2 12.8%, and air 0.2%. According to the provided plot, as the regenerated column of the purifier enters the loop, MS absorbs almost quantitatively CO_2 and saturates in around 4 hours. The same test was repeated five times, with the longest test lasting 12 hours, showing reproducibility of the data. Taking into account the gas flow to the purifier and its composition afterwards, the cumulative flow over time was determined to be approximately 75 litres of CO_2 absorbed per cycle. This is also confirmed by the calculation done during the recuperation process, according to which the CO_2 decreases by around 1% every time the purifier columns swap.

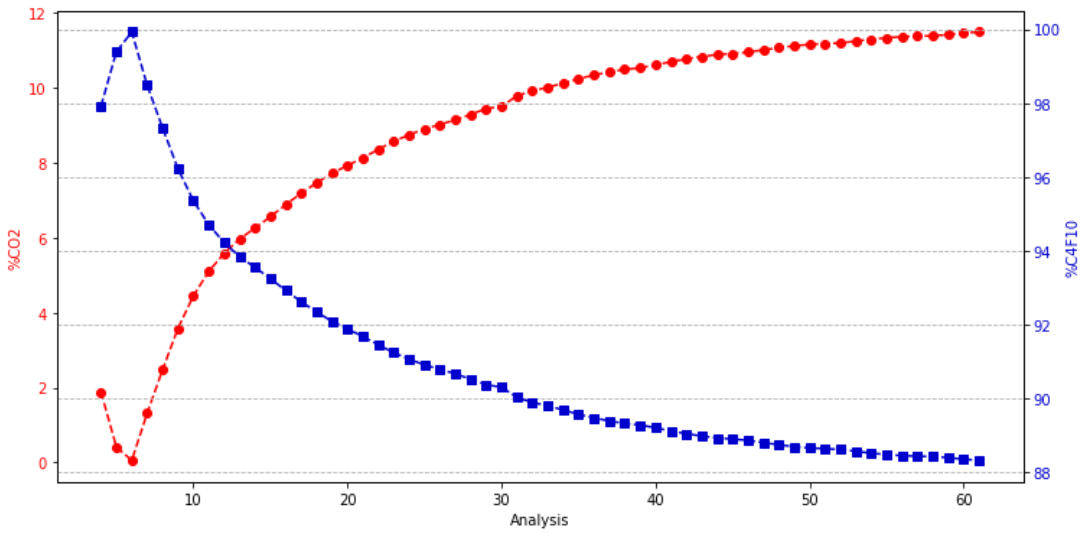

Figure 68 Trends of CO_2 and C_4F_{10} at the output of the purifier module over time.

The second test aimed at understanding if C_4F_{10} could be recovered from the MS during the initial phase of the regeneration of the column under vacuum. The procedure was set to extract the gas from the column by a vacuum pump and send to a small Festo buffer of 0.75 litres, until the pressure inside reached 100 mbarg (Figure 69). At that point, the emptying of the purifier column

was stopped and around 10 µGC analyses of the gas concentration in the volume were performed via µGC. This procedure was repeated until the purifier cartridge reached vacuum. Between each step, all the pipes and the Festo volume purged with Helium and subsequently vacuumed o ensure cleanliness. During the test some parameters were continuously controlled, such as the initial and final pressure of the purifier column at each emptying step, pressure of the Festo buffer and the concentration of C_4F_{10}, CO_2, O_2 and N_2 at each step.

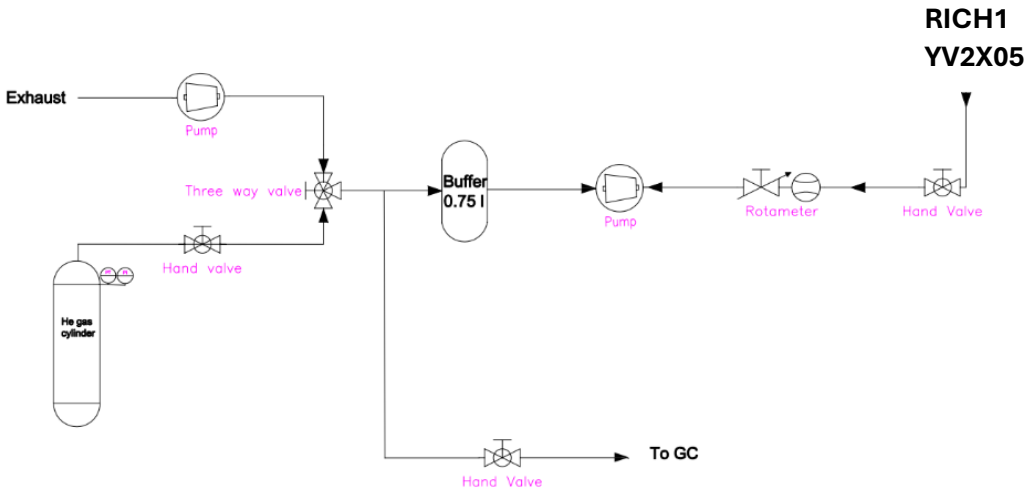

Figure 69 P&ID of the setup used for the RICH1 purifier test.

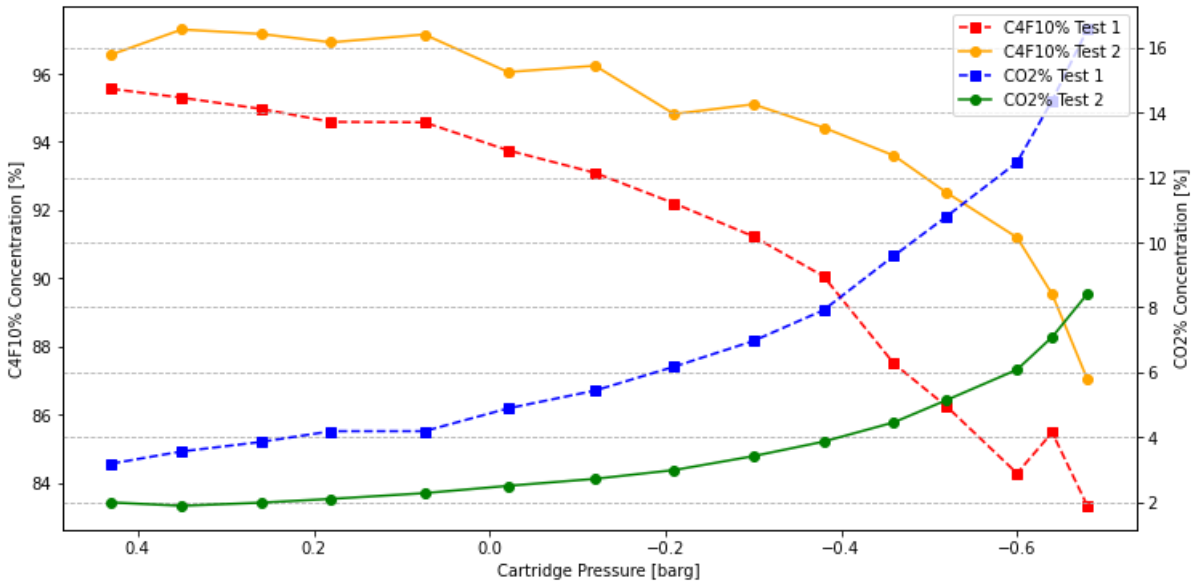

Figure 70 C_4F_{10} and CO_2 concentration VS pressure in the purifier cartridge.

The outcomes of two tests for emptying the purifier module are detailed in Figure 65. Test 1 had a higher CO_2 content in the initial gas mixture compared to test 2 (3.6% vs 2.6%, respectively). The gap is evident for the CO_2 concentration at the beginning and end of the tests. In test 1, the CO_2 started at 3.6% and rose to 16.5% by the end of the extraction; whilst in Test 2, it started at 2.6% and reached a maximum of 8%. It can be concluded that the initial composition of the gas passing through the purifier module impacts the quality of the extracted gas. However, by considering the extracted volume and the buffer pressure, it was possible to calculate that approximately 15 litres of C_4F_{10} and 1 litre of CO_2 were extracted in all the tests performed.

In the final test, the column was heated up and completely emptied, and the extracted gas was analysed through μGC. The results indicated that the gas recovery in this step is not cost-effective, as only 6 out of the 19 litres extracted were C_4F_{10}, with the rest being CO_2.

These results confirmed that it is convenient recovering the gas extracted from the purifier cartridge only during the vacuum regeneration phase. Considering the run volume of the column and the input flow to the module, thanks to this procedure 150 litres of C_4F_{10} are saved per year.

.

3.5 CMS RPC $C_2H_2F_4$ (R134a) Recuperation system

The RPC systems at the LHC are mainly operated using a $C_2H_2F_4/iC_4H_{10}/SF_6$ gas mixture and the total volume of the chambers approaches a value of 15 m^3 each, covering a surface of $\simeq$ 4000 m^2. Due to the large size of the systems, the cost of the mixture, and the use of greenhouse gases, the RPCs are operated using mainly recirculating gas systems, with a recirculation fraction of up to 90%. Unfortunately, it is not possible to increase this fraction due to leaks at the level of the detectors and impurities accumulated in the gas mixture. To keep the quality constant at 90% of recirculation fraction, two different types of purifiers are installed for these detectors: one filled with a mixture of different molecular sieves that absorb water and other impurities such as fluorides, and another one filled with catalyst Cu/Ni able to trap oxygen. Both of them are thermally regenerated before restarting the cycle.

The CMS RPCs work at 90% of gas recirculation fraction and send a flow between 700 and 1000 litres per hour from the mixer module to the chambers. Out of the 700 litres, 200 are lost in the cavern due to small leaks in the plastic pipes caused by ageing, fluoride anions, byproducts due to charge multiplication, and radiation, while 500 litres per hour are continuously exhausted to the atmosphere. For the ATLAS RPC, the volume is even bigger, around 1.2 m^3/h.

The problem of venting the RPC gas mixture is related to the presence of $C_2H_2F_4$ (R134a) and SF_6, which have a GWP of 1430 and 22800, respectively. In one year of CMS operation, the emissions of R134a and SF_6 correspond to 4000 tCO_2 (60% from R134a and 40% from SF_6) released into the atmosphere.

Trying to overcome this problem, a prototype was developed in 2018 to explore the recovery of R134a in ATLAS. Extensive testing revealed that the R134a could be recovered from the RPC gas mixture with a purity of 99.9%. The prototype was then transferred to CMS in 2019 for further testing. Once at CMS, it was discovered that there was an issue in recovering R134a from the $R134a/iC_4H_{10}/SF_6$ mixture in the ratio 95.2/4.5/0.3. Indeed, the combination of Freon and isobutane formed a minimum boiling point azeotrope. Nevertheless, thanks to the initial composition (95/5 $R134a/iC_4H_{10}$), it was still possible to recover pure liquid R134a and release the vapor phase enriched in the azeotropic mixture.

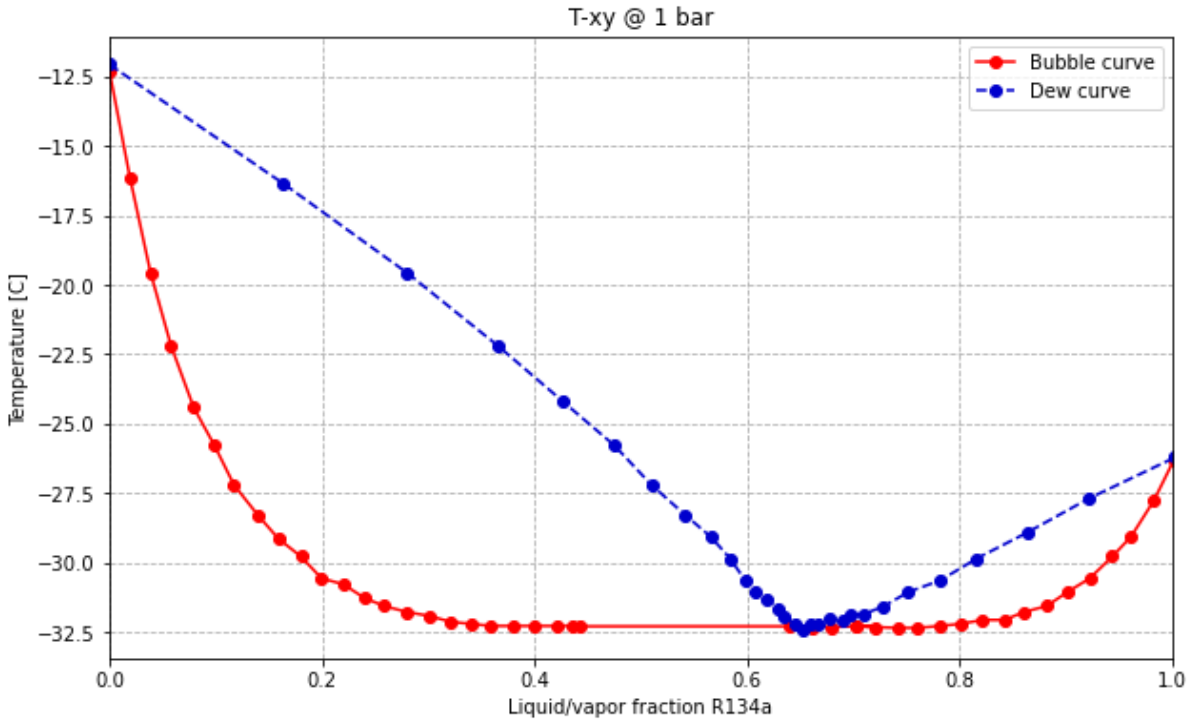

Figure 71 Bubble curve (red) and the dew curve (blue) of the azeotropic mixture R134a/iC_4H_{10}.

Figure 71 displays the bubble curve and the dew curve of the azeotropic mixture R134a/iC_4H_{10} are displayed. This mixture forms when the ratio between the two is 65/35 at a temperature of -32.3°C. Once the mixture is formed, it cannot be separated just by heating the liquid phase, as both gas and liquid phases have the same composition. The only method to separate the two components involves slowly heating liquid, moving within the azeotropic lens on the right side of the diagram, simulating a series of flash distillations at the thermodynamic equilibrium [26].

3.5.1 Recuperation plant

The recuperation plant was designed following the results obtained with the first prototype tested from 2018 to 2022. The results obtained are summarised in the following paragraph.

3.5.1.1 Prototype of the R134a recovery system

The first prototype was tested in two different configurations shown below in Figure 72 and Figure 73.

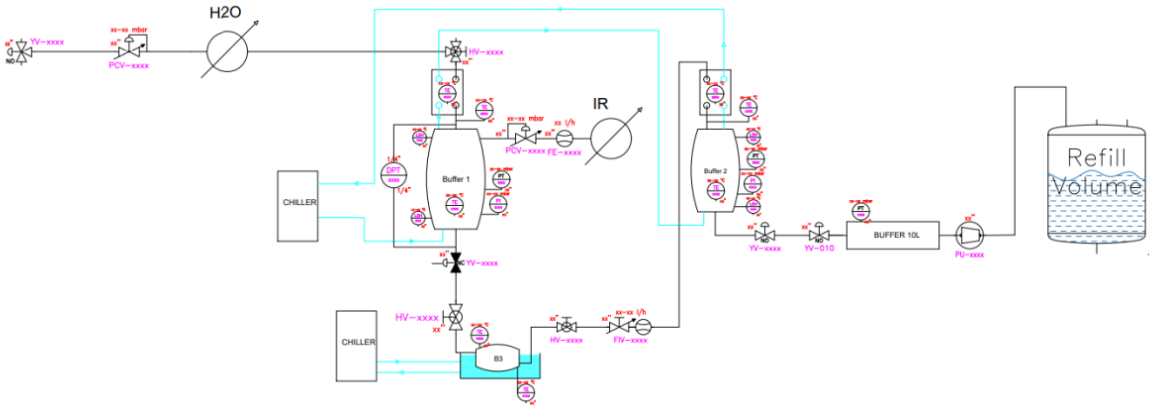

Figure 72 P&ID of the prototype first configuration [27].

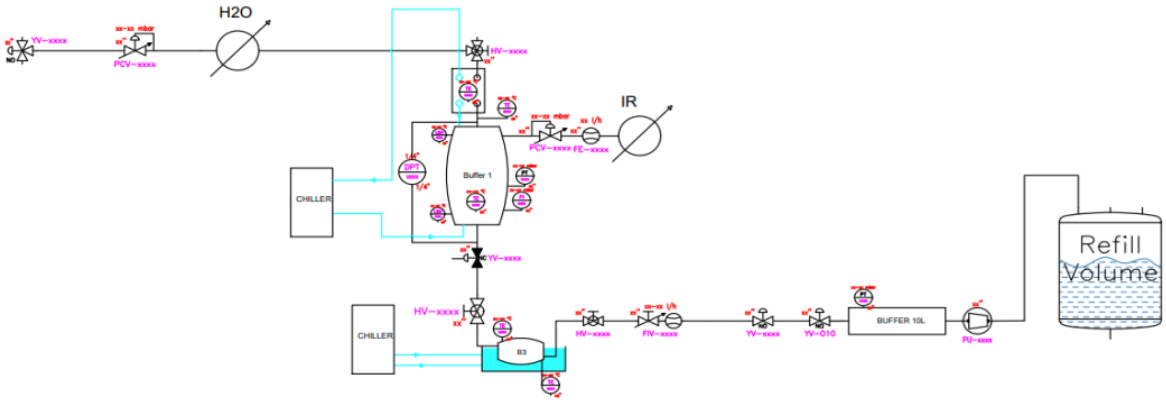

Figure 73 P&ID of the prototype second configuration [27].

The difference between the two configurations lies is the inclusion of the buffer 2 in the first version of the plant (Figure 72), which was later removed in the subsequent version (Figure 73). The tests performed on the first version of the plant aimed at improving the quality of recuperated R134a. For this purpose the process was organised as follows:

1. Condensation of the azeotropic mixture in Buffer 1 (set at -35.5˚C) in order to vent the incondensable, such as nitrogen and SF_6 (-195.8˚C and -67.6˚C, respectively)
2. Distillation process based on the heat exchange between buffer 1 and buffer 3, where the temperature is higher (set between 6 and 9˚C)
3. Cooling down the mixture in buffer 2 (set at -35.5˚C as well) to remove the rest of incondensable
4. Extraction and storage of recuperated R134a in the bottle

Figure 73 shows the second prototype configuration where the main difference from the first one is the removal of the second heat exchanger and buffer2, in which the second liquefaction occurred. The separation working principle is the same as described above, with the advantage that the modification avoids further phase change, reduces the energy demand for the liquefaction process and allows to work in continuous mode with variable flowrates [27].

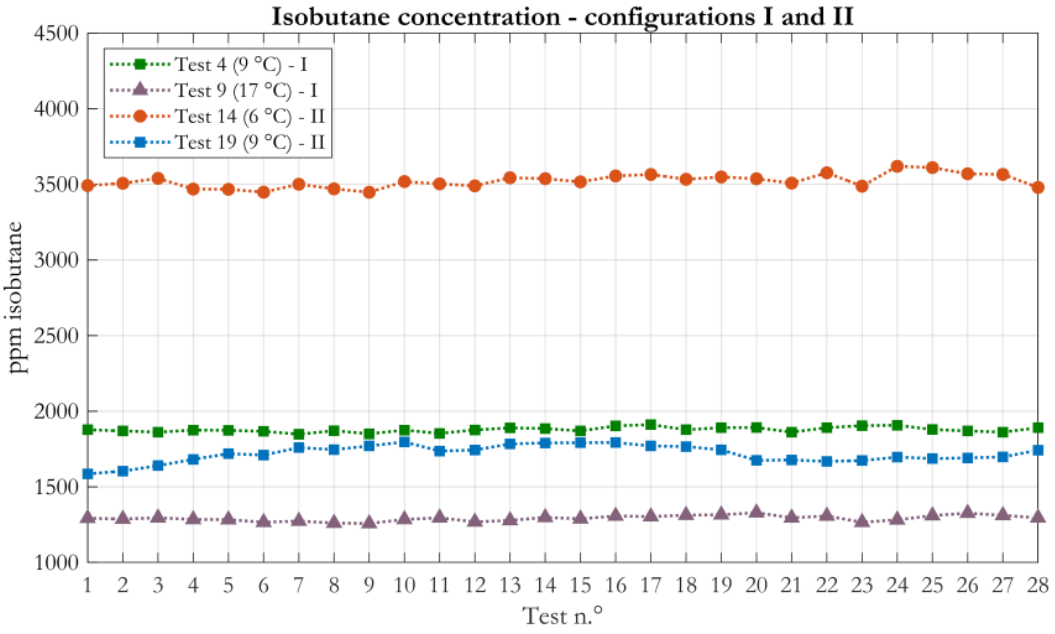

Figure 74 Isobutane concentration vs corresponding analysis number. Comparison between first (I) and second (II) prototype configurations.

The impact of modifications on the prototype were evaluated by μGC analysis and in particular the concentration of isobutane was the marker, as shown in Figure 74 where the two configurations are compared at each temperature of the buffers. Test 4 (blue line, first prototype configuration) and test 14 (green line, second prototype configuration) were performed at the same temperature of buffer 3 and no significant difference in the isobutane concentration can be noticed, confirming that the buffer 2 and the second liquefaction (first prototype configuration) did not improve the separation process.

3.5.2 Commissioning and upgrades of the final plant

Following the tests performed on the prototype, the design and construction of the final plant was commissioned in 2021 and installed at CMS in April 2023. It consists of five units: one electrical rack, two racks dedicated to the four separation units, the pump module and the storage bottle (Figure 75). The P&ID is shown in Figure 76.

Figure 75 Picture of the R134a recovery system installed at CMS.

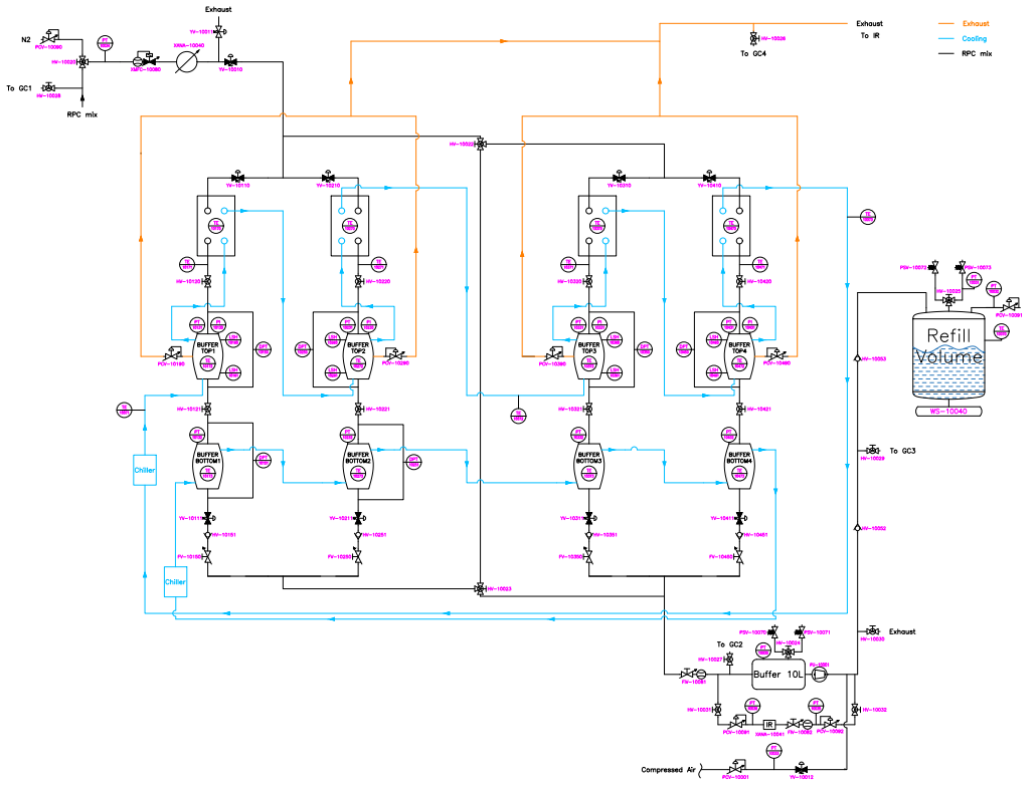

Figure 76 P&ID of the R134a final recuperation plant.

The system was designed to work in continuous and for this reason four identical distillation units have been installed. Each column develops vertically with two buffers located at : the top and the bottom one. In addition, two refrigeration units are connected to the system: the LAUDA Integral XT 280 sets the temperature of the top buffer cooling circuit, while the Huber Ministat 125 controls the temperature of the bottom buffers circuit. Depending on the column, buffers have different dimensions. In particular, columns 1 and 2 have top buffers of 30 cm height and bottom buffers of 10 cm height. On the contrary, columns 3 and 4 have top and bottom buffers of 20 cm height. It was decided to make the buffers of different size in order to evaluate the impact of their dimensions on the heat exchange process with the option to modify the system following the tests.

It was also designed to work both in parallel or in series thanks to the presence of a manual valve on the top of the racks containing the separation units. Since the commissioning of the recovery plant. The working configuration was in parallel. It was also decided to sample the gas not from

the Exhaust module of the RPC gas system but after the Purifier module in order to lower the content of oxygen and in particular of water, and minimize the risk of frost in the top buffer set at around -38˚C.

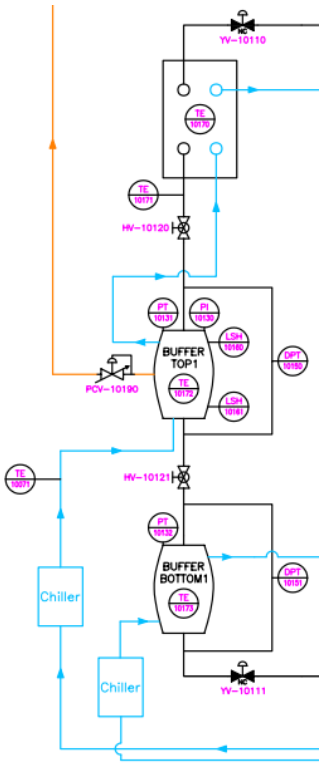

Figure 77 Column 1 P&ID. All columns have the same structure.

Figure 77 shows the P&ID of the column 1 is shown. The recuperation process has two phases: filling and emptying. They are managed by two sensor levels installed at the top and bottom of the buffer. At the start of the filling phase, both sensors are off because the buffer is empty. The filling phase ends when both sensors are on, indicating that the buffer is full.

During the filling phase, the gas from RPC gas system is liquified as it passes through the heat exchanger in which the refrigerant flows counter current with respect to the gas flow. The temperature of the heat exchanger is set between the liquefaction temperature of the azeotropic mixture and the R134a boiling point (-32.3˚C and -26.4˚C at 1 bar, respectively) in order to perform the distillation, and to exhaust immediately only the SF_6 and N_2. The pressure at which

the gas phase goes out from the distillation unit is regulated by a Zimmerli control valve and it is a key parameter for the performance of the plant. Due to gravity, the liquid arrives in the top cold buffer and it immediately flows down to the bottom hot buffer, set at a positive temperature comprised between 10 and 20 degrees. Here, it vaporises immediately and starts the heat exchange starts between liquid and gas phases. The liquid phase is heated very slowly by the gas phase while the vapour phase in contact with the cold liquid condensates, as in a standard distillation column: the release of the condensation heat determines a gradual temperature increase (ideally with infinitesimal steps), forcing the more volatile component in the azeotropic mixture to evaporate and flow out at the exhaust line.

At the initial stage of the operation of the recuperation plant, the process was designed to include a distillation step between filling and emptying. After some tests it was seen that this step did not improve the quality of the recuperated R134a leading to the decision to omit it.

When the buffer is full and the top sensor level turns on, the emptying phase starts. The valve after the bottom buffer opens, the compressor unit starts and the gas phase flows from the distillation unit to the 10 litres buffer, located between the columns and used to dampen the vibrations of the pump and not disturb the separation system. The number of compressor cycles and the pressure of compressed air are regulated to maintain a constant negative pressure in the buffer of -100 mbarg. The gas extracted from the separation plant is sent to the storage bottle which has a pressure equal to the R134a vapour pressure of 4.5 barg at 20°C.

All the R134a recuperated is finally reinjected in the RPC mixer module through a dedicated Mass Flow Controller in a ratio comprised between 30 al 50% with respect to the fresh one, depending on the input flow rate to the recuperation system.

Since the commissioning of the recovery plant in April 2023, several tests have been performed to find the best parameters for the recuperation process. The results of these tests are reported below.

3.5.3 Test results

The recovery system was firstly tested in manual mode and then in auto mode. These tests are devoted to correlate the effects of the operating parameters to the isobutane concentrations of

the recovered mixture and on the system efficiency (or recovery). In addition, the auto mode tests are focused on setting the system to let it run continuously (24 hours per day). The main operating parameters which influence the isobutane concentration in the recovered mixture and the system recovery are found to be:

- temperature of the top buffer (T_{Btop})
- pressure of the top buffer, regulated by the Zimmerli
- temperature of the bottom buffer (T_{Bbot})
- extraction flowrate, regulated by rotameter and needle valves
- distillation time

Top Buffer Temperature

Theoretically, increasing the temperature of the top buffer, the isobutane con centration should decrease. However, it is important to maintain this temperature within the range of -32.3 °C and-26.4 °C, which are the azeotrope and R134a boiling temperatures respectively, at 1 bar. Considering that the columns are cooled in series by the cooling loop, a temperature increment is present between the columns. Therefore, it is necessary to guarantee the column 4 at a temperature lower than 26.4 °C (boiling temperature of R134a) and avoid the complete mixture evaporation. The temperature of the cooling circuit is controlled by the setpoint temperature of the cooling unit and the system was tested under different conditions.

Top Buffer Pressure

Regulating the Zimmerli, it is possible to modify the pressure of the gas phase inside each column can be modified. In particular, the lower the pressure, the more is the gas flowrate leaving the buffer through the exhaust line. The Zimmerli can be manually regulated within a range of 0 and 500 mbar. The tests were conducted at increasing values: 10 mbar, 20 mbar, 35 mbar, and 50 mbar.

Bottom buffer temperature

The temperature regulation in the bottom buffer influences the top buffer temperature. In particular, the higher T_{Bbot} and the higher is the temperature of the vapour formed in the bottom buffer. The vapour releases its sensible and latent heat in the top buffer during condensation, increasing the temperature of the liquid mixture. The system has been tested under the following T_{Bbot} values: 14 °C, 17 °C, 20 °C, and 23 °C.

Extraction Flowrate

The extraction (or emptying) flowrate is defined as the flowrate at which the recovered mixture is sent from the columns to the recuperation bottle, passing through the compressor, and it is controlled by needle valves installed in each column that make them independent from the other ones. According to previous studies, the extraction flowrate influences the gas quality of the recovered mixture, as the higher the flowrate is, the higher is the concentration [27]. The recovery system has been tested with the following extraction flowrates: 500 l/h (real flow 150 l/h), 700 l/h (real flow 200 l/h), and 1000 l/h (real flow 290 l/h).

Distillation Time

The distillation time is defined as the amount of time between the end of filling and the beginning of emptying. The longer the distillation the more should be the isobutane leaving the buffer to the exhaust. The recovery system has been tested under three different distillation times: 0 min, 30 min, and 60 min. An additional parameter, the filling flowrate, does not influence the isobutane concentration of the recovered mixture, but it is fundamental for the system operation in continuous mode. Three filling flowrates were tested: 200 l/h, 300 l/h, and 400 l/h. Finally, it is worth to mention that, not only the isobutane concentration, but also the N_2 and O_2 concentrations must be minimized in the recovered mixture. Accordingly, for each test, C_4H_{10}, N_2, and O_2 concentrations have been analysed with the gas chromatograph.

3.5.3.1 Filling rate

The filling rate is defined as the mixture flowrate at the input of the recovery system. Each column is filled one by one, at a constant flowrate if the system is in manual mode. The influence of the filling rate on the efficiency and isobutane concentration was tested at different filling rates of 400 l/h, 200 l/h, and 300 l/h respectively, involving columns 1 and 3 only.

Filling rate [l/h]	C_4H_{10} [ppm]	N_2 [ppm]	O_2[ppm]	Efficiency[%]
400	1000	170	20	73
300	950	250	30	74
200	1100	47	5	78

Table 6 Summary of filling rates tested and relative gas quality and recuperation efficiency.

According to the results shown in Table 6 the quality of the recuperated R134a is not affected by the filling rate while the efficiency increases of 5% passing from 400 to 200 l/h. Lowering the input flow rate also the temperature of the heat exchanger decreases and therefore a lower amount of gas is lost through the exhaust line.

The status of the filling procedure was monitored through the normalised filling rate measured in mbar/h and described as the Δp in the top buffer for a flowrate of 100 l/h for 1 hour of operation. This parameter was calculated starting from the Stevin's law.

$$\Delta p = \rho g \Delta h$$

According to this equation, when a column is filled for 1 hour at 100 l/h, the maximum Δp achievable is 4.2 mbar [28]. Experimentally, lower values are obtained because a fraction of the gas mixture is lost at the exhaust during the filling phase.

Filling rate [l/h]	C1 [mbar/h @ 100 l/h]	C3 [mbar/h @ 100 l/h]
400.0	4.35	2.65
300.0	3.26	1.57
200.0	2.16	1.07

Table 7 Comparison of normalised filling rates at different filling rates for Columns 1 and 3.

From Table 7 is evident that column 3 has a lower normalized filling rate in all three tests. In particular, its value is almost one half of the corresponding column 1, meaning that a larger amount of gas during the filling phase is sent to the exhaust and the column requires more time

to reach the full state mode. This behaviour may be explained by the temperature increment between C1 and C3, due to the presence of a cooling system connected in series with the four columns.

3.5.3.2 Extraction flowrate

The recovery system was tested in manual mode, under three different conditions of extraction flowrate, to confirm the trend already obtained for the prototype [27]. The tests performed on the prototype shown a better gas quality (lower isobutane concentration in the recovered mixture) by reducing the extraction flowrate. It might be explained by a better heat exchange between liquid and gas phases due to higher time of interaction between the two. Indeed, a well performant heat exchange allows a better gas separation. Therefore, the higher the flowrate, the higher is the iC_4H_{10} concentration, due to the low interaction time between liquid and vapour from the bottom buffer.

Columns 1 and 4 were tested at different extraction rates of 150, 200 and 290 l/h. It was assumed that the behaviour of C2 and C3 was the same of C1 and C4, respectively, since they have the same dimensions. The other parameters were kept constant during the tests.

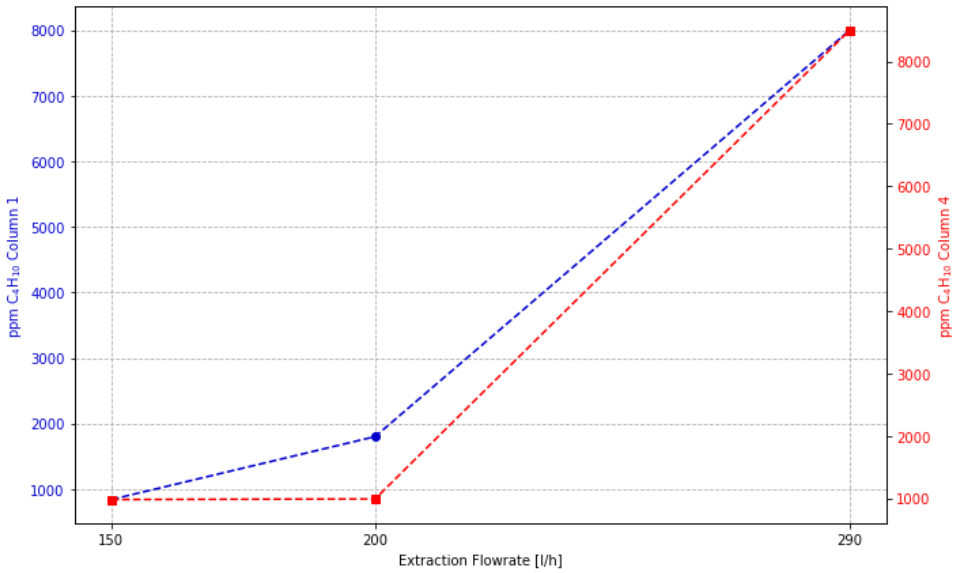

Figure 78 Effect of extraction flowrate on the quality of recuperated R134a for columns 1 and 4.

The plot in Figure 78 summarizes the results obtained for columns 1 and 4. The isobutane concentration for column 1 increases with the flow, reaching the maximum value at 290 l/h. Column 4 has a similar trend but the isobutane concentration is stable at both 150 and 200 l/h and it greatly increases at 290 l/h. The trend observed was the same of the prototype and it might be explained assuming that the distillation process continues during the emptying phase, influencing a lot the final iC_4H_{10} concentration in the recuperated R134a. Slower the extraction phase, lower the isobutane concentration will be in the final gas phase. The differences between column 1 and 4 might be explained by the different dimensions of bottom buffer: the bottom buffers of columns 3 and 4 are bigger than the ones of columns 1 and 2, ensuring a better heat exchange rate.

3.5.3.3 Bottom buffer temperature

One of the two temperatures affecting the performance of the recovery plant is the bottom buffer temperature, controlled by the chiller unit Huber Ministat 125. Top and bottom buffers communicate through a 10 mm diameter pipe and the heat exchange occur in the top buffer between the vapour phase, rising from the bottom buffer and the liquid phase exiting the heat exchanger. In theory, as the temperature of the bottom buffer increases, so does the temperature of the vapor phase, which enhances the heat transfer to the liquid in the top buffer. Consequently, a greater volume of vapor is expelled from the top buffer through the exhaust line. Therefore, a higher T_{Bbot} leads to better gas qualities but worse efficiencies. The system was tested at 14, 17, 20 and 23°C. For this test, the composition of the recuperated R134a was monitored through μGC analyses and the system was set in auto mode.

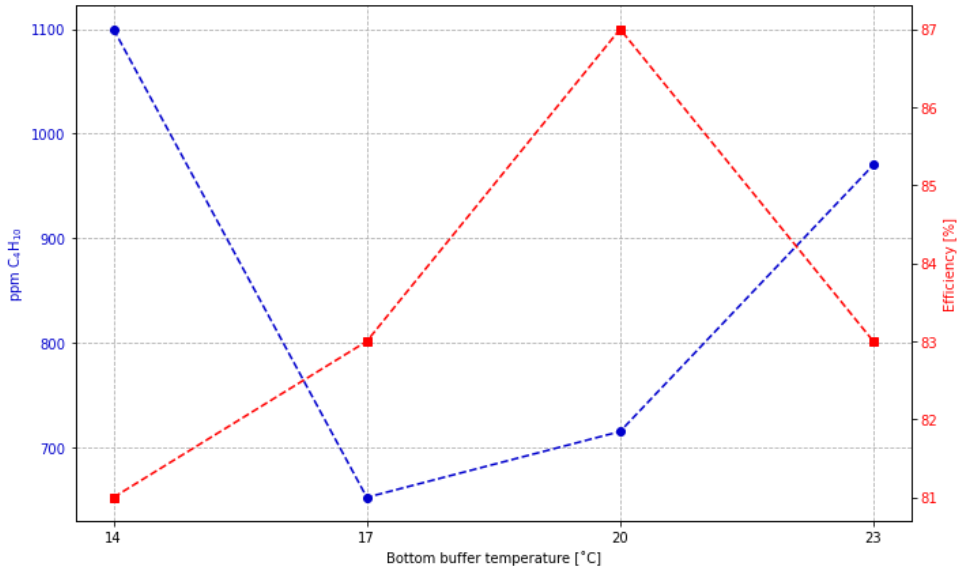

Figure 79 Effect of bottom buffer temperature on the quality of recuperated R134a and recuperation efficiency.

Figure 79 presents the results of the tests conducted to determine the optimal temperature for the bottom buffers. The inconsistent efficiency trend suggests that the bottom buffers may not significantly affect the system's performance. In particular, for columns 1 and 2, the bottom buffers are considerably smaller than the top ones, with a height ratio of 3:1. As a result, even when the bottom buffer temperature is adjusted, the obtained results do not align with the expected values, as previously explained in the paragraph *Top Buffer Temperature*. One potential solution could be to replace the 10 cm buffers in columns 1 and 2 with 20 cm buffers, achieving a height ratio of 3:2. It is worth noting that columns 3 and 4 already have a height ratio of 1:1.

3.5.3.4 Top Buffer Pressure

As already mentioned at the beginning of this paragraph, the top buffer pressure can be regulated manually by the Zimmerli reduction valve installed on each column. Higher the pressure set, lower the amount of gas is released to the atmosphere. This result in the overall efficiency decreases and the improvement of the quality of the recuperated gas improves. The best pressure value is a trade-off between quality and efficiency.

Considering that the temperatures of columns 1 and 2 are lower than columns 3 and 4, attributable to the serial cooling system which enhances gas liquefaction, the Zimmerli pressure was set to 10 mbar to facilitate the complete expulsion of gas through the exhaust system. For columns 3 and 4, three different pressure values were evaluated: 20, 35 and 50 mbar. The results are reported in Figure 80

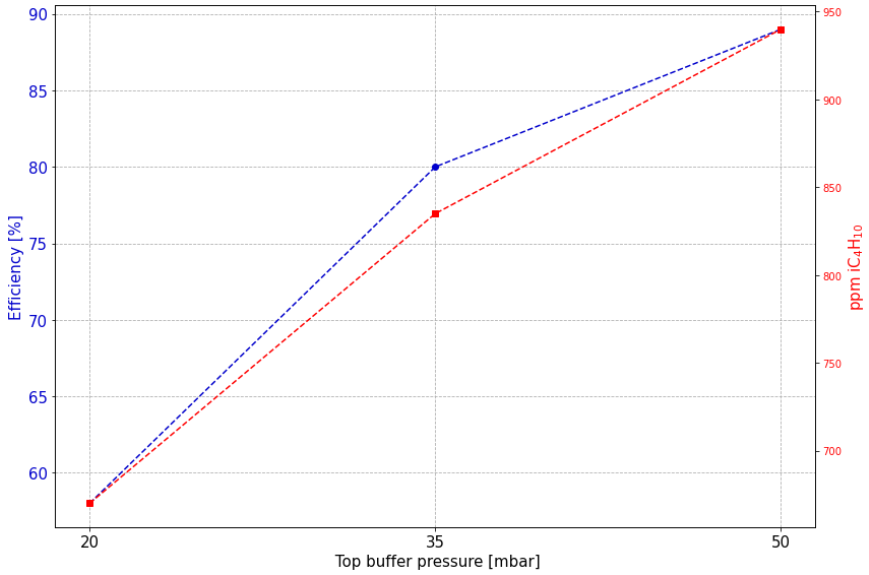

Figure 80 Effect of bottom buffer pressure on the quality of recuperated R134a and recuperation efficiency.

As foreseen theoretically, the recuperation efficiency increases with the pressure of the buffer but the iC_4H_{10} also increases with the same trend, since a lower fraction of gas with impurities leaves the column.

3.5.3.5 Top Buffer Temperature

The efficiency of the R134a recuperation process and the quality of the recuperated R134a are likely most influenced by the temperature of the top buffer. In the earlier part of the paragraph, it was explained that the buffers are cooled down to a temperature range of -32.3 °C and -26.4 °C, which corresponds to the azeotrope and R134a boiling temperatures at 1 bar, respectively.

During the commissioning phase, the system was initially connected to the Lauda Integral XT 280 external cooling unit. However, after a few months, it was replaced with a more powerful cooling unit, the Huber Unistat 915w. Although the refrigerant and cooling pipes remained the same, it was necessary to repeat the tests to regain the original efficiency with the new module. This may be attributed to the distinct positions of the temperature sensors in the two devices, resulting in different temperature differentials (ΔT) in the separation unit [29].

The results of the two sets of tests will be summarised separately below.

Lauda Integral XT 280

Three temperature values were set, -36.5 °C, -36.2 °C, and-36 °C and for each temperature the quality of recuperated R134a and the efficiency of the system were monitored.

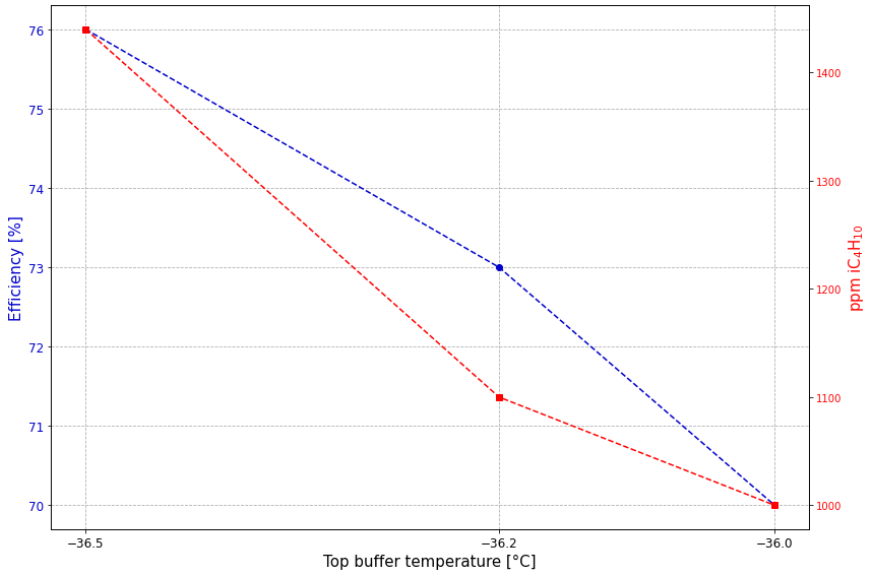

Figure 81 Effect of top buffer temperature on the quality of recuperated R134a and recuperation efficiency using Lauda Integral XT 280 chiller unit.

In Figure 81, the results for different temperatures tested are displayed. Both the recuperation efficiency and the quality of the recuperated R134a exhibit the same trend: as the temperature of the chiller unit increases, both efficiency and isobutane concentration decrease. This can be explained by the fact that higher temperatures in the top buffer correspond to a lower amount of feed gas flow being liquified and more gas being directed to the exhaust. It's worth noting that although this trend summarizes the results obtained with the four columns, each column exhibits different separation efficiency (C1>C2>C3>C4) due to the chiller's low capability to maintain a stable temperature when working in series.

Huber Unistat 915w

The tests on the new chiller unit started on April 2024 and temperatures between -40 °C and -38 °C were investigated, monitoring both the recuperation efficiency and the quality of recuperated R134a. It is important to highlight that the new chiller was tested at 400-500 l/h of feed flow (CMS RPC standard operation conditions), while the Lauda was tested at 150 l/h.

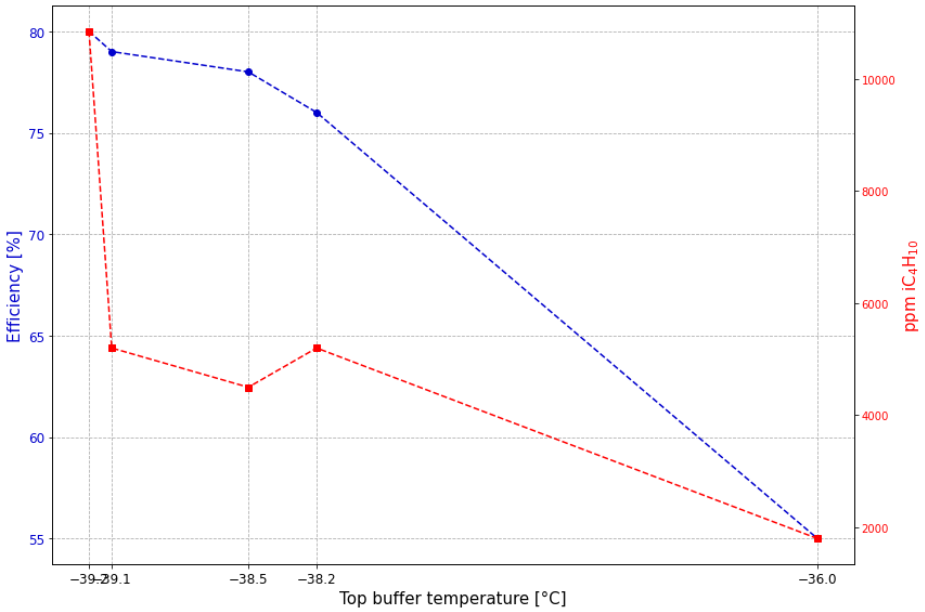

Figure 82 Effect of top buffer temperature on the quality of recuperated R134a and recuperation efficiency Huber Unistat 915w chiller unit.

As depicted in Figure 82, a slight adjustment in the buffer temperature had a significant impact on the concentration of isobutane in the R134a recovery, but in a different extent. The starting setpoint tested was -36 °C, which was the same as the replaced chiller unit. Although the quality was acceptable, the efficiency was too low, so the system was tested at lower temperatures. Between -38 °C and -39.2 °C, the efficiency returned to standard values, but the quality was still not acceptable. Through careful monitoring, it was noticed that the emptying flow of the individual columns was negligible when two or more columns were in extraction mode, despite the presence of needle valves on each separation unit. As a result, one column emptied at half of the set flow, while the other one emptied at a flow rate one-half times higher than the setpoint. As previously demonstrated, higher extraction flow resulted in higher isobutane concentration in the recovery. In order to solve this issue, we made some changes to the pipes between the bottom buffer and the 10L buffer. In the old setup, the output of each column after the needle valves was connected to a single pipe leading to the buffer before the pump. In the new setup, each column is connected to the 10L buffer through an individual pipe that is not linked to the others. This

means that the extraction of each separation unit is now independent from the others, and the flow set by needle valves remains stable.

After this modification, the tests were repeated at -38.5 °C and -38.2 °C. Results are shown in Table 8.

Filling rate [l/h]	Temperature top buffer [°C]	C_4H_{10} [ppm]	Efficiency[%]
500.0	-38.5	4500.0	83.0
500.0	-38.2	3485.0	71.0

Table 8 Summary of the results obtained increasing the top buffer temperature from -38.5 to -38.2˚C.

3.5.4 Final configuration

The recovery system has been optimized for filling and emptying flowrates, top buffer temperature and pressure, and bottom buffer temperature to achieve an efficiency of 80%. The upper limit of isobutane was calculated as 6000 ppm based on the maximum flow of recuperated R134a that can be reintroduced at the RPC mixer, which is 400 L/h, and accounts for 54% of the total mixer flow. This calculation considers a feed flow to the recovery plant of 500 l/h and an 80% efficiency and a final concentration of isobutane introduced with the recuperated R134a of 3200 ppm. To compensate for this quantity of iC_4H_{10}, the concentration of isobutane injected at the RPC mixer was lowered from 4.5% to 4.2% and it is constantly adjusted based on the IR and µGC daily analyses.

The optimal values, obtained during the testing phase, are reported in Table 9 with the average efficiency and gas quality.

Parameter	Value
Filling rate	200-500 l/h
T_{Btop}	-38.5°C
Top buffer pressure	10 mbar (C1&C2) and 35 mbar (C3&C4)
T_{Bbot}	20°C
Emptying rate	220 l/h
Distillation time	0 min
Average isobutane	4700 ppm
Recuperation efficiency	83%

Table 9 Summary of the best working conditions for the R134a recovery plant.

The recovery system has the capacity to operate with four columns in parallel during the filling phase and up to three columns in parallel during the extraction phase. The cooling circuit connected in series alone is insufficient to maintain a uniform temperature across all columns, as each column can affect the temperature of those downstream. During tests, an optimal filling rate of 200 l/h was observed, although this parameter depends on the state of the RPCs. During the LHC running phase, the input flow rate increases to 500 l/h. However, the filling rate does not affect the gas quality of the recovered mixture, and the efficiency may vary by 5%. The Huber Unistat 915 was set to -38.5°C, at which both efficiency and quality are good. The second chiller unit, the Huber Ministat 125, was set to 20 °C in the optimal configuration, even though the bottom buffer temperature has minimal influence on the system efficiency and iC_4H_{10} concentration. The Zimmerli was regulated at 10 mbar for the first two columns to address the issue related to their lower temperatures compared to C3 and C4 and improve the recovered gas quality. On the other hand, C3 and C4 top pressure were set at 35 mbar to reduce the exhaust flow rate and improve the efficiency. Finally, the needle valves were regulated to have and emptying rate of 220 l/h for each column.

Chapter 4
"R&D activities"

4.1 Fluoride ISE measurements of eco-friendly gas mixtures at the GIF++

Many of the gases used in gaseous detectors at the LHC experiments are hydrofluorocarbons (HFCs) and fluorinated gases. CF_4, $C_2H_2F_4$ (R134a), C_4F_{10} and SF_6 are the main contributors for the Greenhouse Gas (GHG) emissions at LHC Experiments due to their high Global Warming Potential (GWP). Additional challenges associated with to the use of those fluorinated gases include their cost, availability, and the increasingly stringent European regulations that mandate the replacement of these gases with more environmentally sustainable alternatives. Some of them are currently under study but many are unsuitable for our purpose due to their toxicity, flammability, or other chemical physical properties. A critical parameter to be assessed in the selection of a fluorinated gas is the reactivity under particular conditions, such as exposure, to humidity, high electric field, or irradiation. Some of them undergo fragmentation processes, producing fluorides anions that can further react with the vapour, and leads to the formation of hydrofluoric acid, according to the following equations:

$$F^- + H_2O \rightarrow HF + OH^-$$

$$HF + H_2O \rightarrow H_3O^+ + F^-$$

Despite of HF is a weak acid, the presence of F atom makes this compound very corrosive for the materials. In the past years, many studies have been performed in order to understand the F^- anions production mechanisms and the long-term effects inside different gaseous detectors, as for example the Resistive Plate Chambers (RPC) [30] that operate with a standard gas mixture of 95.2% $C_2H_2F_4$ + 4.5% iC_4H_{10} + 0.3% SF_6 humidified at 40% relative. The RPC detectors are installed in 3 out of the 4 main LHC experiments: CMS, ATLAS, and ALICE. During normal run periods, the gas mixtures inside these detectors are exposed to large electric fields and high radiation, promoting these fragmentation processes. To perform the experiment, the detector filled with the above mentioned gas mixture is set at its working voltage and irradiated. During detector operation, F^- are generated and collected in an aqueous solution containing 50% of TISAB (Total

Ionic Strength Adjustment Buffer). The presence of TISAB ensures that fluorides are not complexed by other potential interfering substances within the solution. This allows for the accurate measurement of fluoride concentrations without interference. The measurement of the concentration of fluorides produced during the RPC operation was performed by use of an Ion Selective Electrode (ISE) (see 1.5.3 Fluoride ISE).

4.1.1 GIF++ and setup for the ISE measurements

The ISE analyses on RPC detectors here described were performed at GIF++, in which a ^{137}Cs source of 12 TBq is combined with muon beam, in order to simulate the detector operation conditions created at the LHC experiments [31]. In the following plots, the concentration of fluorides is correlated with the physics current of RPC detectors, constant for specific working voltages, that depend in turn on the gas mixture used to fill the detector and on the gamma irradiation source attenuation factor used. The possibility to set different attenuation factors allow to study the performance of the detectors, the ageing processes, and new gaseous mixtures in a shorter period with respect to the standard LHC conditions. To define stable operation conditions, the voltage at which the detector reaches 95% of the maximal efficiency was defined for every gas mixture. The operation voltage was chosen at 150 V above those values, and was referred to as the working point, or WP. The WP depends on the gas mixture, detector specifications and on the irradiation background intensity.

The purpose of this ISE campaign was to measure the concentration of fluorides produced by different gaseous mixtures containing lower amount of R134a than the standard mixture. Different gases as replacement for the R134a were used, as well as CO_2 or R1234ze, an hydrofluoroolefin (HFO) with a GWP=7, shown in Figure 83.

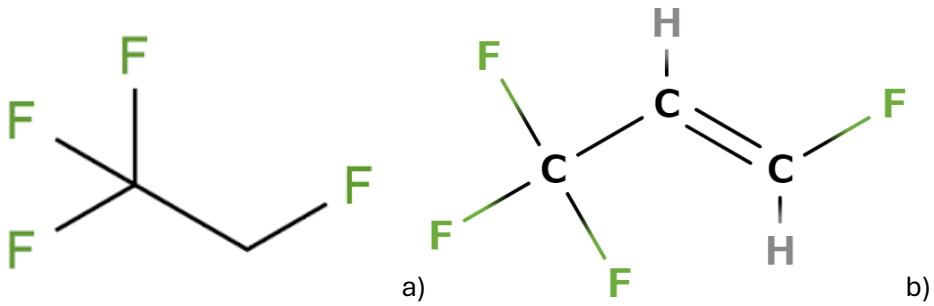

Figure 83 Chemical structure of a) R134a and b) R1234ze (E).

In the first part of the data sets, F^- concentration was measured in both solutions located respectively inside and outside the bunker of GIF++, respectively. For measurements performed inside the bunker, the benefit is derived from the proximity of the sampling point to the chamber, which minimize potential errors associate with gas leaks or absorption of the fluorides in plastic tubes. For measurements conducted outside the bunker, the advantage is the continuous, unrestricted access to the setup, facilitated by the absence of a gamma source. However, to conduct these last measurements, the use of a pump to circulate the gas is necessary, and the length of the tubing. The increased length of the pipes and the greater distance from the chambers contribute to measurements errors. A schematic view of the setups described is given in Figure 84.

For this reason, all the following data refers to measurements performed inside the bunker, which are the most reliable.

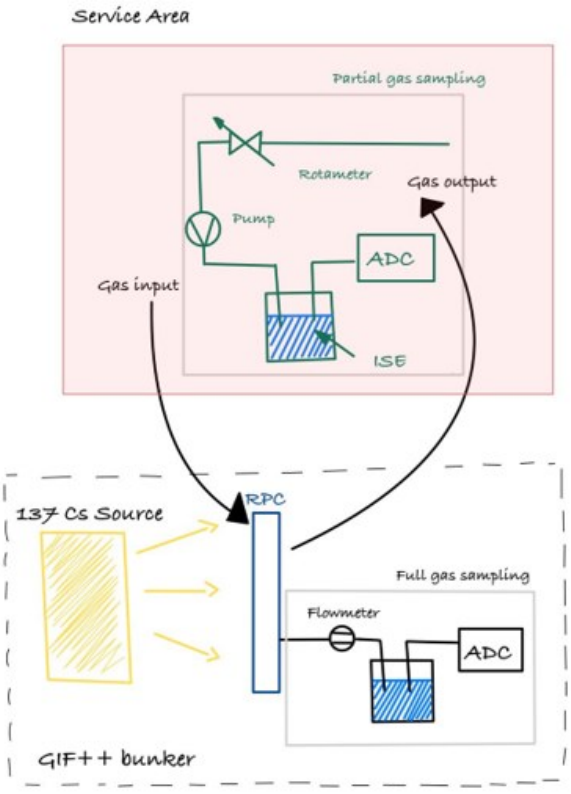

Figure 84 Scheme of the setup used for the ISE measurement at the GIF++.

For these measurements, two different High-Pressure Laminate (HPL) RPCs of 0.7 m x 1 m were used, purchased by the Korea Detector Laboratory (KODEL) [32] and General Tecnica (GT) [33]. The choice of the detector was dictated by the requirement to have two detectors with significantly different resistivities, to explore a potential correlation between this characteristic and fluoride production. In both cases, these are HPL RPC 2 mm gap, flowing at one detector volume per hour, equivalent to 1.5 l/h of gas mixture. The gas outlet was bubbled into an aqueous-TISAB solutions of 20 ml, under vigorous magnetic stirring. To measure the fluoride concentration in the solution, combined ion-selective electrodes from Thermo Fisher [34] were used (shown in Figure 85), and the signal was read using the ISE station from Hanna Instrument [35].

Figure 85 Fluorides electrode Orion™ [34].

During the measurements, gas flow rate, humidity level of the mixture and temperature (except for the tested gas mixtures) were kept constant.

The gas mixtures tested are shown in Table 10, and the results will be discussed following.

Mixture	Abbreviation	Gases	Ratio
CMS RPC standard	Standard	R134a/iC4H10/SF6	95.2/4.5/03
standard + 30% of CO2	Mixture A	R134a/CO2/iC4H10/SF6	65.2/30/4.5/03
standard + 30% of CO2 + 1% of SF6	Mixture B	R134a/CO2/iC4H10/SF6	64.5/30/4.5/1
R1234ze based gas mixture	Mixture C	R134a/CO2/C3H3F4/iC4H10/SF6	22.25/50/22.25/4.5/1

Table 10 Gas mixtures tested at GIF++ as part of the ISE campaign.

4.1.2 Results

4.1.2.1 Results for R134a based gas mixtures: impact of CO_2 co-feed and concentration of SF_6

The aim of this test was to compare the fluorides production using the CMS RPC standard mixture, with Mixture A and Mixture B (see Table 10).

Each gas mixture was tested at working voltage .In particular, the standard mixture was tested at around 10 kV , while Mixture A at 9.5 kV and Mixture B at 9.9 kV. The plot in Figure 86 the plot

displays that fluorides production does not significantly change upon introduction of CO_2 (mixture A) in respect to the standard mixture. This indicates that the fluoride production within the RPC does not strictly depend on the amount of R134a. Hence, only a small fraction of $C_2H_2F_4$ undergoes the fragmentation process, and the addition of CO_2 to the gas mixture does not the final concentration of F^-.This might also suggest that the amount of CO_2 introduced could be even more significant. On the other hand, however, the addition of a small quantity of SF_6 implies an increase in the production of fluorides, especially at higher voltages. This phenomenon was observed in other laboratories but is still subject of study [36].

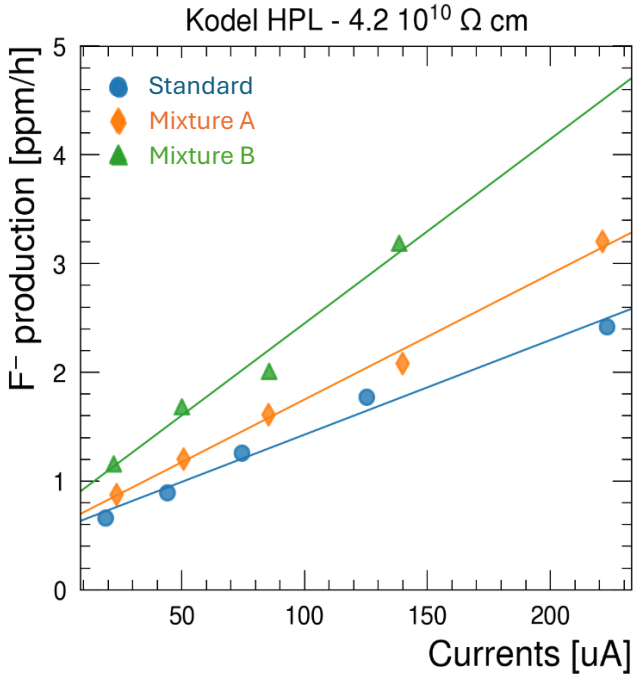

Figure 86 Fluorine ions production at different current value for different gas mixtures: CMS RPC Standard (blue), Mixture A (yellow) and Mixture B (green)

4.1.2.2 Results for R1234ze based gas mixtures: impact of $C_3H_2F_4$ co-feed

In this test, the fluoride production of the CMS RPC standard mixture was compared to the Mixture C (see Table 10), where $C_3H_2F_4$ is used as partial replacement for the R134a.

$C_3H_2F_4$, commonly known as R1234ze, is a hydrofluoroolefin (abbreviated HFO) with a very low Global Warming Potential (GWP) of 7. Each gas mixture was tested at working voltage: for the standard mixture it was around 9.4 kV for the standard one and 10.4 kV for the R1234ze + R134a + 50% CO_2. From the plot in Figure 87, it is evident that the mixture containing HFO has a higher fluoride production rate compared to the standard mixture [36]. A possible mechanism that could justify this phenomenon is as follows: the carbocation formed by fragmentation of R1234ze upon radiation and electric field, is more stable than that formed from R134a. . This indicates that less energy was required to create the ionic form of R1234ze. The enhanced stability can be attributed to the presence of a double bond in its structure, which facilitates resonance within the molecule and allows the positive charge to be distributed across multiple carbon atoms.

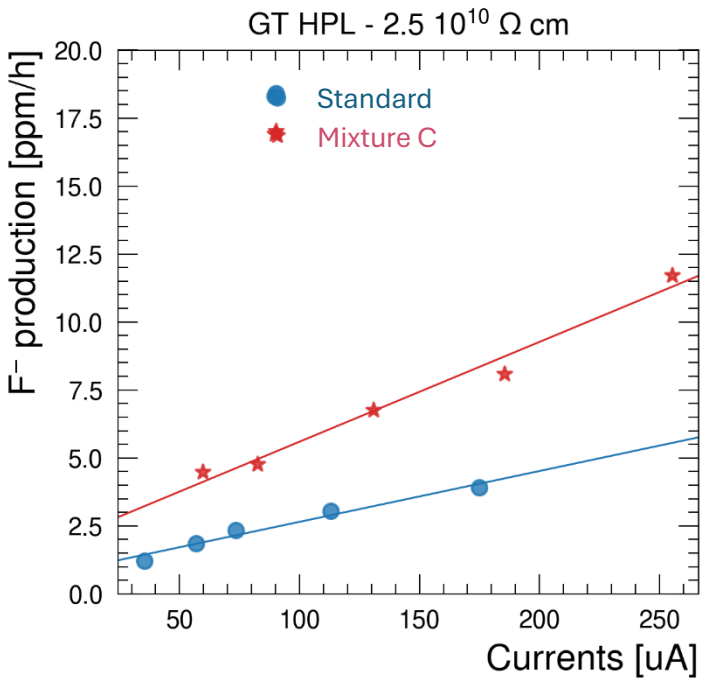

Figure 87 Fluorine ions production at different current value for different gas mixtures: standard mixture (blue) and R1234ze based gas mixture (red).

4.2 Fluoride ISE measurements for ALICE MID detectors

The ALICE Muon Identifier (MID) consists of 72 RPCs arranged in 2 stations of 2 planes each and each plane consists of 18 RPCs. They work with a gas mixture of $C_2H_2F_4/iC_4H_{10}/SF_6$ in a ratio 89.7/10/0.3 at 40% of relative humidity. The fluorinated gas constitutes the higher percentage of gas component inside the detector. The presence of such a huge quantity of this gas and the presence of water vapour led to the formation of Hydrofluoric Acid (HF) inside the detector under the effect of radiation [37]. HF production in RPCs could affect detector performance by damaging the electrode surface: for this reason it is important to study its production and accumulation by monitoring it with a fluoride Ion Selective Electrode. The HF production mechanism is not still completely clear but a hypothesis has been pointed out below exploiting the structure similarity between tetrafluoroethane and perfluorocarbons (see 2.2 Decomposition processes of fluorinated compounds).

The main problem related to the formation of hydrofluoric acid (HF) is its chemical attack to the polymerised linseed oil layer or directly to the Bakelite surface (Figure 88), as revealed by SEM-EDS analysis.

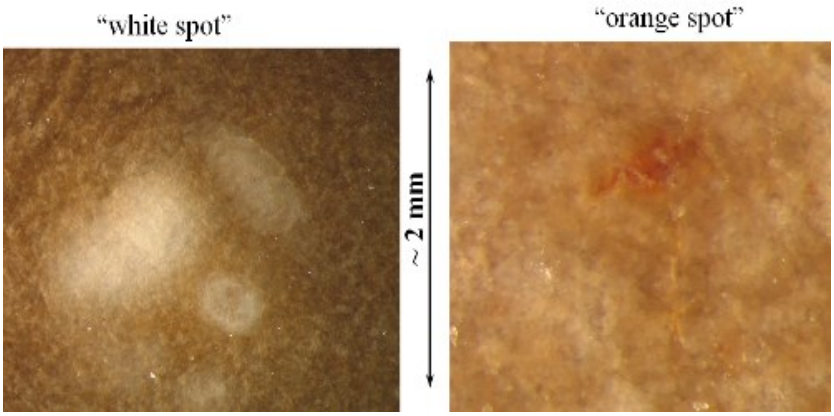

Figure 88 SEM-EDS analysis: White and orange spots due to HF chemical attack to the polymerised linseed oil layer (right) or directly to the Bakelite surface (left) [38].

The chemical composition of HPL electrodes surface was studied using an electronic microscope equipped with an Energy Dispersive X-ray Spectrometer detector (SEM EDS/X-ray):

comparing the sample with a reference, it is clear the presence of a high fluorine peak and Sodium peak (Na) and the depletion of the nitrogen peak, which was initially present in the reference (Figure 89). The relative absence of nitrogen indicates that the Bakelite resin is mainly phenolic; while the erosion of Carbon and appearance of Sodium, belonging to NaOH used to catalyse the production of the phenolic resin, seem to confirm the hypothesis of an etching of the melamine layer because of corrosive action of HF [38].

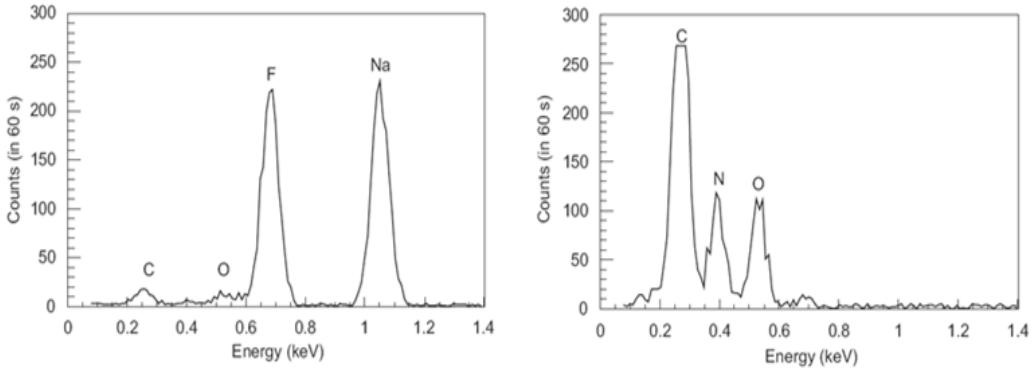

Figure 89 EDX/X-ray spectra comparison: damaged surface (on the left) and reference surface (on the right) [38].

4.2.1 Experimental setup

Fluoride ion selective station is installed in the underground gas room where it is possible to collect the return gases from the detectors (Figure 87):

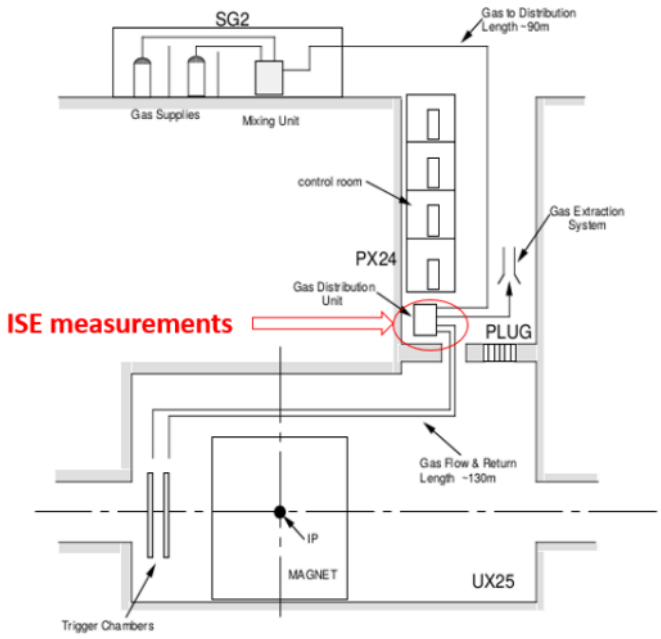

Figure 90 Schematic layout of the gas distribution system in ALICE. The service area where ISE measurements were performed is clearly underlined [39].

Fluoride ions concentration is measured in accumulation mode in two sampling points: before and after the purifier (see Finally, C_4F_{10} is used in RICH detectors due to its higher refractive index, which makes C_4F_{10} particularly suitable for identifying particles within a lower momentum range, and it works well alongside other radiators in RICH systems.

1.4 The LHC gas systems for gaseous detectors). In fact, in ALICE, the purifier is composed by one module with two columns: each column is filled with 50% MS 4Ä (for filtering H_2O), and 25% CuR11 and 25% $NiAl_2O_3$ which are used to remove O_2. Despite the key role of the purifier is the elimination of H_2O and O_2, it is able also to trap other fluorinated impurities such as HF as it will be demonstrated in the following.

The MID gas system works at 88% of recirculation fraction, with a fresh flow injected from mixer of around 25 l/h. The measurement is done by putting a stream of the gas mixture coming from the MID detector, before or after the purifier, inside a 330 ml solution of deionized water and TISAB II.

The gas flowing into the solutions is regulated by two rotameters and set at 1 l/h (calibrated in air). The line coming from the detectors is split into two and a fraction of the gas is sent to a μGC Agilent 990 equipped with two column, one PPU and one MS5A, to monitor the quality of gas mixture at the mixer, before and after the purifier. A simplified scheme is reported in Figure 91.

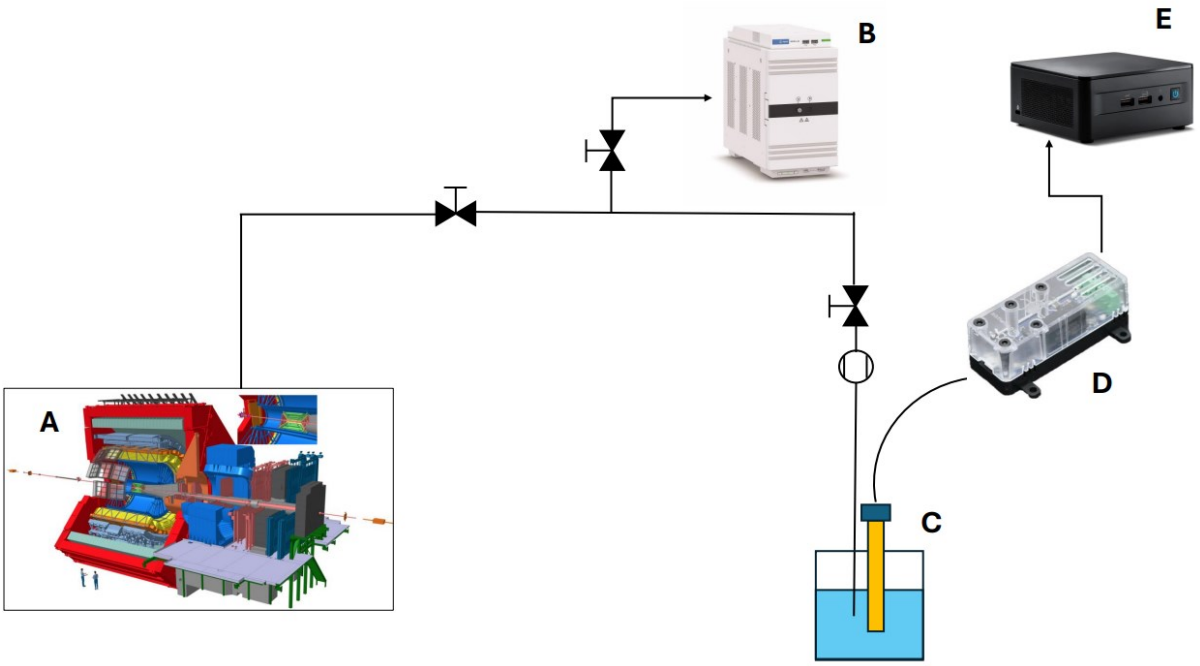

Figure 91 Schematic view of the setup used for ISE and μGC measurements for ALICE MID detectors. A) ALICE cavern, B) μGC Agilent 990, C) 50/50 water/TISAB II solution for ISE analysis, D) Yoctopuce sensor, E) computer for data analysis.

A lot of upgrades have been made since the beginning of these ISE campaign in 2017 [39]. Now two fully dedicated racks are installed in the gas room, one of which is ATEX due to the presence of RPC gas mixture possible flowing out from the ISE solutions. The other one is not ATEX and it is dedicated to the GC setup. They are both show in Figure 92.

Figure 92 Two racks for ISE and µGC analyses installed in ALICE service area.

4.2.2 Results

The goal of the ISE measurements was to measure the fluoride created inside the detector volume as a function of the irradiation (in particular of the integrated luminosity). Luminosity (L) is the ratio of the number of events detected (N) in a certain time (t) to the interaction cross-section (σ):

$$L = \frac{1}{N}\frac{dN}{dt}$$

It has the dimensions of events per time per area and is usually expressed in the cgs units of $cm^{-2} \cdot s^{-1}$ or the non-SI units of $b^{-1} \cdot s^{-1}$. In practice, L is dependent on the particle beam parameters,

such as beam width and particle flow rate, as well as the target properties, such as target size and density. A related quantity is integrated luminosity (L_{int}), which is the integral of the luminosity with respect to time:

$$L_{int} = \int L \, dt$$

The luminosity and integrated luminosity are useful values to characterize the performance of a particle accelerator.

An important fact to point out is that the measurement represents the cumulative amount of fluoride ions in a bottle rather than a punctual assessment of impurities levels in the system at any specific time. This distinction is important for understanding the dynamics and extent of contamination over time, rather than at a single point. The quantity of measured ppm in the sampling solution do not reflect the actual concentration of fluoride ions within the volume of the detector. The results are shown in Figure 93.

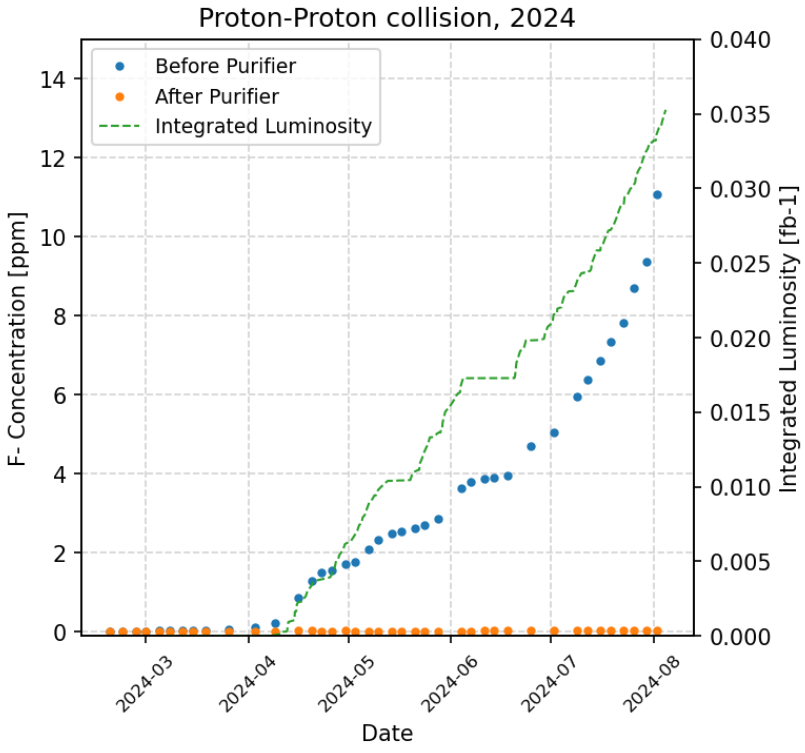

Figure 93 [40] Fluorine ions concentration at the before (blue) and after (yellow) purifier compared with the LHC integrated luminosity [40].

From the plot above it is clearly visible how the concentration of fluoride ions is related to the integrated luminosity. In particular, the slope remarkably increases during run periods while it keeps constant during technical stops (flat areas), meaning that there is not any visible production if the beam is not present. The other important parameter of this plot is the huge difference of fluoride concentration in the two sampling points: the fluoride concentration is constantly lower than instruments detection limit after the purifier, confirming the key role of the purifier in trapping the ions formed in the gas mixture. This additional functionality demonstrates the purifier's comprehensive approach to gas purification, ensuring a cleaner and more controlled chemical environment.

4.2.3 Comparison ISE results LHC RUN2 VS RUN3 [40]

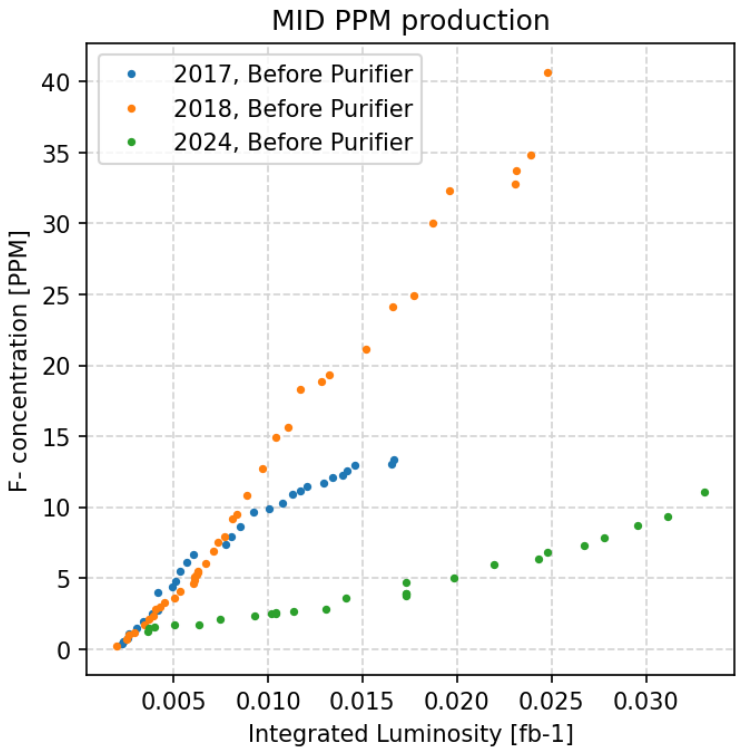

Figure 94 Comparison ISE results LHC RUN2 (blue and yellow) and RUN3 (green) VS integrated luminosity at the sampling point placed before the purifier [40].

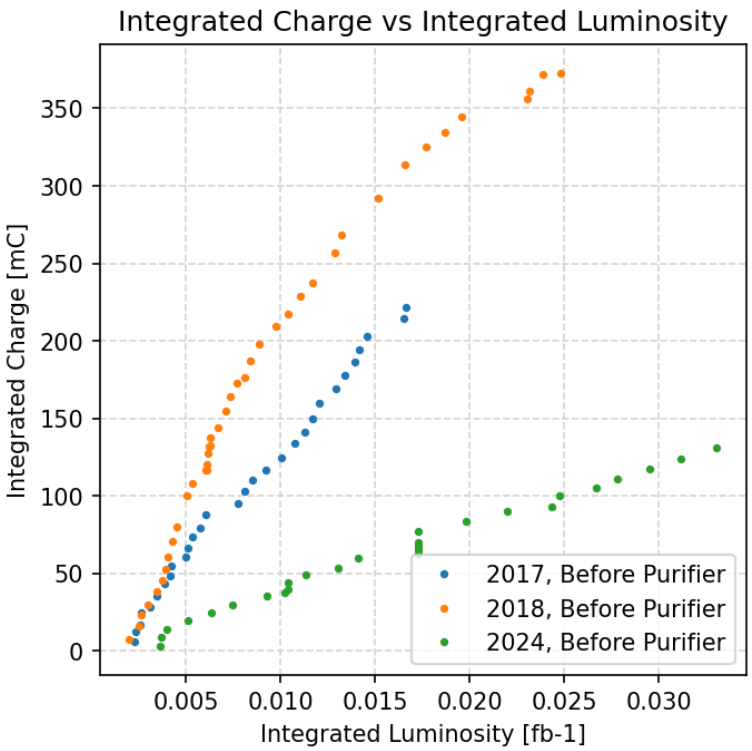

Figure 95 Comparison Integrated charge during LHC RUN2 (blue and yellow) and RUN3 (green) VS integrated luminosity [40].

Figure 94 and Figure 95 show a comparison between ISE measurements performed at the ALICE experiment for the MID detectors during RUN2 (2017 and 2018) and RUN3 (2024).These plots confirm that fluoride ions production is proportional to the accumulated charge and integrated luminosity, as demonstrated during other experiments. However it is clearly visible from the first plot that the concentration of fluoride ions was much higher in 2017 (3 times higher) and in 2018 (4.5 times higher), than in 2024 at the same integrated luminosity value. In the second plot a possible explanation of this behaviour is reported: due to some upgrades in the electronic parts of the MID detectors, the operative voltage was lowered for the RUN3, resulting in a lower integrated charge than RUN2, accounting for the linear production of the F^-.

4.3 VUV and UV-Vis measurements

In the realm of research and development for new, more environmentally friendly gas mixtures to replace the currently used high Global Warming Potential (GWP) gases in gaseous detectors, the chemical-physical characterization of each candidate gas is crucial. This comprehensive analysis is essential to assess the suitability of these gases for particle detection, ensuring that they meet the necessary performance standards while also contributing to environmental sustainability. A particularly valuable parameter for assessing the performance of a gas in LHC operations is its absorbance spectrum, which spans from vacuum ultraviolet (UV) to visible light, as detailed in section 1.5.4 "Vacuum-UV and UV-Vis". This spectrum is expressed in electron volts (eV), providing critical insights into the gas's ability to absorb light at various wavelengths.

The R&D activities were focused on the RPC detectors, which are a type of gaseous avalanche detectors. When charged particles traverse the gas gap of an RPC, they lose a fraction of their kinetic energy by excitation and ionization of atoms or gas molecules. If an atom in the gas is ionized by the inelastic collision of the traversing particle, free charge carriers are deposited close to the position of the encounter. Conversely, if the atom is not ionized but instead excited, it promptly loses the excitation energy by the emission of a photon or an Auger electron, that may create additional ionization elsewhere in the gas. These events are normally undesirable since they may reduce the proportionality of the detector's response. Furthermore, they contribute to the spreading of the avalanche, potentially affecting the accuracy and efficiency of particle detection.

It has been found that the addition of a certain quantity of polyatomic gas, such as Carbon Dioxide (CO_2) or the i-C_4H_{10}, can suppress the photon-induced effects by absorbing the photons in a manner that prevents further ionization. The polyatomic component is integrated in certain concentrations alongside monatomic gases, serving as stabilizing additive. Each muon detector operates with a distinct nominal gas mixture, tailored to optimize performance and stability. (1.3.1 Fill Gases). The energy of the photons produced is usually between 25 and 4 eV that corresponds to wavelengths between 50 and 300 nm [41].

Due to limitations imposed by the instrument, our tests were performed at lower energies, between 9.5 and 1.1 eV.

4.3.1 UV-Vis Setup

During this doctoral project, two distinct sets of measurements were performed: one at CERN chemistry laboratory and another at the physics faculty of the University of Pavia

For the measurements performed at the CERN chemistry laboratory, the single beam Agilent 8453 spectrophotometer was used. Since the analysis was performed on gas phase, a cylindrical cuvette with a path of 100 nm was used at atmospheric temperature and pressure. Nitrogen was used as reference measurement. The analysis was performed in the 190-1100 nm wavelength range. The setup used for these analyses is shown in Figure 96.

Figure 96 Setup used for UV/Vis analysis at CERN chemistry laboratory.

The gases selected for the analyses were: iC_4H_{10}, CO_2, Novec 4710 (C_4F_7N), Novec 5110 ($C_5F_{10}O$) [42] and the HFO R1234ze ($C_3H_2F_4$).

For the analyses performed at the University of Pavia, a Varian Cary 6000i spectrophotometer was employed. It is a double beam device and, in this case, air was used as reference. Also for this

analysis a cylindrical cuvette with a path of 100 mm was used and the measurements were conducted at atmospheric pressure and room temperature with a humility level of 50%, in a wavelength range between 180 and 1800 nm. The setup is shown in Figure 97.

Figure 97 Setup used for UV/Vis analysis at the physics faculty of the University of Pavia.

The gases selected for the analyses were: CO_2, R134a and SF_6.

The results are show following.

4.3.2 UV-Vis results

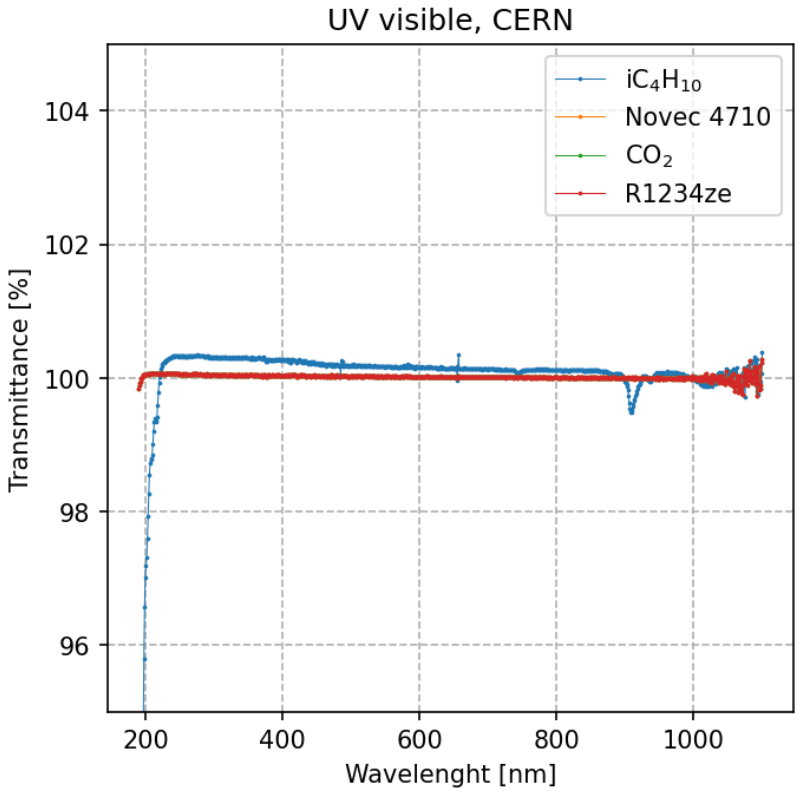

Figure 98 Transmittance VS wavelength for iC_4H_{10}, Novec 4710, CO_2 and R1234ze.

Figure 98 and Figure 99 display the results obtained at the CERN chemistry laboratory are shown. In particular, in the first plot the transmittance of iC_4H_{10}, Novec4710, CO_2 and R1234ze are compared. Among these compounds, isobutane seems to exhibit the strongest absorption in the region between 190 and 240 nm, even though this is the limit of the detector and the error is the highest, and a weak absorption also at 900 nm. The other gases do not show any absorption in the investigated range of wavelength.

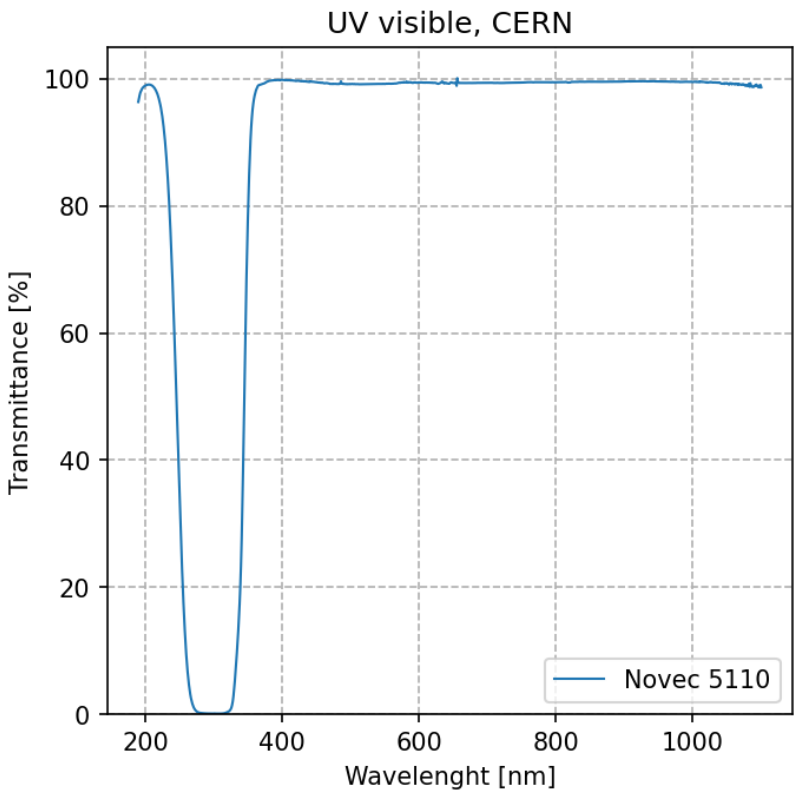

Figure 99 Transmittance VS wavelength for the Novec 5110.

Novec5110, shown in the second plot, presents a strong adsoprtion in the region between 220 and 360 nm, corresponding to the presence of a carbonyl group. The saturation can be due to the condensation of this gas inside the cuvette during the measurement since it is liquid at atmospheric pressure. Except for this strong absorption, it does not show any other interaction with the UV-vis light in the region analysed.

In the following plot, the results obtained at the University of Pavia are depicted.

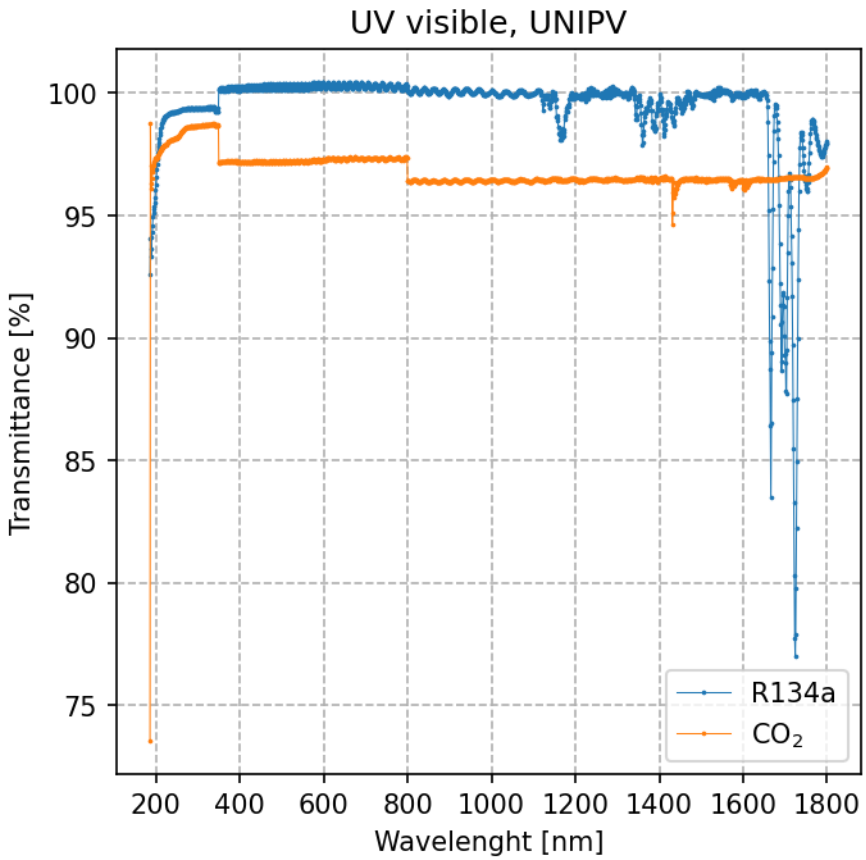

Figure 100 Transmittance VS wavelength for R134a and CO_2.

In Figure 100 the analysis of the CO_2 and R134a ($C_2H_2F_4$) in the range between 180 and 1800 nm is reported. The two "jumps" at around 370 and 800 nm ae due to the instrument and they are not related to the absorption of the compounds. This measurement confirmed what was seen at CERN: CO_2 has not any interaction with light in the range of the analysis. A weak absorption is visible in the IR region.

For the R134a ($C_2H_2F_4$), there is no absorption process in the region of UV-vis but just a very weak interaction in the IR region, which is of minimal interest due to the extremely low energy involved.

4.3.3 VUV setup

The instrument used for the VUV measurements, called ASSET, is the one shown in Figure 101 [43].

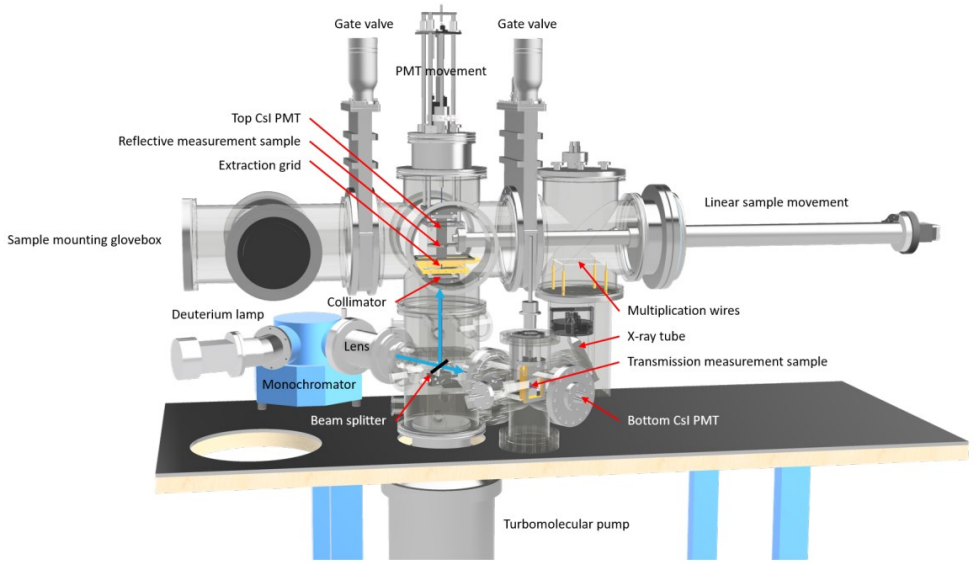

Figure 101 VUV spectrophotometer installed at the GDD laboratory at CERN [43].

Measurements are done by the use of UV light from a system consisting of a deuterium lamp [29] and a VUV monochromator [30]. The system can be purged with high purity nitrogen in order to avoid any absorption of the short wavelength part of the UV spectrum. The monochromator is attached to the measurement chamber via an extension containing a MgF2 collimating lens with the aim of focusing the light. A beam splitter divides the light into two separate beams. The light intensity is monitored by two calibrated CsI PMTs, one of which is used to measure the amount of light in the sample position, while the other one monitors stability of the light during measurements. The wavelength range that the measurements are conducted in is limited to about 130 nm on the low-wavelength side due to the MgF2 lens transparency and at about 170 nm on the high wavelength side due to the intensity of light from the deuterium lamp. The highest light intensity is observed at 160 nm (Figure 102).

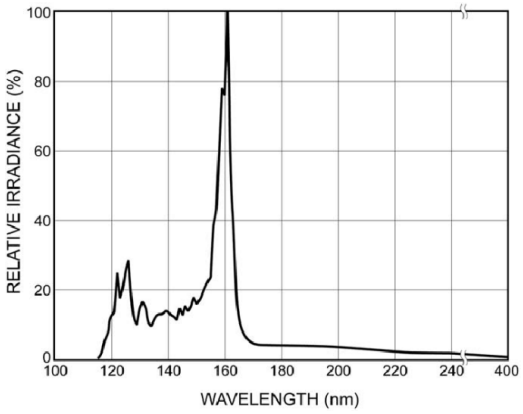

Figure 102 Deuterium lamp spectrum.

The setup permits reflective as well as transmission mode measurements. The reflective mode allows to measure the quantum efficiency of the photocathodes, while the transmission mode enables the measurements of the quantum efficiency as well as the transparency. Both measurements are done in the vacuum on the level of 10^{-7} mbar obtained by pre-pumps and turbomolecular pumps. The setup contains gate valves that permit a separation of the volumes and pump only the measurement chamber or flush only the irradiation chamber. A sample movement arm enables a linear transfer of the sample from one part of the chamber to another.

For our purpose, the setup was used in transmission mode (Figure 103): the UV beam, which is transmitted through the beam splitter, goes through a MgF2 window that separates two volumes and preserves vacuum in main chamber, and it arrives to a collimator. The light intensity is monitored by two calibrated CsI PMTs.

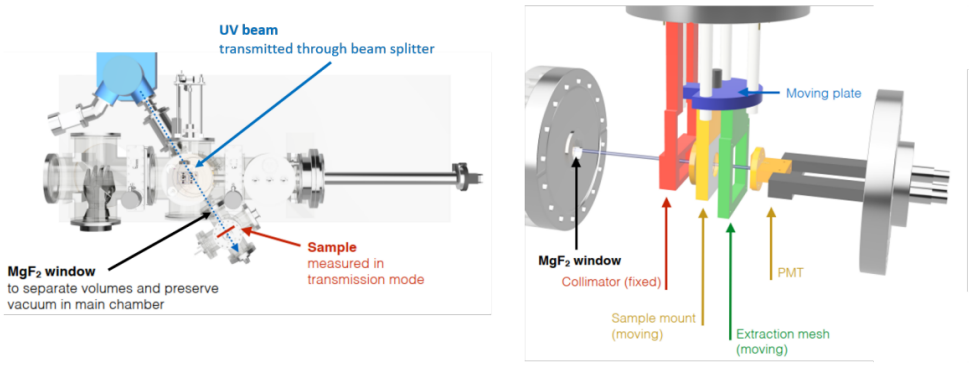

Figure 103 The scheme of the transmission mode [43]

4.3.4 VUV results

These measurements were performed at the GDD laboratory at CERN [44] with the ASSET instrument described above. The range of wavelength investigated was between 130 and 220 nm, corresponding to a range of energy between 9.5 and 5.6 eV. R134a, CO_2 and a mixture of R134a/iC_4H_{10} in a ratio 95/5 were analysed. Some gases, such as R134a and R134a/iC_4H_{10} were analysed at different pressures to examine the extent to which this variable affects the absorption process. All the plots shown following are expressed in terms of transparency VS wavelength.

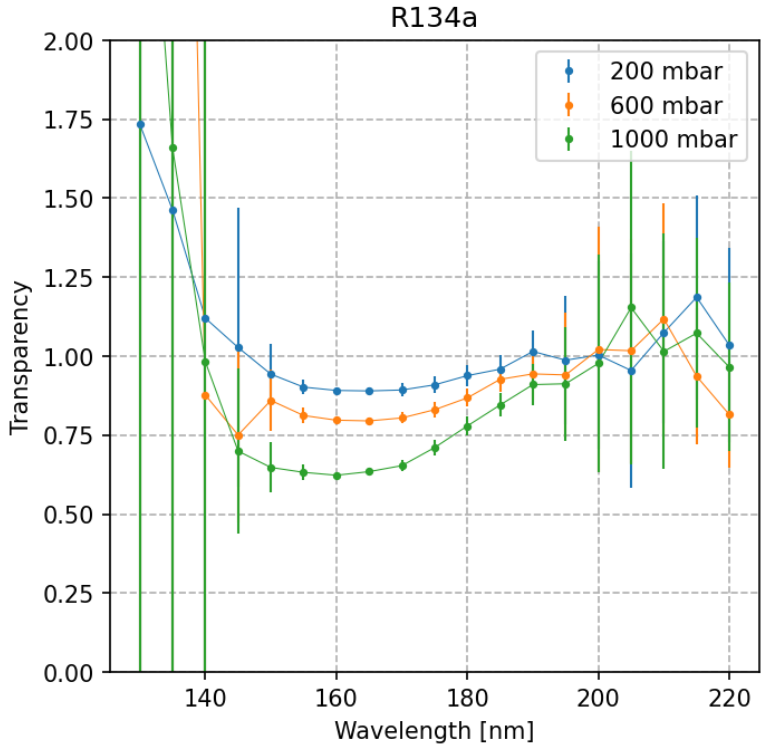

Figure 104 Transparency VS wavelength spectra for the R134a analysed at different pressures

Figure 104 summarizes the results obtained for the R134a at 200 mbar, 600 mbar and 1000 mbar are summarised. The maximum absorption intensity is in the region between 145 and 170 nm, corresponding to the maximum light intensity of the deuterium lamp. It is evident that increasing the pressure, the transparency decreases, as a result of a stronger absorption. The peak in that region can be explained with a $n \rightarrow \sigma^*$ transition, typical of alkyl halides.

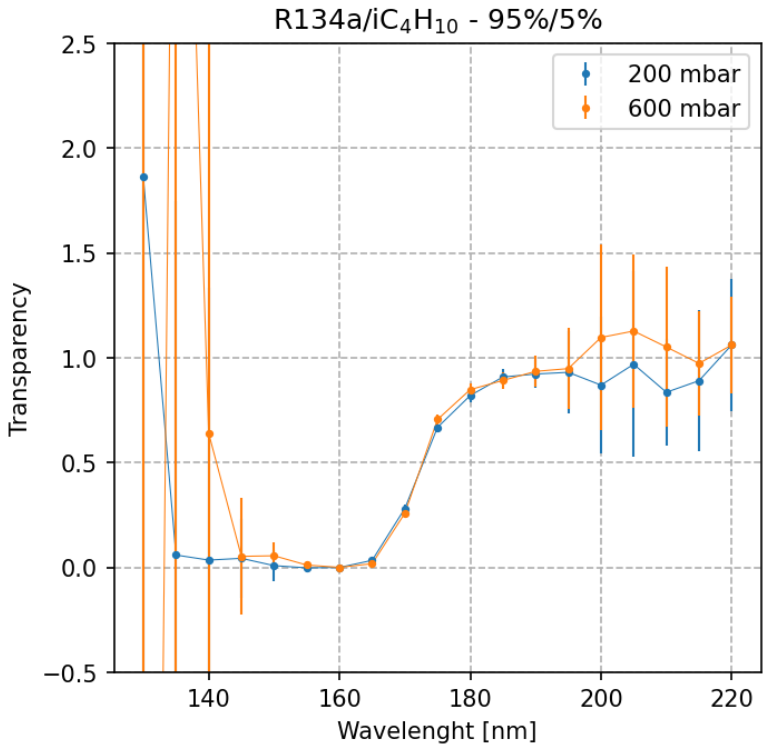

Figure 105 Transparency VS wavelength spectra for the R134a/iC_4H_{10} 95/5 analysed at two different pressures

The plot in Figure 105 refers to the measurements performed using a mixture of R134a/iC_4H_{10} in a ratio 95/5. Two analyses at 200 mbar and 600 mbar were conducted, while it was not tested at 1000 mbar for safety reason due to the flammability of the gas mixture. However, it is clearly visible that at 200 mbar there is a cutoff between 145 and 165 nm already. It means that increasing the pressure does not increase the absorption process. The difference with the previous plot is the presence of isobutane and the strong absorption may be explained with a $\sigma \rightarrow \sigma^*$ transition typical of alkanes at that specific energy of 8 – 9 eV.

Other measurements were performed on several gases by F. M. Brunbauer that are interesting for the R&D activities, shown in Figure 106. All the analyses were performed at 1000 mbar.

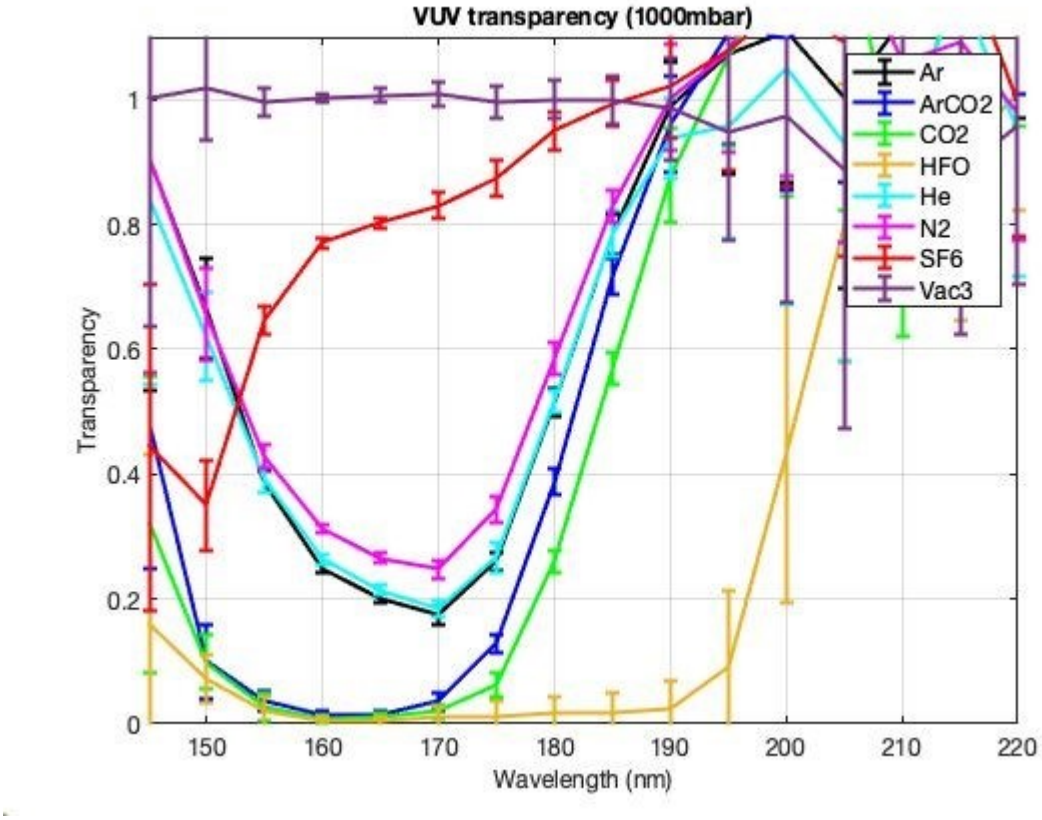

Figure 106 Transparency VS wavelength spectra for different gases analysed at 1000 mbar

The compounds exhibiting the highest absorption are the HFO, CO_2, and the mixture Ar/CO_2 in a ratio of 70/30. N_2, He, and Ar show a moderate absorption in correspondence with the maximum light intensity of the deuterium lamp, while SF_6 does not interact with photons except for the region between 140 and 155 nm.

Further studies on these gases and also new, more eco-friendly gases are scheduled for the next months.

Chapter 5
“Conclusions”

The purpose of the PhD project described in this thesis is twofold: primarily, to reduce GHG emissions, by enhancing the efficiency of recovery systems for fluorinated gases utilized in LHC experiments, specifically targeting CF_4, C_4F_{10}, and $C_2H_2F_4$ within the CMS and LHCb setups; secondly, and secondly, to explore and develop new possible more eco-friendly alternatives to the gases currently used in particle detectors.

There are currently two different recovery plants of CF_4, one for each experiment, used for the CMS CSC detector and the LHCb RICH2, respectively. In the first case, CF_4 is recovered from a mixture containing $CF_4/CO_2/Ar$ in a ratio of 10%/50%/40%. The process is divided in three stages. Initially, membranes are employed to remove 97% of the initial CO_2 and 75% of the Ar. Subsequently, a 5A absorber eliminate the remaining CO_2, while in the final stage, a 13X MolSieve is used for the adsorption of CF_4 and the removal of the main contaminants, such as Ar and nitrogen. Thanks to the studies and optimizations carried out on the membrane module and on the CF_4 absorber module, the recovery efficiency has increased from below 50% to the current level of 70%,resulting in an annual saving of over 800 kg r of CF_4. This reduction is equivalent to approximately 10,000 tCO_2e and a financial saving of 60 kCHF per year.

The second recovery system for the CF_4 installed in LHCb differs from the first one because it was not designed to work in continuous operation. Instead, it is used only when the detector needs to be filled or emptied, that usually occurs at the start and at the end of the LHC RUN. The recovery system is made of two modules, the membrane and the purifier ones. The membrane module is primarily used to remove a significant portion of CO_2 and Ar from the gas mixture. Following this initial purification, the purifier module, which may include technologies such as 5A absorbers and 13X Molecular Sieves, further cleanses the gas by eliminating remaining impurities and adsorbing CF_4. This structured approach ensures efficient recovery and purification of the gas.

The last emptying of the detector was performed in 2018 and the last filling in 2021. Thanks to the recovery system the CF_4 consumption was of 255 kg instead of 1020 kg, saving 5600 tCO_2e and 41 kCHF. The system reached a 75% of efficiency thanks to the fine tuning followed with the use of µGC and IR.

Many improvements were also done on the recovery system for the C_4F_{10}, installed in LHCb for the RICH1 detector. Before this PhD project the recovery plat worked with an efficiency of 70% especially for the lack on the software control but thanks to gas chromatograph analysis and some hardware improvements, such as the installation of a flowmeter at the exhaust of the plant, we have been able to reach nowadays a recovery efficiency of 83%. The gas chromatography was crucial to monitor not only the quality and the gas composition inside the detector, but also to improve the quality of the gas already recuperated inside the recovery tank. It was possible to perform a cleaning of the bottle, to spot the difference in composition between gas and liquid phase and to understand the solubility of CO_2 in the C_4F_{10}. Moreover, we found out that nitrogen solubilizes more than oxygen in the C_4F_{10} liquid, leading to a gas mixture in which the ratio between the two is not 1:4 but 1:2. The study on the purifier modules permitted to save perfluorobutane that was wasted in the atmosphere before. These studies brought to 285 kg of C_4F_{10} saved in the past three years, equivalent to 2600 tCO_2e.

The last year of this PhD project was focused on the commissioning of the recovery system for the $C_2H_2F_4$ installed in CMS for the Resistive Plate Chambers detectors. This system required extensive work due to the uniqueness of the plant and the operational difficulties related to the formation of a minimum boiling point azeotrope between R134a and iC_4H_{10}. Many GC and GC/MS analyses were performed to characterize the R134a recovered during the tests in which several parameters have been modified. The parameters most affecting the performance of the recovery plant were identified as: temperature and pressure of top and cold buffers, input and extraction flow rate . Once the parameters were identified, the system was modified to obtain a good final product. In particular, needle valves and new pipes were added to improve the extraction procedure which resulted in the isobutane concentration passing from 10000 ppm to 4500 ppm, maintaining an efficiency higher than 80%. This recovery system will help to save more than 17000 tCO_2e and 100 kCHF per year.

Beside the recovery systems, many studies were carried out to characterize the gas mixtures used in particle detectors in order to understand the breakdown mechanisms of fluorinated gases in the LHC conditions which help in finding new more ecofriendly alternatives to the GHGs currently used at the CERN LHC experiments. One of the parameters that must be verified in the choice of a fluorinated gas is the reactivity of these gases in specific conditions, such as humidity, high electric field, or irradiation. Some of them go through fragmentation processes, producing fluorides anions that can react with the water present in the gaseous mixture leading to the

formation of hydrofluoric acid. Part of the R&D activities focused on ISE measurements for fluorine ions at the Gamma Irradiation Facility (GIF++) at CERN where a charged muon beam is combined with a 12 TBq ^{137}Cesium source thanks to which it is possible to simulate the HL-LHC conditions in a short period of time. For this experiment two RPCs were used and all the gas passed through the chambers was bubbled in water solutions 50/50 water/TISAB II. The measurements were done in continuous and the fluoride production of the standard gas mixture (95.2% $C_2H_2F_4$ + 4.5% iC_4H_{10} + 0.3% SF_6 humidified at 40% relative) was compared to mixtures in which part of the R134a was replaced by CO_2 or HFO. Both gaseous mixtures resulted in a fluoride concentration higher than the standard mixture, confirming that F^- ions are not proportional to the quantity of fluorinated gas in the mixture. At the same time it could be explained considering the higher stability of carbocation formed starting from the HFO with respect to the one formed from R134a.

The tests at the GIF++ were useful to optimize the setup for the ISE analyses and to improve the data acquisition that were then used at the ALICE LHC experiment for MID detectors. Before the LHC RUN3, two racks completely dedicated to ISE and μGC analyses were installed. Three sample points arrive in the racks, from mixer module, before and after the purifier module. They are all analysed by μGC while only before and after purifier are bubbled in two different water solutions made 50/50 water/TISAB II for ISE measurement. During RUN2 it was demonstrated that purifier is able to trap different kind of impurities among which also fluorine ions. The analysis campaign started in September 2023 confirmed this trend: the fluorides concentration after the purifier module is lower than instrument's detection limit while before the purifier it has the same trend of the integrated luminosity and it reached a value of 20 ppm in 7 months. These measurements are very useful also to understand the correlation between fluorides and detectors parameters such as currents, irradiation, humidity and quantity of fluorinated gases.

Last part of R&D activities focused on the UV-visible characterization of the gases used in the gaseous particle detectors, mainly Resistive Plate Chambers. For this purpose, many gases have been analysed in the wavelength range between 140 and 1800 nm, using different device for each range. As concern the near UV and visible range, most of the analysed gases have not any interaction with photons, with a resulting absorbance close to zero, except for the Novec 5110 which shown a cutoff between 220 and 360 nm. Different results were obtained for the range between 140 and 220 nm: all the gases analysed shown absorption peaks in correspondence of the deuterium lamp maximum light intensity at 160 nm. The mixture 95/5 R134a/iC_4H_{10} was the

one showing a cutoff between 145 and 165 nm, confirming the capacity of this gas mixture of absorbing photons at higher energy.

The work done in the past three years helped to save more than 60000 tCO_2e and more than 300 kCHF. Thanks to the improvements done on the recovery plants, more tCO_2e and kCHF will be saved in the next years. The studies performed on the fluorinated gases contributed to the advances in the understanding of the complex processes which take place inside the gaseous detectors that however still require further studies.

Bibliography

[1] G. Martinez, «The Muon Spectrometer of the ALICE experiment,» *Nuclear Physics A,* pp. 313-319, 2005.

[2] P. Fonte e V. Peskov, On the physics and technology of gaseous particle detectors, Plasma Sources Science and Technology, 2009.

[3] The ATLAS Collaboration, G. Aad e E. Abat, «The ATLAS Experiment at the CERN Large Hadron Collider,» *Journal of Instrumentation,* 2008.

[4] CERN, «ATLAS EXPERIMENT,» [Online]. Available: https://atlas.cern/Discover/Detector/Muon-Spectrometer.

[5] P. Paolucci, «The CMS Muon system,» CMS-CR-2006-006, Geneva, CERN, 2005.

[6] A. Alves Jr e et al., «Performance of the LHCb muon system,» *JINST,* 2013.

[7] LHCb collaboration, «The LHCb Detector at LHC,» *Journal of instrumentation,* 2008.

[8] Buchtela and G. Steinhauser, “"Gas Ionization Detectors.",” in *Handbook of Radioactivity Analysis, Academic*.

[9] M. Corbetta, «Studies on Gas Mixture and Gas Recirculation Effects on GEM “Studies on Gas Mixture and Gas Recirculation Effects on GEM,» 2018.

[10] P. Camarri, R. Cardarelli, A. Di Ciaccio e R. Santonico, «Streamer suppression with SF6 in RPCs operated in avalanche mode,,» *Nuclear Instruments and Methods in Physics Research Section A: Accelerators, Spectrometers, Detectors and Associated Equipment,,* 1998.

[11] «PROFIBUS and PROFINET International,» [Online]. Available: https://www.profibus.com/.

[12] M. Corbetta, «Development of Gas System for Gaseous Detector Operation at HL-LHC,» Geneve, CERN, 2021.

[13] «Jeol,» [Online]. Available: https://www.jeol.com/products/science/gcms.php.

[14] Directorate-General for Climate Action, «European Commission,» [Online]. Available: https://climate.ec.europa.eu/eu-action/fluorinated-greenhouse-gases/achievements_en.

[15] G. Salierno, «On the Chemical Pathways Influencing the Effective Global Warming Potential of Commercial Hydrofluoroolefin Gases,» *ChemSusChem,* pp. 1-19, 2024.

[16] R. Guida, M. Corbetta, B. Mandelli e G. Rigoletti, «Strategies for reducing the use of greenhouse gases from particle detectors operation at the CERN LHC experiments,» in *40th International Conference on High Energy physics - ICHEP2020*, Prague, Czech Republic (virtual meeting), 2020.

[17] R. Guida, B. Mandelli e M. Capeans, «Strategies for reducing the environmental impact of gaseous detector operation at the CERN LHC experiments,» *Nuclear Instruments and Methods in Physics Research A,* vol. 845, pp. 253-256, 2016.

[18] F. Bazzarelli, G. Lidietta e E. Piacentini, «Dense Membranes,» in *Encyclopedia of Membranes*, 2016.

[19] M. Mulder, «Basic Principles of Membrane Technology,» in *Basic Principles of Membrane Technology, Dordrecht, The* , 1996.

[20] X. Y. Chen, S. Kaliaguine, N. Tien-Bihn e D. Rodrigue, «POLYIMIDE MEMBRANES FOR GAS SEPARATION: SYNTHESIS, PROCESSING AND PROPERTIES,» in *Polyimides*, 2017.

[21] D. W. G. Robert H. Perry, «Distillation,» in *Perry's Chemical Enginers'*, Mc Graw Hill, 1999.

[22] A. Wisecarver, «Gas Mixture Longevity Studies for the CMS Cathode Strip Chambers in Preparation for HL-LHC,» in *2019 APS Meeting of the Division of Particles & Fields*, 2019.

[23] M. C. Arena, «OPTIMIZATION OF CF4 RECUPERATION FROM THE GAS MIXTURE USED IN THE CSC GAS SYSTEM AT THE COMPACT MUON SOLENOID (CMS) EXPERIMENT AT CERN,» University of Pavia, 2021.

[24] F. Falbo, F. Tasselli, A. Brunetti, E. Drioli e G. Barbieri, «Polyimide hollow fiber membranes for CO2 separation from wet gas mixtures,» *Separation Processes Braz. J. Chem. Eng,* 2014.

[25] J. Wang, S. Deng, R. Zhao, J. Zhao, J. Xue, Z. Wu e Y. Bai, «Performance comparison of three adsorption cycles for CF4 recovery from waste gas using 13X zeolite,» *Journal of Cleaner Production,* vol. 337, 2022.

[26] M. Arena, R. Guida, B. Mandelli e G. Rigoletti, «Recuperation systems for fluorinated gases at the CERN LHC Experiments,» *Nuclear Instruments and Methods in Physics Research Section A: Accelerators, Spectrometers, Detectors and Associated Equipment,* vol. Volume 1068, 2024.

[27] M. Di Toma, Development of a prototype for the recovery of R134a from the mixture of RPCs detectors, Politecnico di Torino, EP-DT-FS gas group, March 2023.

[28] M. Bruno, R134a recuperation system for the resistive plate chambers at CMS experiment, CERN: Politecnico di Torino, 2023.

[29] «Huber,» [Online]. Available: https://www.huber-online.com/fr/produits/systemes-de-thermoregulation-dynamique/unistats-jusqua-120c/unistat-915w. [Consultato il giorno 2024].

[30] R. Santonico e R. Cardarelli, «Development of resistive plate counters,» *Nuclear Instruments and Methods in Physics Research,* pp. 377-380, 1981.

[31] M. Jakel, «CERN GIF++ : A new irradiation facility to test large-area particle detectors for the high-luminosity LHC program,» *Proceedings of Science,* n. Technology and Instrumentation in Particle Physics 2014, 2014.

[32] CERN, «CERN COURIER,» 23 September 1998. [Online]. Available: https://cerncourier.com/a/kodel-establishes-korea-as-major-physics-player/.

[33] GENERAL TECNICA. [Online]. Available: https://www.generaltecnica.it/online/.

[34] «Thermo Fisher scientific,» [Online]. Available: https://www.thermofisher.com/order/catalog/product/9609BNWP?SID=srch-srp-9609BNWP.

[35] «Hanna Instruments,» [Online]. Available: https://hanna.it/ise/ise-da-banco/.

[36] R. Guida, B. Mandelli e G. Rigoletti, «Measurements of fluoride production in resistive plate chambers,» *Nuclear Instruments and Methods in Physics Research Section A: Accelerators, Spectrometers, Detectors and Associated Equipment,* 2023.

[37] R. Santonico, «RPC understanding and future perspectives,» *Nuclear Instruments and Methods in Physic Reasearch,* pp. 1-6, 2004.

[38] M. Abbrescia, A. Colaleo e R. Guida, «'Results about HF production and bakelite analysis for the CMS Resistive Plate Chambers,» *Nuclear Methods in Physics Research,* n. A 594, pp. 140-147, 2008.

[39] L. Alvigini, Studies on impurities in the gas mixture of CERN LHC particle detectors, CERN: University of Pavia, 2019.

[40] M. Verzeroli, M. C. Arena e et al., *Studies of F- Impurities Formation in ALICE MID RPC Detectors:A Comparison Between RUN2 and RUN3,* Santiago de Compostela (Spain): RPC 2024, 2024.

[41] M. Abbrescia, V. Peskov e P. Fonte, Resistive Gaseous Detectors, 2018, pp. 81-90.

[42] M. Arena, R. Guida, S. Juks, B. Mandelli, G. Rigoletti e M. Verzeroli, «Towards more eco-friendly gaseous detectors,» *Nuclear Instruments and Methods in Physics Research Section A: Accelerators, Spectrometers, Detectors and Associated Equipment,* vol. 1068, 2024.

[43] M. Lisowska, Photocathode characterisation and ageing studies for precise-timing gaseous detectors, Wroclaw: Politechnika Wroclawska, 2021.

[44] CERN, «GDD-Gas Detectors Development Group,» [Online]. Available: https://gdd.web.cern.ch/.

[45] F.Sauli, « ''Gaseous radiation detectors: fundamentals and applications",» Vol. 36, Cambridge University Press.

[46] W. L. Hosch, «Britannica,» [Online].

[47] R. Guida e B. Mandelli, «R&D strategies for optimizing greenhouse gases usage in the LHC particle detection systems,» *Nuclear Instruments and Methods in Physics Research Section A: Accelerators, Spectrometers, Detectors and Associated Equipment,* vol. Volume 958, 2020.

[48] S. Colafranceschi, L. Benussi e other, «Performance of the Gas Gain Monitoring system of the CMS RPC muon detector and effective working point fine tuning,» *Journal of Instrumentation,* vol. Volume 7, 5 December 2012.

[49] A. Sabliic, in *Environmental and ecological chemistry - Volume I*.

[50] D. Wiedner, «The use of n-perfluorocarbons as rich radiators,» *Nuclear Instruments and methods in Physics research A,* vol. 595, pp. 216-219, 2008.

[51] W. Zheng, L. Jia e F. Huang, «Vacuum-Ultraviolet Photon Detections,» *iScience,* vol. 23, n. 6, 2020.

[52] «Horiba,» [Online]. Available: https://www.horiba.com/int/scientific/technologies/vacuum-ultra-violet-spectroscopy/vacuum-ultra-violet-spectroscopy/.

[53] «3M,» [Online]. Available: https://www.3m.com/3M/en_US/p/d/b00000619/.

[54] «3M,» [Online]. Available: https://www.3m.com/3M/en_US/p/d/b40006511/.

[55] «sinteco,» sinteco srl, [Online]. Available: https://www.sinteco-srl.com/prodotti/gas-refrigeranti/r1234ze/.

[56] CERN, «Environment Report,» 2021-2022.